

UCLA

UCLA Electronic Theses and Dissertations

Title

Identifying Deep-brain Contributions to Consciousness for Clinical Intervention in Severe Brain Damage with Transcranial Focused Ultrasound

Permalink

<https://escholarship.org/uc/item/167194s4>

Author

Cain, Joshua Alan

Publication Date

2022

Peer reviewed|Thesis/dissertation

University of California

Los Angeles

Identifying Deep-brain Contributions to Consciousness for Clinical Intervention in
Severe Brain Damage with Transcranial Focused Ultrasound

A dissertation presented in partial satisfaction of the requirements for the degree Doctor of
Philosophy in Psychology

by

Joshua Alan Cain

2022

© Copyright by

Joshua Alan Cain

2022

ABSTRACT OF THE DISSERTATION

Identifying Deep-brain Contributions to Consciousness for Clinical Intervention in
Severe Brain Damage with Transcranial Focused Ultrasound

by

Joshua Alan Cain

Doctor of Philosophy in Psychology

University of California, Los Angeles, 2022

Professor Martin Monti, Chair

The disorders of consciousness (e.g., coma, the vegetative state) which often follow severe brain damage are the medical conditions which arguably pose some of the greatest cost on developed societies—both in terms of the economic cost and the suffering produced. While advances in the field of long-term intensive care have made the maintenance of life in patients recovering from brain injury highly feasible, little can be done to promote functional recovery in DOC patients who do survive with severe impairments in consciousness or cognitive functioning. This remaining gap in the medical treatment of DOC is contrasted starkly by a rapidly growing scientific understanding

of the mechanisms behind impairment in DOC. The distance between the science and treatment of DOC stems from the many as-yet-undiscovered approaches necessary to move what we know about the neural correlates of (un)consciousness in DOC into suitable treatment options. For instance, circuits involving the basal ganglia and thalamus have been highlighted in recent decades for their apparent involvement in the DOC pathology. Prior to this dissertation, however, there were no methods for influencing the function of these nuclei directly without a surgery whose risks preclude use in most DOC patients. The work of this dissertation aims to assess the feasibility of using low intensity focused ultrasound (LIFU) as a way to selectively, but non-invasively, modulate deep brain structures in the context of DOC. LIFU in healthy subjects was used to better understand the neural response to LIFU applied to the deep brain, while acute and chronic doc patients were administered thalamic LIFU and monitored for the observation of changes in responsiveness. We observe significant behavioral improvement in both DOC cohorts, while fMRI data from three cohorts (2 DOC, 1 healthy) suggest acute inhibition may occur during LIFU but that complex changes in connectivity may underlie the observed recovery in DOC. Finally, this dissertation includes the production of a system for rapidly estimating how skull affects LIFU beam properties (an enduring challenge in this field), which should assist newcomers to the technology. In all, this work aims to be a suitable foundation from which to build a better scientific understanding of and treatment options for DOC through LIFU.

The dissertation of Joshua Alan Cain is approved.

Barbara Knowlton

Marco Iacoboni

David Clewett

Martin Monti, Committee Chair

University of California, Los Angeles

2022

Dedication

To those who, tripping and stumbling, dare light candles in particularly dark rooms.

Table of Contents

Chapter 1: General Introduction.....1

Disorders of Consciousness (DOC).....1

Thalamus.....4

Focused Ultrasound Neuromodulation10

Chapter 2: Establishing the presence of fMRI correlates of concurrent (Online)

LIFU exposure using two parameter sets in healthy individuals.....13

Abstract.....13

Introduction13

Methods15

Results27

Discussion37

Chapter 3: Establish the feasibility, preliminary efficacy, and neural correlates

of thalamic LIFU in acute and chronic patient populations.....46

Abstract46

Introduction47

Methods48

Results59

Discussion69

Chapter 4: Establish improved methods for rapidly estimating the effects of

skull on transcranial focused ultrasound.....82

Abstract82

Introduction	82
Methods	84
Results	88
Discussion.....	90
Chapter 5: This Work in Context.....	92
Appendices	100
Chapter 2 Appendix.....	100
Chapter 3 Appendix.....	108
References	109

List of Tables

Chapter 2

(Appendix) Table 2-S1: 100Hz Sonication Compared to Baseline, 10Hz Sonication.....100

Chapter 3

Table 3-1: Relevant patient-specific information in subjects.....50

List of Figures

Chapter 2

Figure 2-1: Sonication Parameters, Experimental Design, and Water Tank Measurements of Beam Properties.....	28
Figure 2-2: Numerical Modeling through Bone and Water.....	29
Figure 2-3: ROI analysis results.....	32
Figure 2-4: Whole brain results.....	36
Figure 2-S1: Aggregating LIFU Mode 1 and LIFU Mode 2 data.....	101
Figure 2-S2: Comparisons between Run1 and Run2 for LIFU in Mode 1 (PRF = 100Hz).....	102
Figure 2-S3: Comparisons between Run1 and Run2 for LIFU in Mode 2 (PRF = 10Hz).....	103
Figure 2-S4: Whole-Brain Perfusion Linear Model.....	104
Figure 2-S5: ASL ROI Putamen.....	105
Figure 2-S6: ASL ROI Left Globus Pallidus.....	106
Figure 2-S7: ASL ROI Left Thalamus.....	106
Figure 2-S8: Cumulative Pressure Over Time.....	107

Chapter 3

Figure 3-1: Study protocol involving LIFU parameters and CRS-R.....	52
Figure 3-2: Acute Behavioral Results.....	60
Figure 3-3: Acute Whole Brain Results.....	63
Figure 3-4: Chronic Behavioral Results.....	65

Figure 3-5: Chronic Whole Brain Results.....68

Figure 3-S1: Group Wide Activations in Subject Space.....108

Chapter 4

Figure 4-1: SMART_FUS workflow.....87

Figure 4-2: SMART_FUS outputs.....89

Chapter 5

Figure 5-1: Scholarly mentions (results on google scholar) since 1999 of “ultrasound neuromodulation” and “transcranial magnetic stimulation”

Figure 5-2: Scholarly mentions (results on google scholar) since 1999 of “ultrasound neuromodulation” (blue) and “transcranial magnetic stimulation” (orange), normalized by the total results from each search query since 1999.

Figure 5-3: Scholarly mentions (results on google scholar) since 1999 of “ultrasound neuromodulation”

Acknowledgements

Julia Crone, Evan Lutkenhoff, and Joel Frolich, whose expertise was indispensable. Micah Johnson, who's frequent help and spirit kept me going. Martin Monti and Caroline Schnackers, who trusted me with so much. The patients and their loved ones, without whom our study of disorders of consciousness would be impossible.

Joshua Cain Ph.D. Curriculum Vitae

EDUCATION

Ph.D. Student in Cognitive Neuroscience, UCLA, 06/28/17 – Present, Ph.D. Candidate from 05/01/2021, GPA: 3.9

M.S. Cognitive Neuroscience, UCLA, 12/30/18

B.Sc. in Neuroscience, Drake University, May 2016, GPA: 3.99

B.Sc. in Psychology, Drake University, May 2016, GPA: 3.99

AWARDS

Ursula Mandel Fellowship (\$20,000) 2020-2021 Academic Year

Graduate Research Mentorship Program (\$20,000) 2019-2020 Academic Year

ISTU Conference Student Award (\$1,000) Spring 2019

Graduate Summer Research Mentorship Program Award (\$6,000) Summer 2018

Summa Cum Laude Drake University Spring 2016

RESEARCH

Overview:

Graduate Student under Dr. Martin M. Monti at UCLA 06/01/2017-Present

Research Assistant under Dr. Brian J. Sanders at Drake University 10/01/2013– 18/05/2016

Research Intern under Dr. Jonathan Crystal at Indiana University 5/15/2015-7/25/2015

Published Studies:

J Cain*, AI Luppi*, LRB Spindler*, UJGórska*, D Toker, AE Hudson, EN Brown, MN Diringer, RD Stevens, M Massimini, MM Monti, EA Stamatakis**, M Boly**, the Curing Coma Campaign and its contributing collaborators. Mechanisms Underlying Disorders of Consciousness: Bridging Gaps to Move Towards an Integrated Translational Science. Neurocritical Care. Accepted. *co-first authors **co-senior authors.

Cain, J. A., Visagan, S., Johnson, M. A., Crone, J., Blades, R., Spivak, N. M., Shattuck, D. W., & Monti, M. M. (2021). Real time and delayed effects of subcortical low intensity focused ultrasound. *Scientific Reports*, 11(1), 6100. <https://doi.org/10.1038/s41598-021-85504-y>

Cain, J. A., Spivak, N. M., Coetzee, J. P., Crone, J. S., Johnson, M. A., Lutkenhoff, E. S., Real, C., Buitrago-Blanco, M., Vespa, P. M., Schnakers, C., & Monti, M. M. (2021). Ultrasonic thalamic stimulation in chronic disorders of consciousness. *Brain Stimulation: Basic, Translational, and Clinical Research in Neuromodulation*, 14(2), 301–303. <https://doi.org/10.1016/j.brs.2021.01.008>

Iglehart, C., Monti, M., Cain, J., Tourdias, T. & Saranathan, M. A systematic comparison of structural-, structural connectivity-, and functional connectivity-based thalamus parcellation techniques. *Brain Struct Funct* 225, 1631–1642 (2020).

Bratch, A., Kann, S., Cain, J. A., Wu, J.-E., Rivera-Reyes, N., Dalecki, S., ... Crystal, J. D. (2016). Working Memory Systems in the Rat. *Current Biology*, 26(3), 351–355. <http://doi.org/10.1016/j.cub.2015.11.068>

In Review:

Cain, J. A., Spivak, N. M., Coetzee, J. P., Crone, J. S., Johnson, M. A., Lutkenhoff, E. S., Real, C., Buitrago-Blanco, M., Vespa, P. M., Schnakers, C., & Monti, M. M. (2022) Ultrasonic Deep Brain Neuromodulation in Acute Disorders of Consciousness: A Proof-of-Concept. (In review at *Brain Sciences*)

Cain, J. A., Visagan, S., & Monti, M. M. (2021) S.M.A.R.T. F.U.S: Surrogate Model of Attenuation and Refraction in Transcranial Focused Ultrasound. (In review at *Brain Stimulation*)

Students Papers:

Phuc Nguyen, Joshua Cain. "A New Frontier in Fighting Brain Cancer: Cutting Edge Magnetic Resonance Imaging Techniques" *Journal of Student Research*. (In review at *Journal of Student Research*)

Invited Talks:

J. Cain, MM Monti, C Schnakers, N. Spivak, PM Vespa (2022) Ultrasonic Deep Brain Neuromodulation in Acute and Chronic Disorders of Consciousness: A Proof-of-Concept.
Oral Presentation; North American Neuromodulation Society (NANS), 25 minutes

J. Cain, MM Monti, C Schnakers, N. Spivak, PM Vespa (2019) Recovering consciousness: Thalamic sonication in chronic post-coma recovery.
Oral Presentation; Allen Institute, Tiny Blue Dot Foundation Meeting, 45 minutes

J. Cain, MM Monti, C Schnakers, N. Spivak, PM Vespa (2019) Recovering consciousness: Thalamic sonication in chronic post-coma recovery.
Oral Presentation; Association for the Scientific Study of Consciousness (ASSC), 35 minutes

J. Cain, MM Monti, C Schnakers, N. Spivak, PM Vespa (2019) Recovering consciousness: Thalamic sonication in chronic post-coma recovery.
Oral Presentation; International Society for Therapeutic Ultrasound (ISTU), 10 minutes

J. Cain, MM Monti, C Schnakers, N. Spivak, PM Vespa (2019) Recovering consciousness: Thalamic sonication in acute post-coma recovery.
Oral Presentation; International Brain Stimulation Conference, 20 minutes

J. Cain, S. Visigan, R. Blades, and M. Monti, Ph.D. (2019) Thalamic Low-Intensity-Focused-Ultrasound-Pulsation Enhances Cortical BOLD and Blood Perfusion.
Oral Presentation; Annual World Congress of the Society for Brain Mapping and Therapeutics (SBMT), 20 minutes

Chapter 1: General Introduction

1.1 Disorders of Consciousness (DOC)

1.1.1 The Mesocircuit Hypothesis, DOC, and the Deep Brain

Disorders of Consciousness (DOC) are a spectrum of disorders defined by a disruption in either wakefulness or awareness (Laureys, 2005; Monti et al., 2010). This spectrum encompasses, for instance, Coma, the Vegetative State, and the Minimally-Conscious state, conditions which often occur following traumatic (e.g., blunt force trauma) or non-traumatic (e.g., hypoxia) brain damage. The vegetative state, characterized by eye opening or reflexive behavior, is defined as wakefulness without awareness, which distinguishes it from Coma where neither are present. On the contrary, the minimally conscious state may present with some level of awareness and some level of arousal despite one or both qualities being severely diminished or perturbed (Monti & Sannita, 2016).

For over two decades, neuroimaging techniques such as positron emission tomography (PET) and functional magnetic resonance imaging (fMRI) have consistently observed downregulation of cortical metabolism as well as a disruption in frontoparietal connectivity in DOC patients (Laureys et al., 1999; Monti & Sannita, 2016). In recent years, information theoretic measures of cortical network activity have also consistently predicted DOC symptoms (Casarotto et al., 2016). While these phenomena may consistently describe the type of forebrain dysfunction observed in DOC, clinical approaches to treating DOC have largely focused on the reinvigoration of forebrain function by targeting its background conditions—namely subcortical output to the cortex. While functional dysregulation of large-scale cortical networks is perhaps an obligatory feature of DOC, the DOC pathology is highly heterogeneous in terms of structural damage, suggesting that disruption of any singular component of principle circuits involved in forebrain regulation could

result in lost consciousness and reinvigoration of those damaged components may reverse that loss.

Schiff identifies that the broad forebrain dysregulation that must underlie the severe impairments observed in DOC may arise from 1) direct and expansive damage to forebrain neurons, 2) physical deafferentation of forebrain neurons from sensory input and arousal regulating centers or 3) functional changes in circuit-level dynamics (Schiff, 2010a). Importantly, option 3 does not depend on permanent cellular damage, providing hope for restorative techniques which reverse the circuit-level dysfunction observed in DOC. Logically, reversal of aberrant circuit dynamics is thought to underlie spontaneous recovery from DOC.

Though necessarily an oversimplification, Schiff's "mesocircuit" hypothesis focuses on a pathway involving cortical input to the striatum's medium spiny neurons (MSN), which inhibit the globus pallidus interna, which itself tonically inhibits the thalamus and its excitatory projections to cortex (Schiff, 2010a). The high firing threshold of MSN's (Grillner et al., 2005) ensures that a reduction in cortico-striatal input, which is likely in the case of severe cortical damage, is primed to severely reduce striatal output to the globus pallidus and, ultimately, excitatory thalamic output to cortex. It can be safely stated that all of the promising treatment mechanisms for DOC that have emerged in recent years are thought to act on some component of this circuit from amantadine's action in the striatum, zolipem's purported action on the globus pallidus, and DBS stimulation of the central thalamus (Schnakers & Monti, 2017). However, the thalamus, as the final bottleneck towards cortical activation, has received disproportionate attention. While recent studies have revealed

direct pallido-cortical connections (Zheng & Monti, 2019), a view of the thalamus as the primary gateway to cortex for the subcortical components of the mesocircuit retains heuristic value.

1.1.2 The Thalamus and DOC

Damage to the thalamus and its connections with cortex have been widely associated with the symptoms of disorders of consciousness following severe brain damage (Monti & Sannita, 2016). For instance: Infarct of the central thalamus is associated with a loss of consciousness in some patients (Castaigne et al., 1981). Damage to the thalamus has been characterized as a principle neural correlate of the persistent vegetative state (Monti et al., 2010). A meta-analysis of 13 fMRI studies in DOC patients reported reduced activity in the mediodorsal nucleus of the thalamus (Hannawi et al., 2015) in DOC patients. Furthermore, atrophy of the thalamus predicts the degree of symptoms in DOC (e.g., reduced arousal, reduced ability to respond to commands) (Lutkenhoff et al., 2015) as well as future recovery (Lutkenhoff et al., 2013; Lutkenhoff, Wright, et al., 2020) while DOC symptoms are further predicted by thalamocortical functional (Crone et al., 2014; Laureys et al., 2000; Zhou et al., 2011) and structural (Zheng et al., 2017) connectivity as well as disturbances in intrathalamic network properties (Crone et al., 2014).

What remains unclear is the precise relationship between thalamic damage and DOC: 1) Does thalamic damage indeed cause DOC symptoms? 2). What specific symptoms of DOC does thalamic damage explain—i.e., arousal, cognitive functioning, motor output? 3) Is stimulation of thalamic output capable of improving symptoms in (all) DOC patients? Indeed, stimulation of the central thalamus has famously been shown to improve symptoms in one DOC patient (Schiff, 2010a), who displayed improvements in both areas of arousal as well as the complex motor responsivity associated with cognitive functioning. However, many mysteries remain. What is the mechanism by which this subject regained function and, given that follow-up case studies

demonstrated no improvement(Magrassi et al., 2016), why did this subject respond particularly well to thalamic stimulation and why? In order to make sense of these findings, tailor future treatments to individual subjects, and investigate new methods for subcortical stimulation in DOC, we must better understand how the thalamus contributes to those qualities lost in DOC: arousal and cognitive functioning.

1.2 Thalamus

It has become clear what the Thalamus is not: it is not the passive sensory relay system it was once characterized as; recent multimodal data continues to support the notion that the thalamus plays a broad modulatory role on cortical functioning. What remains unclear is what precise mechanisms underlie thalamic influence in cognition and, by extension, what mechanisms underlie pathologies associated with damage to the thalamus. Like the symptoms of DOC, thalamic function can arguably be broken down into two constructs: arousal and cognitive functioning.

1.2.1 Arousal and Cognitive Functioning?

Since the formation of the Yerkes Dodson law in 1908 (Yerkes & Dodson, 1908), an interaction between arousal and cognitive functioning has been apparent. As pointed out by Koch and Crick(Crick & Koch, 1995), arousal is necessary for cognition but not sufficient for it. The interaction of these two constructions complicates our understanding of the DOC pathology as damage in one area may impede both arousal and cognitive functioning by only impacting the arousal observed in other functionally connected regions that are the true computational engines of cognition. This is particularly apparent when considering the thalamus because of its clear role in both constructs.

1.2.2 Thalamic Anatomy

The thalamus is well-positioned by its anatomy in the regulation of both cognitive functioning and arousal. While their proportions may change, all thalamic nuclei contain “core” cells, which have highly localized cortical projections as well as “matrix” cells, which project more diffusely. Respectively, these may facilitate the sensory relay functions of the thalamus as well as its role in broad cortical modulation in either arousal regulation or cognitive control mechanisms.

Arousal:

The thalamus receives massive inputs from brainstem and basal forebrain arousal regulating systems(Saper & Fuller, 2017), suggesting a role in arousal. The intralaminar nuclei (IL) of the central thalamus receive a disproportionate quantity of these inputs while cholinergic and glutamatergic input arriving to the thalamus from the brainstem as well as the basal forebrain(Kolmac & Mitrofanis, 1999; Parvizi & Damasio, 2001; Schiff, 2010a); moreover, the IL receive a bulk of the noradrenergic and serotonergic inputs stemming from the brainstem(Schiff, 2008). Many thalamic nuclei receive the majority of their inputs from cortex. These “higher-order” nuclei tend to project widely throughout the cortex but especially to the large association areas of the frontal and parietal cortices with the IL perhaps projecting most widely. This feature seems obligatory for a region conducting broad arousal modulation.

Moreover, subsets of thalamic neurons known as matrix cells project diffusely within superficial cortical layers and are thus thought to conduct modulatory roles, such as arousal regulation on cortical processing in comparison to the more “sensory relay” roles of more locally-projecting thalamic neurons. Supporting a role in arousal, optogenetic stimulation of these matrix cells within the IL nuclei was able to wake rodents from sleep (Honjoh et al., 2018).

Cognition:

Similar to arousal, the broad projecting nature of thalamic nuclei and of some thalamic cells also allows for thalamic modulation in high-order cognitive functioning. While the general lack of interconnection within the thalamus itself may suggest a limited role for the thalamus in the computations of cognition, the thalamus has been depicted as a “mental blackboard” or the “*conductor of the cortical orchestra*”. Parallel thalamocortical loops that span the breadth of the cortex may gift the thalamus an abstracted, yet privileged and integrated, vista on cortical activity. Thus, it may be privileged in its ability to regulate cortical activity in response to changing cognitive needs. Convergence of signals from virtually all sensory modalities has been suggested to play a role in the binding of modal-specific information (Crick, 1984; Jerath & Beveridge, 2019; Jones, 2009; Ward, 2011) in the thalamus. Some (Ward, 2011) have gone as far as to postulate this convergence onto the thalamus as *the* principle bottleneck through which cortical processing passes before emerging into the integrated and unitary (Edelman & Tononi, 2000) global workspace (Cho et al., 1997) of conscious experience.

Thalamic anatomy also allows for the many mechanisms required of such a cognitive system. For instance, the center-surround architecture seemingly so important for some aspects of visual attention has been proposed to originate, in part, from the center-surround responsivity of the thalamic reticular nucleus and its connections to the pulvinar thalamus (Saalmann & Kastner, 2009). Moreover, the thalamus has long been observed to generate the cortical oscillations thought so important for many aspects of cognition (Buzsáki, 2006) while its physical location may further aid in its use of oscillatory mechanisms; as thalamic tissues are located in the center of the brain and thus roughly equidistant from all points of the cortical mantle, thalamic tissues may be

particularly well-positioned to coordinate the clocking of oscillations in cognition without accounting for variable axon-potential delays between cortical targets(Buzsáki, 2006).

1.2.3 Cognition and The Thalamus

The thalamus is unambiguously involved in cognitive functioning across multiple domains from working memory (Bolkan et al., 2017) to visual attention(Saalman et al., 2012). Disruption of select thalamic nuclei consistently impairs cognitive functioning (Mitchell & Chakraborty, 2013; Pergola et al., 2018) while neuronal activity in the thalamus (e.g., mediodorsal thalamus) appears to play a role in maintaining specific cortical representations over others(Schmitt et al., 2017). Thus, the role of the thalamus in cognition is expansive and goes beyond simply maintaining broad cortical arousal. However, understanding the potential role of the thalamus in arousal and its interaction with cognition is highly important to understanding DOC and its potential treatments.

1.2.4 The Question of Arousal and the Thalamus

The activity and structural integrity of the thalamus and its cortical connections are unambiguously correlated with states of arousal. However, a closer look at the role of the thalamus in arousal suggests that, while it appears to have some role in modulating cerebral arousal, perhaps as it relates to cognitive functioning, it has less to do with transitions in arousal (between normal waking and sleep, anesthesia, DOC) than other structures.

For instance, the firing rate of thalamic neurons decreases in sleep as cells enter a state of rhythmic bursting(Buzsáki, 2006; Steriade & Timofeev, 2003), paralleled by decreased blood flow to the region(Hofle et al., 1997; Kajimura et al., 1999). Like sleep, a principal neural correlate of the loss of consciousness during anesthesia is reduced thalamic activity, assessed via regional metabolism and blood flow in humans(Alkire et al., 2008) while thalamo-cortical connectivity also appears reduced and dynamically altered in anesthesia(Guldenmund et al., 2013; Murphy et al., 2011).

Moreover, central thalamic activity appears correlated with short term fluctuations in arousal. The firing rate of central thalamic neurons increases during the delay period of simple reaction time “vigilance” tasks(Schiff et al., 2012). Activity in the central thalamus has been shown to increase with increasing vigilance during attention tasks using PET(Kinomura et al., 1996) and fMRI(Paus, 2000) over a periods of seconds(Kinomura et al., 1996; Nagai et al., 2004; Naito et al., 2000) to minutes(Paus, 2000). Short term enhancement of activity(Kinomura et al., 1996) as well as gamma power(Schiff et al., 2012) in central thalamic nuclei may reflect task-dependent modulations of cortical arousal.

However, associations between the thalamus and arousal become less compelling when more discriminating methods are employed. For instance, the effect of anesthesia on thalamus appears secondary to reduced cortical activity. Indeed, the transition of thalamic cells into rhythmic bursting as well as their reduced metabolic activity under anesthesia disappears when cortico-thalamic connections are severed(Alkire et al., 2008). Moreover, altered electrophysiological properties of the cortex begin at the moment of lost consciousness under anesthesia while altered thalamic activity trails this by roughly 10 minutes(Alkire et al., 2008). Furthermore, causal modelling of altered network properties in anesthesia support the notion that pallidocortical instead of thalamofugal effective connectivity was related to loss of consciousness under propofol anesthesia(Crone et al., 2017).

Work to separate the arousal and cognitive symptoms of DOC more compellingly implicates extra-thalamic mechanisms of arousal than thalamic ones. While thalamic damage, assessed by MRI, predicts DOC symptoms broadly, it does not appear to predict the arousal sub-score in neuropsychiatric tests of DOC symptoms, rather predicting complex motor-responsivity which is more closely associated with cognitive functioning. Instead, aspects of the globus pallidus have

been associated with the arousal sub-score(Lutkenhoff et al., 2015). Supporting a pallidal arousal mechanism, cell body lesions of globus pallidus pars externa produce increased delta power(Qiu et al., 2010), a classical correlate of low-arousal states such as sleep. While traditional models of basal ganglia connectivity implicate basal-ganglia-thalamo-cortical pathways in mediating pallidal influence on cortex, direct pallido-cortical pathways have recently been identified and associated with the maintenance of electrocortical arousal(Chen et al., 2015; Saunders et al., 2015; Zheng & Monti, 2019). The pallidum may maintain arousal independent of thalamic involvement.

Indeed, cell-body specific ablations of the thalamus suggest, strikingly, that the thalamus may not be necessary for the maintenance of wakefulness at all. Destruction of cell bodies in nearly the entire thalamus has been shown to produce little effect on sleep-wake cycles or on electrophysiological-correlates of arousal(Fuller et al., 2011; Vanderwolf & Stewart, 1988) while elimination of all thalamic afferents to a cortical region again does not lead to the bursting characteristic of sleep and anesthesia(Constantinople & Bruno, 2011). These results stand in stark contrast to the immediate coma-like state caused by similarly vast cell-body lesions created in the basal forebrain(Fuller et al., 2011).

However, stimulation of the central thalamus (emphasizing the central medial (CM), central lateral (CL), and paracentral nucleus (PC)), suggests that the thalamus can modulate arousal states, if it not altogether necessary for maintaining arousal. Famously, a single minimally-conscious DOC patient regained some functioning following deep brain stimulation of the CL nucleus, including in the arousal sub-score(Schiff et al., 2007). Recent work in macaques seem to confirm this effect where electrical CL stimulation can induce wakefulness from sleep and anesthesia(Donoghue et al., 2019; Redinbaugh et al., 2019), producing eye-opening and increasing responsivity. Moreover, cell-body specific stimulation via optogenetics(Honjoh et al., 2018; Liu et al., 2015) and from

chemical(Alkire et al., 2007; Mair et al., 2011) and anti-antibody(Alkire et al., 2009) injections into the CL and CM nuclei (but see discussion of CM specificity in Honjoh et al.(Honjoh et al., 2018)) has produced similar effects.

In sum, it remains clear that thalamic activity is highly related to arousal and can induce arousal when stimulated; yet, it is much less clear that the thalamus maintains the waking state, where brainstem projections to cortex, directly or via the nuclei of the basal forebrain and basal ganglia (e.g., GP, Striatum)(Chen et al., 2015; Crone et al., 2017; Saunders et al., 2015; Zheng & Monti, 2019), may be more relevant to this function.

1.3 Focused Ultrasound Neuromodulation

1.3.1 Background

While routinely used to modulate the cortex non-invasively, more established neuromodulatory techniques such as transcranial magnetic stimulation (TMS) and transcranial electrical stimulation (tES) remain limited in both the domains of spatial precision and the depth of their influence(Bestmann & Walsh, 2017; Deng et al., 2013). Because such non-invasive protocols are unable to selectively target structures below the cortical mantle, reversible neuromodulation of the deep brain has been limited to invasive techniques, such as deep brain stimulation (DBS), which involve the surgical implantation of electrodes and are thus limited to (severe) patient populations. However, the emerging technology of low-intensity focused ultrasound (LIFU) has increasingly been shown to address this gap; indeed, LIFU has demonstrated the capacity to both inhibit as well as excite subcortical tissues safely and reversibly in model organisms (i.e., rats (B.-K. Min, Bystritsky, et al., 2011; B.-K. Min, Yang, et al., 2011; Yang et al., 2012; Yoo, Bystritsky, et al., 2011; Yoo, Kim, et al., 2011), pigs (Dallapiazza et al., 2017), and macaques(Folloni et al., 2019), as well as, recently, healthy human subjects(Legon et al., 2018)) with a spatial precision far

exceeding that of TMS or tES(Bestmann & Walsh, 2017; Bystritsky et al., 2011; Dallapiazza et al., 2017; Deng et al., 2013; Kubanek, 2018) and which may be measured in millimeters instead of centimeters. The promise of precise and reversible subcortical modulation opens many doors to the study of the subcortical components of the DOC pathology. Moreover, the properties of focused ultrasound suggest it may represent a sensible evolutionary step in obtaining subcortical neuromodulation in DOC patients, avoiding, for instance, the risks inherent to DBS—including hemorrhage and infection(Fenoy & Simpson, 2014)—and the non-selectivity of pharmaceuticals thought to impact this system (e.g. zolpidem and amantadine(Schnakers & Monti, 2017)).

1.3.2 Limitations for Use in Basic Research

Despite the promise of LIFU, many mysteries remain which limit its effective use in clinical and research settings. Thus, the field of LIFU, as it stands, contributes great effort not only to its use in basic science but, concurrently, to the betterment of LIFU as a technique. For instance:

1) A great deal of uncertainty surrounds the relationship between the various parameters of LIFU (e.g., fundamental frequency, pulse schemes, intensity) and its effect on neural tissues. A trend has been observed that low duty cycles (the proportion of time LIFU is on for any given time-window) result in inhibitory effects while higher duty cycles can cause excitation(Plaksin et al., 2016). Yet, exceptions have been observed and the valence of LIFU's influence may depend on the targeted tissue(Blackmore et al., 2019). The relationship between LIFU parameters and stimulation valence is further hampered by elusive neuroimaging signatures observed during LIFU. Like in some TMS studies, observation of altered BOLD signal in targeted tissues has been challenging(Ai et al., 2016) and only once observed in subcortical tissues (Cain, Visagan, et al., 2021), impeding the process of attempts to use LIFU as a treatment for DOC.

2) While the theoretical accuracy of LIFU is extremely high, the prediction of skull-refractory effects on the LIFU focal point, both in terms of intensity and in its position, remains difficult without the CT images usually only taken in medical settings. Thus, in research settings, the realized precision of LIFU is greatly diminished. Currently, the most widely accepted method for estimating the effect of skull on LIFU is computational modelling through surrogate CT images or binarized skull masks derived from CT or MRI images (Mueller et al., 2017). However, this process is intensive and likely unrealistic going forward as LIFU becomes more widely used. While skull shape and density are highly important, so too are the many parameters of the LIFU waveform. These have yet to be fully mapped to the attenuation/refraction experienced when LIFU is passed through bone. Such a mapping would greatly reduce the complexity of planning LIFU experiments as well as providing an estimate of these effects prior to the involvement of subjects.

Chapter 2: Establish the presence of fMRI correlates of concurrent (Online) LIFU exposure using two parameter sets in healthy individuals.

Abstract

Deep brain nuclei are integral components of large-scale circuits mediating important cognitive and sensorimotor functions. However, because they fall outside the domain of conventional non-invasive neuromodulatory techniques, their study has been primarily based on neuropsychological models, limiting the ability to fully characterize their role and to develop interventions in cases where they are damaged. To address this gap, we used the emerging technology of non-invasive low-intensity focused ultrasound (LIFU) to directly modulate left lateralized basal ganglia structures in healthy volunteers. During sonication, we observed local and distal decreases in blood oxygenation level dependent (BOLD) signal in the targeted left globus pallidus (GP) and in large-scale cortical networks. We also observed a generalized decrease in relative perfusion throughout the cerebrum following sonication. These results show, for the first time using functional MRI data, the ability to modulate deep-brain nuclei using LIFU while measuring its local and global consequences, opening the door for future applications of subcortical LIFU.

Introduction

While routinely used to modulate the cortex non-invasively, established neuromodulatory techniques such as transcranial magnetic stimulation (TMS) and transcranial electrical stimulation (tES) remain limited in both the domains of spatial precision and the depth of their influence (Bestmann & Walsh, 2017; Deng et al., 2013). Because such non-invasive protocols are unable to selectively target structures below the cortical mantle, reversible neuromodulation of the deep brain has been limited to invasive techniques, such as deep brain stimulation (DBS), which

involve the surgical implantation of electrodes and are thus limited to (severe) patient populations. However, the emerging technology of low-intensity focused ultrasound (LIFU) has increasingly been shown to address this gap; indeed, LIFU has demonstrated the capacity to both inhibit as well as excite subcortical tissues safely and reversibly in model organisms (i.e., rats (B.-K. Min, Bystritsky, et al., 2011; B.-K. Min, Yang, et al., 2011; Yang et al., 2012; Yoo, Bystritsky, et al., 2011; Yoo, Kim, et al., 2011), pigs (Dallapiazza et al., 2017), and macaques (Folloni et al., 2019), as well as, recently, healthy human subjects (Legon et al., 2018)) with a spatial precision far exceeding that of TMS or tES (Bestmann & Walsh, 2017; Bystritsky et al., 2011; Dallapiazza et al., 2017; Deng et al., 2013; Kubanek, 2018).

The ability of LIFU to selectively modulate subcortical tissue non-invasively potentially makes way for causal inferences in the study of subcortical networks as well as the treatment of many neurological conditions. The lentiform nuclei are of particular interest for their role in a cortico-basal ganglia-cortical circuit ostensibly mediating motor refinement, cognitive functioning, and arousal (Lanciego et al., 2012; Schiff, 2010a). Moreover, these structures are relatively accessible to LIFU through the temporal window, the thinnest section of the temporal bone and, thus, the ideal cranial entry-point for minimizing ultrasound attenuation and refraction through skull when utilizing a single-element transducer. Despite the centrality of basal ganglia-cortical circuits to several aspects of human cognition (Lanciego et al., 2012), knowledge of their precise structure and function remains incomplete, yet evolving. Only recently, for instance, has the field begun appreciating the contribution of the lentiform nuclei to maintaining electro-cortical and/or behavioral arousal (Qiu et al., 2016; Yuan et al., 2017), as evidenced by both animal models and human studies, putatively through a recently identified extra-thalamic direct pallido-cortical

pathway(Chen et al., 2015; Saunders et al., 2015; Zheng & Monti, 2019). LIFU thus promises the unprecedented ability of performing causal investigation into the role of these circuits in healthy volunteers. While clinical translation of this technique is already ongoing(Monti et al., 2016) in the context of Disorders of Consciousness(Schiff, 2010a)(DOC) after severe brain injury, pallidal LIFU is likely to be applicable to other conditions such as obsessive-compulsive disorder(Greenberg et al., 2010), Tourette syndrome(Schrock et al., 2015), treatment-resistant depression,(Brunoni et al., 2016) Huntington's disease, and Parkinson's disease.(Agnesi et al., 2013; Edwards et al., 2012)

Here, we administered two sessions of deep-brain LIFU in 16 healthy volunteers. In each session we delivered two 5-minute doses of LIFU aimed at the left globus pallidus. Each dose was administered in 30-second blocks separated by 30-second rest intervals. Given the current uncertainty with respect to how different sonication parameters (e.g., duty cycle, pulse repetition frequency, tone burst duration) relate to local and distal brain modulation, two sonication modes modeled after prior work(B.-K. Min, Yang, et al., 2011; Yang et al., 2012; Yoo, Bystritsky, et al., 2011; Yoo, Kim, et al., 2011) were administered, one per session. Online (during sonication) brain responses to each sonication were assessed with T2*-weighted blood oxygenation level dependent (BOLD) signal. Offline (post- sonication) effects were assessed before and after sonication with perfusion-weighted arterial spin labeling (ASL). The main aims of the work were to assess the online and offline topography (local and global) and valence (i.e., up-/down-modulation) of the brain response to each sonication setting.

Methods

Participants

Participants included 16 healthy individuals (15 male; age = 18–44 years ($M = 25.25$; $SD = 7.78$)). Participants were screened for eligibility, reporting no history of neurological/psychiatric disorder or medical condition that may preclude safe entry into an MR environment. Participants were instructed to have the hair around their left temple below 0.5 inches during LIFU sessions due to the potential of hair to trap air bubbles and attenuate ultrasound. This requirement resulted in a high proportion of males. Participants received \$150 compensation for taking part in the experiment. Written informed consent was obtained from all subjects according to the procedures approved by the UCLA Institutional Review Board. All procedures were performed in accordance with relevant guidelines and regulations.

Experimental Design and MR Image Parameters

All participants underwent three discrete sessions in the 3 Tesla Siemens Prisma Magnetic Resonance Imaging (MRI) scanner at the Staglin IMHRO Center for Cognitive Neuroscience at UCLA. During **session 1**) baseline structural and functional BOLD data was collected. This included a T1-weighted structural sequence (MPRAGE, $TR = 2000$ ms, $TE = 2.52$ ms, voxel size 1 mm^3), T2-weighted structural sequence ($TR = 1500$ ms, $TE = 104$ ms, voxel size 1 mm^3), a baseline arterial spin labeling image ($TR = 4.6$ ms, $TE = 16.18$ ms, 8 sequential slices, voxel size 1 mm^3 ; inversion time = 1990ms, tag-controlled pulsed ASL (PASL), bolus duration = 700ms), a baseline functional image (T2*- weighted Gradient Recall Echo sequence, $TR = 700$ ms, $TE = 33$ ms, 1000 interleaved slices, voxel size 1 mm^3), and a white-matter nulled T1-weighted image used to better capture the fine structure of subcortical nuclei. During **sessions 2 and 3**) LIFU was applied. Firstly, a T1-weighted MPRAGE sequence (see parameters above) was captured followed by transducer placement. ASL data was collected immediately following transducer placement (see parameters above). Sonication was administered in 30-second blocks for 10-minutes while

functional BOLD data (see parameters above) were collected. ASL data were again collected immediately post-sonication while another sonication was administered during the collection of BOLD data (see parameters above) immediately thereafter for a total of 2, 10-minute rounds of sonication delivered in 30 second blocks or 10-minutes of sonication total. Following Sonication 2, ASL data were again collected. Sonication parameters were always held constant within sessions but differed between Mode 1 and Mode 2 for each participant between sessions, order counterbalanced between participants.

Ultrasound Positioning

During sessions 2 and 3, the ultrasound transducer was positioned so that its center lay on the left temple (approximately 1/3 of the distance from the corner of the left eye to the left tragus for each participant and superior 2cm). Ultrasound gel (aquasonic) was firstly applied to this region in an area subsuming the diameter of the transducer and rubbed into any hair present so that no hair permeated the gel layer in order to minimize air bubbles and ensure a smooth surface for coupling. A thin layer of gel was applied to the surface of the transducer and bubbles were similarly smoothed from this layer. The transducer was then coupled to the head with gel filling any concavity between the transducer membrane and the scalp. Two straps—one horizontal and one vertical—secured the device to the participant. Next, we acquired a rapid (95 s) T1-weighted structural sequence (TR = 1900 ms, TE = 2.2 ms, voxel size 2 mm³). Using a circular MR fiducial and the visible center of the transducer, reference lines were drawn using the scanner console in the transverse and coronal planes to locate the target of the LIFU beam visually in three dimensions. Adjustments to the positioning were made iteratively until the trajectory of our ultrasound beam passed through the temporal bone, through the anterior dorsal aspect of the left globus pallidus transversely as well as coronally and terminating into the left thalamus. This

portion of the GP was chosen for its apparent direct structural connectivity with frontal cortex(Zheng & Monti, 2019) and our interest in the role of GP in cognitive functioning. The dimensions of the -3 decibel focus of our transducer when measured in water (see Figure 2-1) and simulated through bone (see Figure 2-2), as well as the orientation of the ultrasound beam, suggests that this targeting ensures the beam consistently subsumes aspects of the left GP, with the adjacent left putamen and left thalamus also likely impacted directly by LIFU.

Ultrasound Waveform

A BXPulsar 1001, Brainsonix Inc. ultrasound device was used in two modes. While both modes employ a 650kHz carrier wave, the distinction between them is a high PRF (100 Hz) with low Pulse Width (0.5ms) for Mode 1 and a low PRF (10Hz) with high Pulse Width (5ms) for Mode 2. Pulsation was administered in 2, 10-minute sessions on each of 2 different days and thus in 4, 10-minute sessions total. Within each 10-minute session, pulsation alternated between 30s of LIFU and 30s of no-LIFU for a total of 10, 30s trains of pulsation per sonication (5-minutes of LIFU total per 10-minute session) - a standard block design amenable to BOLD MRI. For both modes, Duty Cycle = 5%, $I_{spta.3} = 720 \text{ mW/cm}^2$; $I_{sppa.3} = 14.40 \text{ W/cm}^2$ (see Figure 2-1). This intensity falls under the safety guidelines for ultrasound imaging of the cranium provided by the FDA(Duck, 2007).

Ultrasound Simulation

We simulated the propagation of the ultrasound waveform through a human skull using acoustic wave equations implemented in MATLAB using k-Wave (v1.1)(Treeby & Cox, 2010), a k-space pseudospectral solver toolbox. We applied these equations to computational head models derived from imaging data from the Visible Human Project®(Spitzer & Whitlock, 1998), provided courtesy of the U.S. National Library of Medicine. Specifically, we used the head CT (dimensions

: 512 x 512 x 512 voxels) and its paired T1-weighted MRI (dimensions : 196 x 231 x 67 voxels) data from the Visible Human® Male (VHM) dataset (Spitzer & Whitlock, 1998). The VHM MRI data were aligned to the VHM CT using FSL's FLIRT program (6DOF model) and resampled to the voxel grid of the CT data. We manually defined a target beam trajectory through the temporal bone and into the left pallidum on a reference MRI brain atlas (MNI152, 1mm). This enabled improved identification of relevant anatomy for landmark selection as compared to the visible human® dataset's male MRI, which is of relatively low resolution. The trajectory was defined by selecting two anatomical points in the MNI152 atlas: 1) a target point in the anterodorsal pallidum, at which the ultrasound was aimed from the left side of the head; and 2) a point denoting the center of the transducer's face outside the head at the point of contact with the skin. Care was taken to ensure the transducer's membrane was flush with the skull, as was the case in our experimental setting. We registered the MNI152 atlas to the transformed VHM MRI data using FLIRT (12 DOF model), and used this transform to map the target and transducer points to the space of the VHM CT data.

Head models were derived from the CT data as follows. We first resampled the CT data into a 512x512x512 volume with isotropic voxels (0.489mm x 0.489mm x 0.489mm) using trilinear interpolation. This defined the simulation grid, whose dimensions enabled us to take advantage of the speed offered by the Fast Fourier Transform used in k-Wave's Fourier collocation method when calculating spatial gradients. We generated three 3D arrays based on the CT scan that modeled the 1) density, 2) speed of sound, and 3) nonlinearities of the varying materials (e.g., scalp, skull, brain) at each position in the grid. These values were derived using mappings of CT intensity,

based on Hounsfield unit values, to corresponding values for medium density, speed of sound, and absorption using the porosity method, as performed by Legon et al.(Legon et al., 2018)

These rectilinear grids were then used to simulate LIFUP from a fixed simulated transducer on the subject's head. We modeled a 72mm diameter single-element transducer positioned in the grid based on the transformed transducer point. We defined a focal point tracing forward 55 mm (the length of our transducer's focal depth from its membrane) along the line from the transducer point to the pallidal target point. Wave propagation from the transducer converging toward this focal point was simulated in the grid. We modeled the pressure wave emitted from the transducer as a three-dimensional sinusoidal wave using parameters obtained from water tank experiments (Acetera), specifically including a pressure at the face of the transducer of 1.0558 MPa and a carrier frequency of 650kHz. We simulated the propagation of this pressure wave from the transducer by solving coupled 1st-order nonlinear differential equations on the rectilinear grids of values representing density and speed of sound. The combination of these equations yields the generalized form of the Westervelt equation(Wise & Treeby, 2013). We solved this system of equations using k-Wave(Treeby & Cox, 2010). The maximal pressure and particle velocity values encountered at every voxel over time in the rectilinear grid simulation domain were recorded for analysis.

This scheme was simulated for a length of time corresponding to one pulse of the mode 2 parameter set used here (see ultrasound waveform for a complete description of parameter sets). In the mode 2 (10Hz Pulse Repetition Frequency) scheme, our pulse is on for 0.005 seconds and off for 0.095 seconds (0.1 seconds Pulse Period for a duty cycle of 5%). We thus simulated a duration of 0.005 seconds, or 3250 cycles at 650kHz (Carrier Frequency). We performed the simulation twice, first

using the CT-derived head model and then using a free-water model, applying the same trajectory in both cases. For each simulation, the peak intensity inside the brain (the majority of energy deposition is in the skull when it is present) as well as its voxel coordinate were captured. We calculated the distance between the simulated point of highest intensity in free water and through bone in order to capture the degree of refraction expected to occur due to propagation through skull. Similarly, the peak intensity in both free-water and CT simulations were compared in order to quantify the degree of peak pressure attenuation expected due to skull. The cumulative energy deposition over time was calculated for the voxel of peak intensity for the through-skull simulation. Energy deposition over time was highly linear, suggesting that the shorter pulse width used here, 0.5ms, in terms of energy deposition, behaves the same as the longer pulse (see Figure 2-S8) and that the results presented generalize to both pulse widths.

BOLD Data Analysis

fMRI as well as ASL preprocessing and analysis was conducted using FSL (FMRIB Software Library v6.0.1)(Jenkinson et al., 2012) with in-house Bash shell scripts. In addition, second level data analysis was performed using JASP. JASP Team (2019). JASP (Version 0.11.1).

Preprocessing

Prior to analysis, preprocessing was performed including brain extraction (optibet(Lutkenhoff et al., 2014)), spatial smoothing (using a Gaussian kernel of 5 mm full-width half-max), slice timing correction (Fourier-space time-series phase-shifting), highpass temporal filtering (Gaussian-weighted) at .01 Hz, and motion correction (MCFLIRT)(Jenkinson et al., 2002, 2012). None of the collected BOLD data exhibited motion greater than 3 mm translation or 3 degrees of rotation. Registration from functional to structural space for each subject was performed using FSL's Boundary-Based Registration (BBR)(Greve & Fischl, 2009), with the exception of two subjects

for which this failed; functional to structural space registrations for these subjects were performed using FSL FLIRT(Jenkinson et al., 2002, 2012) (Normal Search 12 DOF). Registration of functional to standard space for each run was performed using FSL FLIRT(Jenkinson et al., 2002, 2012) (Normal Search 12 DOF) and FSL's nonlinear registration tool, FSL FNIRT(Jenkinson et al., 2012) (Warp resolution of 10 mm). Registration from structural to functional space as well as functional to standard space was confirmed visually for each run.

BOLD – Whole Brain:

LIFU-BOLD data sequences were first analyzed employing a univariate general linear model (GLM) approach(Monti, 2011) including a pre-whitening correction for autocorrelation (FILM). For each LIFU-BOLD sequence for each participant, a univariate analysis was conducted using a single “task” regressor—onset time of 30s blocks of LIFU administration; moreover, 24 extended motion regressors were employed, including motion in 6 directions as well as first derivatives, second derivatives, and their difference. Thus, here, “baseline” refers to inter-sonication periods where no LIFU is applied. For each BOLD sequence, we computed 2 contrasts: LIFU > no LIFU and LIFU < no LIFU. Data from LIFU Mode 1 and data from LIFU Mode 2 were aggregated respectively and assessed statistically using a mixed effects FLAME 1 + 2 model. At level 2, these results were aggregated between runs of the same LIFU parameter set while the following contrasts were calculated on a per-subject basis: Mean LIFU Mode 1, Mean LIFU Mode 2, LIFU Mode 1 – LIFU Mode 2, LIFU Mode 2 – LIFU Mode 1, LIFU Mode 1 + LIFU Mode 2. At level 3, data were aggregated between subjects. Data were cluster corrected for multiple comparisons using a cluster-level threshold of $z > 3.09$ (corrected $p < .05$). A separate level 3 analysis was conducted with cluster correction at $z > 2.57$ (corrected $p < .05$).

BOLD – ROI:

Based on the trajectory of our ultrasound beam, three subcortical ROI's (Left Putamen, Left Globus Pallidus and the Left Thalamus) were selected to determine if FUS modulated the BOLD signal in targeted regions and/or in adjacent regions. For each subject, masks for each region were created by using FSL's automatic segmentation for subcortical nuclei (FIRST)(Jenkinson et al., 2012) for subcortical extraction on high resolution T1 images. Each subcortical ROI was binarized and confirmed for correct extraction visually. For each statistical z-score map produced in the GLM contrast of no LIFU blocks (see Block Design above) with LIFU blocks (LIFU > no LIFU), voxel-wise z-scores were averaged inside the area of each ROI using FSL's tool for extracting the mean selected voxels in a 3D image (fslmeants)(Jenkinson et al., 2012). Registration via FSL's linear registration tool (FLIRT(Jenkinson et al., 2002, 2012), Normal search, 12 DOF) of each z-score map to structural masks was confirmed visually. This leaves us with one number denoting the z-scored difference in BOLD between LIFU-on and baseline (LIFU-off) within each ROI for each LIFU run for each subject.

A 2 x 2 x 3 repeated measures ANOVA was performed with Parameter Set (Mode 1 or Mode 2), Run (Sonication 1 or Sonication 2 within session), and ROI (Left Putamen, Left GP, Left Thalamus) as factors. Follow-up 2 x 2 repeated measures ANOVAs were performed for each ROI with Parameter Set (Mode 1 or Mode 2), Run (Sonication 1 or Sonication 2 within session) as factors. In each of these follow-up ANOVAs, marginal means were computed for each parameter set and statistically assessed against zero in order to assess if an influence from each parameter set existed irrespective of the other. Šidák correction was used to correct for multiple comparisons across marginal mean test. Mauchly's test of sphericity was found to not have been violated. The Shapiro Wilk test confirmed normality in the data. Several outliers existed in this data. A separate

analysis was conducted with outliers excluded; this did not change results and so outliers were left in the data presented here.

In addition to frequentist testing, a 2 x 2 x 3 Bayesian repeated measures ANOVA was performed with Parameter Set, Run (Sonication 1 or Sonication 2 within session), and ROI (Left Putamen, Left GP, Left Thalamus) as factors. For all Bayesian t-tests employed throughout this study, a Cauchy distribution with a width parameter of 0.707 was used while, for all Bayesian ANOVAs, a r scale prior width of 0.5 was used; see JASP documentation for a discussion of Markov chain Monte Carlo (MCMC) settings, which are determined in a black-box manner by the JASP program. Follow-up 2 x 2 Bayesian repeated measures ANOVAs were also performed for each ROI. Bayes factors (BF) reported reflect the ratio of evidence for each alternative hypothesis (H1) against the null hypothesis(H0). A BF_{10} indicates the Bayes factor in favor of H1 over H0. A $BF_{10} > 3$ is widely considered as positive and substantial evidence for the alternative hypothesis(Kass & Raftery, 1995). $BF_{Included}$ denotes the evidence in support of the inclusion of effects (e.g., interaction terms) in the model over and above that of other terms. In order to estimate BF for marginal means, a separate analysis was performed in which runs were averaged. Bayesian one-sample one-sided t tests were conducted for each parameter for each ROI against zero in which the alternative hypothesis stated the data was below zero. Statistical analysis was performed in JASP.

Connectivity Psychophysiological Interaction (PPI):

Psychophysiological analysis was conducted to determine which, if any, regions of the whole brain changed their connectivity with the left globus pallidus during 30s blocks of sonication as compared to non-sonication blocks. The same masks used for the BOLD ROI analyses (see Block

Design BOLD ROI) were used here. This was done for data from each BOLD sequence (4 per subject) using FSL's tool for extracting the time points of selected voxels in a 4D image (fslmeants)(Jenkinson et al., 2012). Using FSL FEAT, each LIFU-BOLD data sequence was first analyzed employing a multivariate general linear model (GLM) approach including our block design, the time series of the ROI, and importantly, their interaction. Finally, lower-level results from each LIFU mode were aggregated respectively using a mixed effects FLAME 1 + 2 model. Aggregated data were regressed on subject of origin. Data were cluster-corrected for multiple comparisons using a cluster-level threshold of $z > 3.09$ (corrected $p < 0.05$), as well as, in a separate third level analysis, $z > 2.57$ (corrected $p < 0.05$).

Arterial Spin Labeling (ASL)

ASL – Whole Brain

In order to quantify the degree of blood perfusion throughout the brain at three time points for each subject visit—pre LIFU 1, post LIFU 1, and post LIFU 2—each ASL sequence was analyzed using standard processing methods in FSL Bayesian Inference for Arterial Spin Labeling MRI(Chappell et al., 2009) (BASIL), using the command-line tool `oxford_asl`. Analysis was set to conform to the assumptions concerning the kinetic model and T1 values outlined in the BASIL white paper(Chappell et al., 2009). The standard T1 value of atrial blood (T1b) was used (1.65). The inversion efficiency of pASL was set at 0.98. Estimation of bolus duration was disabled and supplied at 700ms. Spatial regularization(Groves et al., 2009) as well as motion correction(Jenkinson et al., 2002, 2012) was used while artifact correction for ASL signal within the microvasculature was disabled . The resultant perfusion images were registered to standard space; the quality of these registrations was confirmed visually. At level 2, two linear and two “L” models were applied to the three estimates of perfusion derived from level one, for each mode

(10Hz vs 100Hz) and for each subject. One linear model described a descending trend in blood perfusion through the session (1 0 -1) while the other, an ascending trend (-1 0 1). One “L” model described a descending trend in blood perfusion after LIFU 1 but decreasing no further (1 -.5 -.5) while the other, an ascending trend after LIFU 1 but then increasing no further (-1 .5 .5). At level 3, data was aggregated within respective modes and across subjects as well as statistically assessed using FSL randomise’s(Winkler et al., 2014) nonparametric permutation t test for voxel-based thresholding. A single-sample two-sided t test was run with threshold free cluster enhancement (TFCE)(S. M. Smith & Nichols, 2009), correcting the resultant *p*-values for multiple comparisons across space.

ASL – ROI

The ROI’s investigated in BOLD were also analyzed using ASL data. These included the Left Putamen, Left Globus Pallidus, and Left Thalamus. The same masks used for the BOLD ROI analyses (see Block Design BOLD ROI) were used here. Each perfusion image was registered to subject structural space using `oxford_asl`. Intensity of perfusion images were averaged inside the area of each ROI using FSL’s tool for extracting the mean selected voxels in a 3D image (`fslmeants`)(Jenkinson et al., 2012) for each perfusion image for each subject (16 images; 3 time points per 2 parameter sets).

The resultant intensity values were run in a 2 by 3 by 3 repeated measures ANOVA was run with Parameter Set (Mode 1 or Mode 2), Time Point (Pre LIFU 1, Post LIFU 1, Post LIFU 2) and ROI (Left Putamen, Left GP, Left Thalamus) as factors. A “Repeated” contrast was run for Time Point, which directly compares Pre LIFU 1 with Post LIFU 1 and Post LIFU 1 with Post LIFU 2. Follow-up 2 x 3, two-way repeated measures ANOVA’s were run for each ROI with Parameter Set (Mode

1 or Mode 2) and Time Point (Pre LIFU 1, Post LIFU 1, Post LIFU 2) as factors. A “Repeated” contrast was run for Time Point, which directly compares Pre LIFU 1 with Post LIFU 1 and Post LIFU 1 with Post LIFU 2 for each of these follow-up tests. Mauchly’s test of sphericity was found to be violated in several of these ANOVAs, thus the Greenhouse-Geisser correction for sphericity was applied to these. The Shapiro Wilk test confirmed normality in the data. No outliers were found in these data.

In addition to frequentist testing, a 2 by 3 by 3 Bayesian repeated measures ANOVA was run with Parameter Set (Mode 1 or Mode 2), Time Point (Pre LIFU 1, Post LIFU 1, Post LIFU 2) and ROI (Left Putamen, Left GP, Left Thalamus) as factors. In order to estimate BF for “Repeated” models, a follow-up comparison between Time Points was conducted. Statistical analysis was performed in JASP.

Results

We present the results of this work in three main sections. First, we describe our sonication settings as well as the spatial characteristics of our ultrasound beam when passed through free water (measured empirically) and bone (simulated using k-wave(Treeby & Cox, 2010) in Matlab). Second, we report online local and global effects of LIFU sonication with an ROI analysis of the principal target (left GP) and proximal structures (i.e., left putamen and left thalamus), as well as a full brain analysis of the same BOLD data. Finally, we describe offline effects of LIFU both locally, with an ROI analysis of ASL perfusion data, and globally, with a full-brain analysis of the same perfusion data.

Ultrasound Waveform Through Water and Bone

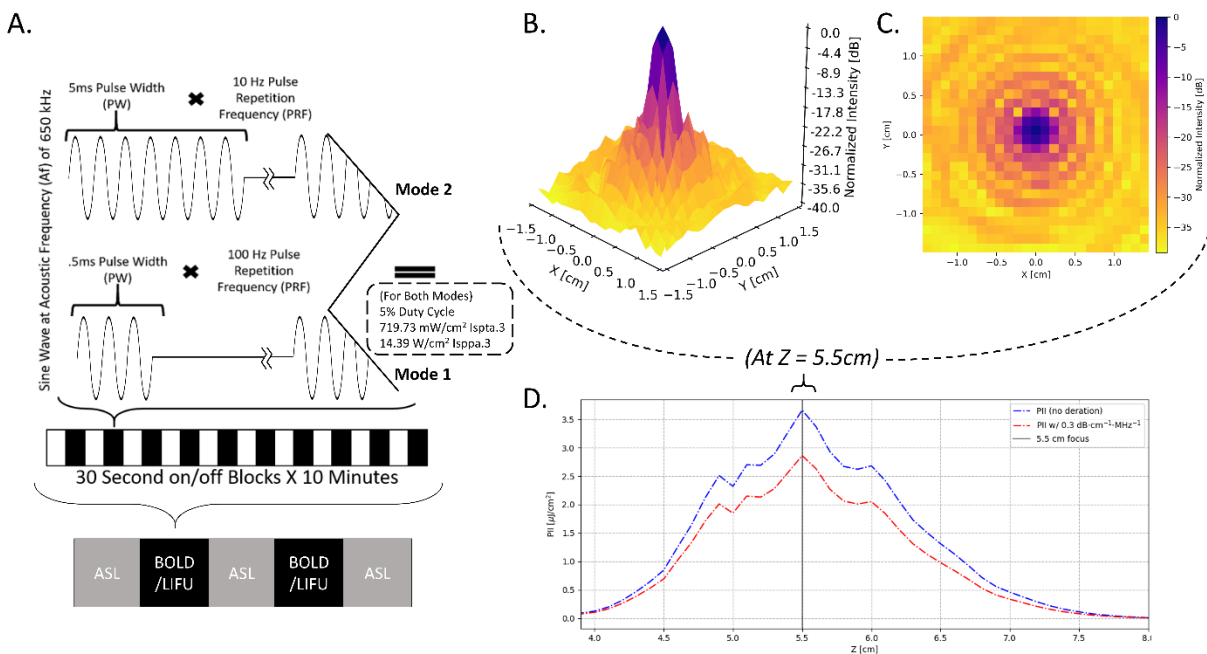


Figure 2-1. Sonication Parameters, Experimental Design, and Water Tank Measurements of Beam Properties. **A)** Parameters for each LIFU mode utilized including pulsing schedule, block design, and intensity. $I_{sppa.3}$ = Spatial Peak Pulse Average Intensity. $I_{spta.3}$ = Spatial Peak Temporal Average Intensity; “.3” denotes deration (attenuated intensity at 0.3 dB/cm-MHz) through human tissue. Here, we have applied LIFU in two sessions, utilizing different parameter sets in each with LIFU Mode 1 having a pulse repetition frequency (PRF) of 100Hz PRF and a pulse width (PW) of 0.5ms PW while LIFU Mode 2 = 10Hz PRF, 5ms PW; all other factors including duty cycle (DC) = 5% and intensity $I_{spta.3}$ (Spatial Peak Temporal Average)(Duck, 2007) = 720 mW/cm² ; $I_{sppa.3}$ (Spatial Peak Pulse Average)(Duck, 2007) = 14.40 W/cm² were held constant. **B,C)** Intensity in the radial plane (X/Y plane, extending from focal point of ultrasound beam 5.5cm from transducer surface) shown in both 3 (**B**) and 2 (**C**) dimensions. A 50% (-3dB) reduction in peak intensity occurs in an area approximately 0.5 cm in width. Note that the decibel scale is nonlinear and -3 dB approximately corresponds to a 50% reduction in intensity; this scale is normalized to

maximal intensity, where peak intensity equals 0dB. **D)** Intensity in the longitudinal plane (Z plane, extending from transducer) in absolute (pulse intensity integral (PII); “.3”denoting absorption in human tissue at 0.3 dB/cm-MHz) values of Z correspond to distance from the transducer surface. Note the peak intensity 5.5 cm from the transducer surface and that a 50% (-3dB) reduction in peak intensity is found in an area approximately 1.5 cm in length.

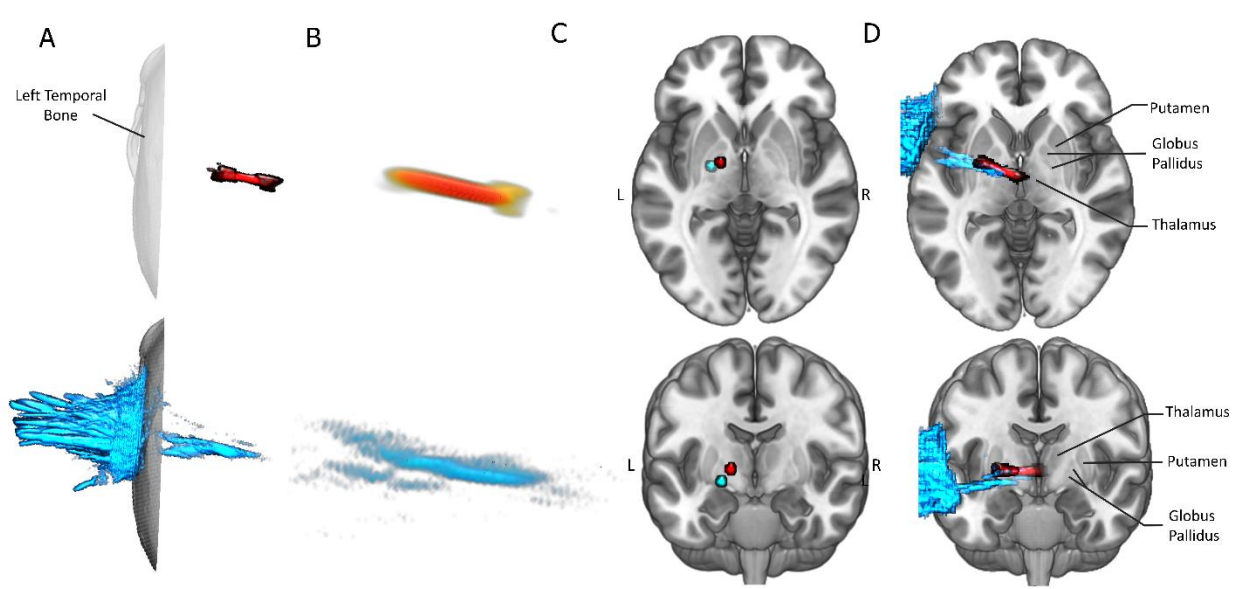


Figure 2-2: Numerical Modeling through Bone and Water. Here, one 5ms pulse (corresponding to 1 pulse of Mode 2) of our ultrasound beam is simulated twice, in water (red), and through the temporal bone of a human computed tomography (CT) image (cyan). The same trajectory, which targets the left GP, was used in both simulations. The maximal pressure for each voxel over the course of the simulation is visualized. Only Voxels exceeding 50% (-3dB) of the maximum in-brain pressure are presented. **A)** Depiction of the effect of bone on beam shape and position. Note that bone (bottom, cyan) appears to flatten, deform, and laterally retract the ultrasound beam

compared to the water condition (top, red). However, the general expression of an elongated beam and its general location is retained. Note that most energy (A bottom) is deposited into and reflected off bone when it is present. **B)** Higher-resolution depiction of ultrasound beam in water (B top) and through bone (B bottom). **C)** Location of maximum pressures following propagation through water (red) and through bone (cyan). Points were mapped into MNI space for visualization. Note that both reside inside the left pallidal target. While the effect of bone moves the peak pressure somewhat ventral and lateral, the total translation is 0.93 cm. **D)** Depiction of whole ultrasound beam through water (cyan) and bone (red). Simulations were mapped into MNI space for visualization. Note that energy deposition into portions of the left lentiform nuclei and left thalamus exceeded the threshold of -50% maximum pressure.

Previous simulations of ultrasound propagation have demonstrated the general maintenance of focal shape and focal location when passing through the human skull, including through the temporal bone (Mueller et al., 2017). To ensure that these results generalize to our LIFU parameters (see Figure 2-1) and our trajectory, we have simulated, in three dimensions, 5ms (equivalent to 1 pulse in LIFU Mode 2) of LIFU propagation at our parameters through the temporal bone of a high-resolution CT (visible human® (Spitzer & Whitlock, 1998)) and into the left GP. Regarding refraction, the point of maximum pressure of this simulation, compared to simulation through water alone, deviated by 0.93 cm, in the range of previous findings (Brinker et al., 2019; Mueller et al., 2017). As depicted in Figure 2-2 C and D, our results suggest that energy deposition remains inside the targeted left GP while not significantly impacting ventral or dorsal structures (e.g., left hippocampus), despite some expected deviation. The thresholded (-50%) pattern of energy deposition subsumes portions of the left thalamus and left putamen, supporting the attention given

here to these structures (Figure 2-2 D, Cyan). Regarding attenuation, skull bone attenuated the energy reaching the brain significantly, as expected, resulting in a peak in-brain pressure 12.35% of that simulated in water alone. It is important to note that the depictions of our ultrasound beam here, for both water and bone simulations, are thresholded at an arbitrary value: (-50%) from maximal in-brain pressure. While the skull deforms and “flattens” the energy deposition to some extent, resulting in a larger area exceeding that -50% threshold (see Figure 2-2 B), an oblong focus of high intensity remains with a degree of refraction (0.93cm) that retains energy deposition into pallidal tissues. Note that cumulative energy deposition over time was recorded at the point of max intensity and is highly linear (see Figure 2-S8), suggesting that these results also generalize to the shorter 0.5ms pulse.

Region of Interest (ROI) Analysis

BOLD – ROI:

We assessed the local influence of sonication during sonication using both parameter sets on BOLD signal as compared to baseline (30 second inter-sonication blocks when no ultrasound is applied). A 2 x 2 x 3 repeated measures ANOVA (as well as its Bayesian equivalent) was performed with Parameter Set (Mode 1 or Mode 2), Run (Sonication 1 or Sonication 2 within session), and ROI (Left Putamen, Left GP, Left Thalamus) as factors; this revealed a significant effect of Parameter, $F(1,15) = 5.442$, $p = .034$, $BF_{\text{Inclusion}} = 78.620$. A significant interaction (in the frequentist but not Bayesian approach) between Parameter Set, Run, and ROI was found $F(1,15) = 9.055$, $p = 8.36e^{-4}$, $BF_{\text{Inclusion}} = 0.647$). Based on this finding as well as our a-priori expectation of regional effects from LIFU (see Discussion), a follow-up two-way ANOVA was performed for each ROI. While no significant effects were found for the Left Putamen, a significant effect of parameter was found in both the Left GP ($F(1,15) = 4.585$, $p = .049$, $BF_{\text{inclusion}} = 2.49$) as well as the Left Thalamu

s $F(1,15) = 5.115$, $p = .039$, $BF_{inclusion} = 1.53$) with reduced BOLD found during sonication in LIFU Mode 1 as compared to LIFU Mode 2 for both ROIs. To assess if either parameter set induced a change in BOLD signal from baseline, marginal means were assessed for each parameter set for each ROI. A reduction in BOLD from baseline during sonication in Mode 1 was found in the Left GP, $t(15) = -2.923$, $p_{\text{Sidak}} = .013$, $BF_{10} = 5.54$, and the Left Thalamus, $t(15) = -2.436$, $p_{\text{Sidak}} = .042$, $BF_{10} = 3.62$. These results suggest that sonication in Mode 1 significantly reduced BOLD signal in the Left GP and the adjacent Left Thalamus when compared to sonication in Mode 2 and when compared to baseline. Sonication in Mode 2, despite its identical intensity and DC of 5% as compared to Mode 1, induced no significant influences on BOLD in these regions.

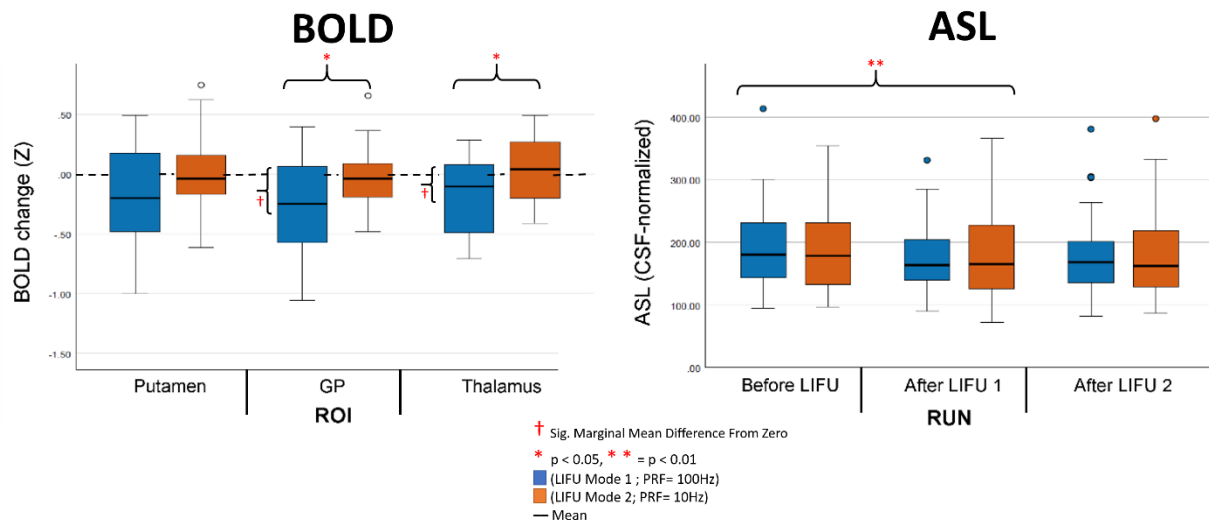


Figure 2-3: ROI analysis results. Left: online changes in BOLD signal during LIFU sonication blocks compared to inter-sonication blocks (i.e., baseline) for the target Left GP ROI and in the proximal Left putamen and Left thalamus ROIs during Mode 1 (blue) and Mode 2 (orange) sonication, compared to baseline (Red crosses indicate a significant difference from baseline for an individual condition while red Asterisks indicate significant difference across conditions).

Right: offline changes in ROI perfusion before LIFU, after sonication 1, and after sonication 2 for each sonication mode (Red Asterisks indicate significant difference across conditions). Whiskers represent 1.5 times the interquartile range above the 75th percentile and below the 25th percentile.

ASL – ROI:

To assess longer-term effects of pallidal LIFU on relative brain perfusion, we performed a three-way repeated measured ANOVA, as well as its Bayesian equivalent, including sonication parameter (Mode 1, Mode 2), time point (Pre LIFU 1, Post LIFU 1, Post LIFU 2) and ROI (Left Putamen, Left GP, Left Thalamus) as factors. As depicted in Figure 2-3, we only observed a main effect of time point ($F_{Greenhouse-Geisser}(1.303, 19.547) = 7.926, p = .007; BF_{Inclusion} = 10.174$). Post-hoc analysis revealed that this effect was driven by a large decrease in perfusion, within the ROIs, following LIFU 1 ($t(15) = 3.231, p_{holm} = .006; BF_{10} = 138.915$), with no additional decrease observed following LIFU 2 ($t(15) = .399, p = .693; BF_{10} = 0.175$). No main effect of sonication parameter was found ($F_{Greenhouse-Geisser}(1,15) = .177, p = .680; BF_{Inclusion} = 0.164$). An interaction between time-point and ROI was also observed ($F_{Greenhouse-Geisser}(2.290, 34.353) = 3.180, p = .048$) albeit with weak support ($BF_{Inclusion} = 0.055$) consistent with the fact that follow-up 2-way repeated measures ANOVAs, one per ROI, generally revealed the same pattern of decreased relative perfusion over time seen in the 3-way analysis.

In the Left Putamen, a main effect of Run was found ($F_{Greenhouse-Geisser}(1.396, 20.102) = 4.873, p = .028; BF_{Inclusion} = 0.824$). Follow up revealed a more linear trend with no significant difference between run 1 and 2 ($t(15) = 2.537, p_{holm} = .074; BF_{10} = 0.654$) or between run 2 and 3, ($t(15) = .840, p_{holm} = .407; BF_{10} = 1.325$). In the Left GP, a main effect of Run was found ($F_{Greenhouse-Geisser}(1.141, 18.739) = 7.543, p = .011; BF_{Inclusion} = 1.719$). Follow up revealed a significant difference

between run 1 and 2 was found 2 ($t(15) = 2.867$, $p_{holm} = .015$; $BF_{10} = 1.159$) with no difference between run 2 and 3 found. In the Left Thalamus, a main effect of Run was found ($F_{Greenhouse-Geisser}(1.629, 21.512) = 7.816$, $p = .004$; $BF_{Inclusion} = 3.707$). Follow up revealed a significant difference between run 1 and 2 ($t(15) = 3.561$, $p_{holm} = .004$; $BF_{10} = 8.242$) with no difference between run 2 and 3 found.

Whole Brain Analysis

BOLD – Whole Brain:

Full-brain analysis of the BOLD response during LIFU sonication revealed several foci of reduced BOLD response during Mode 1 (PRF = 100Hz, PW = 0.5ms; see Figure 2-4). Significant clusters included right and left pre- and post-central gyri, frontal polar cortex, posterior cingulate cortex, and Heschl's Gyrus (see also Table S1). Given the known conservative bias of FSL-FLAME 1+2 (Eklund et al., 2016; Woo et al., 2014) in single-sample t-tests at the employed cluster defining threshold (CDT; equivalent to $p=0.001$; see Figure 2-1A,B in ref 31 (Eklund et al., 2016)), results are shown at two CDT values (Figure 2-4; $p=0.001$, in violet, and $p=0.005$, in blue). At this lower threshold, an additional cluster is visible in the medial frontal cortex and significant clusters expand to subsume portions of the dorsal thalamus. No area of increased BOLD response was observed at either CDT during LIFU Mode 1 sonication. Furthermore, no significant foci of increased or decreased BOLD signal were observed during LIFU Mode 2 (PRF = 10Hz, PW = 5ms) sonication at either CDT.

Direct comparison of the BOLD response under the two stimulation modes revealed no significant differences at a CDT of $p < .001$. When displayed at the lower CDT (Figure 2-4 bottom left),

however, some foci of significant difference were observed in the very foci reported for Mode 1 (pre- and post-central gyri and posterior cingulate cortex/ left dorsal thalamus).

ASL – Whole Brain

Given the ROI result, full-brain relative perfusion images were analyzed by contrasting the average brain perfusion after LIFU (i.e., the average of time-point 2 and time-point 3) to the relative perfusion prior to LIFU (as shown in Figure 2-S4, the results are qualitatively unchanged when the data were analyzed with a linear model [i.e., time-point 3 versus time-point 1]). As shown in Figure 2-4, a nonparametric permutation t-test, corrected for multiple comparisons with threshold-free cluster enhancement, TFCE,(S. M. Smith & Nichols, 2009) revealed broad decrease in perfusion throughout the cerebrum for both LIFU modes. In accordance with our ROI results, no significant difference was found when directly comparing sonication modes, and no increase in perfusion was found for either mode.

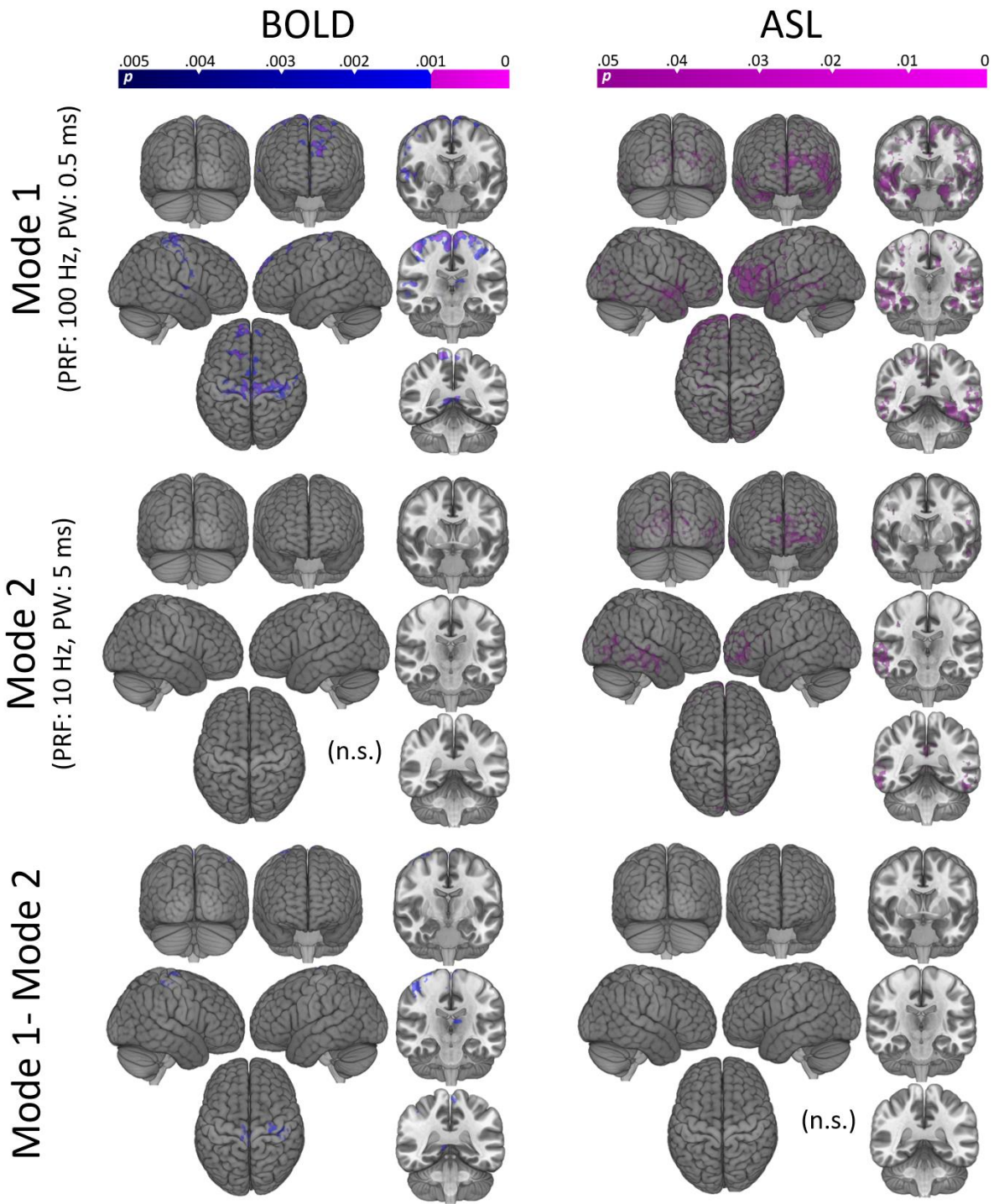


Figure 2-4: Whole brain results. Left: Regions of significant decrease in BOLD signal during sonication Mode 1 (top) and Mode 2 (middle) compared to inter-sonication periods (i.e., baseline). Subtraction of these results are also shown (bottom). Statistical maps were obtained using a mixed effects model (FLAME 1+2) as implemented in FSL(S. M. Smith et al., 2004), and are shown at two levels of cluster correction for multiplicity (CDT set at $p < 0.005$, in blue, and at $p < 0.001$ in violet). Significant reduction in BOLD is found in several cortical regions, at both thresholds, for Mode 1. No regions of increased BOLD signal were observed for Mode 1. No regional increase or decrease was observed for Mode 2. Right: Regions of significant decrease in relative perfusion after sonication in Mode 1 (top) and Mode 2 (middle). Subtraction of these results are also shown (bottom). Statistical maps were obtained with a non-parametric approach (FSL randomise), as implemented in FSL, and are here shown at a level of $p < 0.05$ corrected for multiplicity with threshold free cluster enhancement (TFCE). No significant increase in ASL was observed for either sonication mode.

Discussion

This study is the first demonstration of a group-wide(Ai et al., 2016) MRI response from subcortical focused ultrasound in humans. Taken together, our results suggest that, when targeting the GP and adjacent structures: **1)** LIFU, across two modalities (i.e., BOLD, ASL), in Mode 1 appears neuroactive both during (i.e., online) and after (i.e., offline) sonication. **2)** The valence of online, offline, local, and distal effects all appear inhibitory. **3)** LIFU parameters (PRF and PW) indeed appear to impact the acute effect of LIFU (on the order of 30s, as observed with BOLD), while statistically similar changes in perfusion suggest long-term effects (on the order of minutes, as observed with ASL) may not be as susceptible to these differences, perhaps adding a temporal dimension to the parameter-space of LIFU.

Firstly, we asked if online LIFU could modulate BOLD signal in the target of interest as well as throughout the brain. We found an apparent inhibition of our intended target nuclei, as well as the adjacent left thalamus, during 30-second trains of LIFU in Mode 1 but not in Mode 2 (see Figure 2-3). At the whole-brain level we also found an online inhibitory effect of LIFU in Mode 1, but not Mode 2, within the primary somatomotor cortex, left dorsal thalamus, as well as frontal and posterior cingulate association cortex concurrent with pallidal sonication (see Figure 2-4, Table 2-S1). It remains to be seen if LIFU induces changes in neurovascular coupling irrespective of changes in neural activity; certainly, higher intensity ultrasound may cause vasoconstriction (Pichardo et al., 2006). This could theoretically explain BOLD changes in our targeted structures but is much less relevant to our findings distal to the targeted nuclei. Regardless, the absence of any BOLD response in Mode 2 either locally or distally provides a negative control, suggesting that our results are specific to the parameters employed and argues against the notion that these results stem from artifact (i.e., neurovascular, MRI (Ai et al., 2016), and/or auditory (Sato et al., 2018)) or from inflated type 1 error (Eklund et al., 2016).

While GP connectivity remains elusive, the results presented here demonstrate a plausible pattern of effects. Inhibition of the left pallidum significantly affects all other components of the cortico-basal ganglia-thalamo-cortical circuit underlying motor refinement (Lanciego et al., 2012) and cognitive functioning (Schiff, 2010a), either by way of thalamus as conduit (Schiff, 2010a) or through direct pallido-cortical projections (Chen et al., 2015; Crone et al., 2017; Saunders et al., 2015; Zheng & Monti, 2019). Our BOLD results—primarily found in frontoparietal cortex and thalamic tissues—fit within this framework. Recording activity from both the target of interest and

globally is key to understanding the valence of LIFU's direct influence on neural tissue and the network effects this may bring about. Despite this, direct measurement from targeted subcortical structures is rare in LIFU studies (a notable exception being a recent study in macaques(Folloni et al., 2019)) while it is completely absent in humans until this point, rather being inferred from downstream impacts on cortical activity(Dallapiazza et al., 2017; Legon et al., 2018; Yoo, Kim, et al., 2011). Dual local and distal effects found here bolster the notion that fMRI can be used to effectively understand LIFU and its parameter space in healthy human subjects. On the contrary, only distal effects could have been found, which is often the case in TMS-fMRI(Bestmann & Feredoes, 2013), and which would have severely impaired valence-specific conclusions about LIFU's direct influence. These results, which are based on a the contrast of 30s blocks of LIFU compared to 30s inter-sonication baseline blocks, suggest that the effects of LIFU can vary over a time-course of seconds, despite our own findings in relative perfusion as well as prior results demonstrating sustained influence from LIFU lasting minutes(Yoo, Bystritsky, et al., 2011) or hours(Folloni et al., 2019; Fouragnan et al., 2019; Verhagen et al., 2019). This finding supports the feasibility of classical block designs in future studies and invites investigation of online behavioral impacts from LIFU. Furthermore, our findings of pallidal as well as cortical (most relevantly in the primary somatomotor cortex) effects of pallidal LIFU also mirror the results of studies using contemporaneous neuroimaging and pallidal DBS(Jech, 2008; H.-K. Min et al., 2012), potentially suggesting that this non-invasive technique might be employed in the future to evaluate patient suitability for invasive stimulatory procedures or as a treatment intervention itself.

In addition, we used ASL to characterize the relative longer-term effects of our sonication (i.e., minutes, rather than seconds following cessation). Unlike BOLD, which is derived from more

complex interactions between blood flow and acute neural activity, ASL quantifies cerebral blood perfusion alone. This reduces the inter-subject and inter-trial variability of ASL relative to BOLD(Aguirre et al., 2002), making ASL preferable for detecting disparate neural activity between distant time points. Here, we again found an apparent inhibition (decreased perfusion) of our target nuclei (and the adjacent putamen, thalamus) in the minutes following sonication. Again, this inhibition was extended to the cortex, where decreased perfusion was found throughout the cerebrum (see Figure 2-4). However, here, we find the same pattern of results following sonication in both Mode 1 and Mode 2.

These results corroborate other findings of an offline influence from LIFU(Dallapiazza et al., 2017; Folloni et al., 2019; Fouragnan et al., 2019; Kubanek, 2018; Verhagen et al., 2019). However, the estimated focal intensities used here are approximately an order of magnitude lower than recent studies in pigs(Dallapiazza et al., 2017) and macaques(Folloni et al., 2019; Fouragnan et al., 2019; Verhagen et al., 2019). The time course of LIFU's influence on neural activity remains unclear and appears to vary dramatically between experimental paradigms, ranging from seconds(King et al., 2013) to over an hour(Folloni et al., 2019; Fouragnan et al., 2019; Verhagen et al., 2019) with a trend towards long-term, offline effects occurring following longer sonication periods(Kubanek, 2018). An offline impact may be expected here given that the 10 minutes of total sonication utilized far exceeded the 40 seconds necessary to elicit effects in the tens of minutes to hour range(Folloni et al., 2019; Fouragnan et al., 2019; Verhagen et al., 2019), despite the lower intensities used here. A significant perfusion effect of LIFU in Mode 2 (PRF = 10Hz) here despite null effects on BOLD suggests either the heightened discriminability of ASL compared to BOLD(Aguirre et al., 2002) in this context or that modifying LIFU parameters may impact the time-course of LIFU's

influence. Given the recent offline behavioral effects found in non-human primates(Fouragnan et al., 2019), these results further support investigation into offline behavioral effects in humans at these intensities more comfortably within the range deemed safe for ultrasound imaging of the human cranium(Duck, 2007). A growing consensus surrounding the offline impact of LIFU supports its potential use in clinical applications seeking persistent impacts on neural activity(Bystritsky & Korb, 2015; Monti et al., 2016). However, these early results should be replicated—ASL measures, like BOLD, may be confounded by changes in physiological arousal(J. C. Smith et al., 2010) and its consequences (i.e., blood CO₂ content(Chang & Glover, 2009), and blood pressure(Hajjar Ihab et al., 2010)), as well as any as-yet undiscovered direct impacts of LIFU on neurovascular coupling.

Others have reported differential neuromodulatory effects from LIFU applied at different PRFs when intensity is held constant(King et al., 2013); however, these differences are slight in comparison to alterations of other parameters, such as intensity or duty cycle(King et al., 2013). LIFU parameters such as PRF are likely to interact with duty cycle, intensity, etc. in a high dimensional parameter space that is far from fully characterized, as evidenced by divergent findings between studies despite similar parameters (e.g., apparent disruption(Dallapiazza et al., 2017) as well as excitation(Yoo, Bystritsky, et al., 2011) at PRF = 10Hz with duty cycles near 50%). A possible explanation for these apparent contradictions, it is likely that LIFU modulation may be tissue-type selective. While the mechanisms underlying neuromodulation through LIFU remains debated, principle theories concern an interaction of mechanical pressure on neural tissue and lipid bilayer and/or membrane protein dynamics which brings about depolarization by altering membrane permeability or capacitance(Plaksin et al., 2016; Tyler, 2011). Tissue-specific effects

are thus likely to be driven by differential expression of membrane proteins or the variable membrane dynamics between cell types. For instance, it has been proposed that inhibition through LIFU is achieved through preferential excitation of GABAergic interneurons rather than hyperpolarization of single cells (Plaksin et al., 2014, 2016) and that this is the mechanism underlying a general trend of inhibition during lower duty cycles. While much more work is needed to assess how LIFU interacts with the microstructure of the basal ganglia, these results support the notion of inhibition using low duty cycles, a step towards clinical applications for LIFU in our targeted tissues which absolutely requires valent-specific interventions.

The dimensions of the ultrasound beam produced with our single-element transducer ensure energy deposition into adjacent structures when targeting the GP due to its small size. This, indeed, is a limitation (as discussed below) in the use of LIFU for basic science of the GP alone. However, this may be of benefit to scientific and clinical applications aimed at broader basal-ganglia-thalamo-cortical (Lanciego et al., 2012; Schiff, 2010a) circuits, whose subcortical components are ideally positioned for LIFU modulation through the temporal bone. Apparent inhibition of these circuits' components here, if proved consistent, may make way for clinical use, with an emphasis on the modulation of basal-ganglia-thalamo-cortical (Lanciego et al., 2012; Schiff, 2010a) communication that is presumed to underlie the efficacy of pallidal DBS in treating some individuals with obsessive-compulsive disorder (Greenberg et al., 2010), Tourette syndrome (Schrock et al., 2015), treatment-resistant depression (Brunoni et al., 2016) and movement disorders such as Huntington's disease and Parkinson's disease (Agnesi et al., 2013; Edwards et al., 2012). These results are also highly relevant to the continued study of LIFU's influence in Disorders of Consciousness (Monti et al., 2016) as DOC symptomatology has also

been linked to basal-ganglia-thalamo-cortical communication(Schiff, 2010a) and GP atrophy specifically(Lutkenhoff et al., 2015). The properties of focused ultrasound suggest it may represent a sensible evolutionary step in obtaining subcortical neuromodulation in these applications, avoiding, for instance, the risks inherent to DBS—including hemorrhage and infection(Fenoy & Simpson, 2014)—and the non-selectivity of pharmaceuticals thought to impact this system (e.g. zolpidem and amantadine(Schnakers & Monti, 2017)). These findings represent a pioneering step towards such applications as well as an early foothold for the use of MR-guided LIFU in human neuroscience more broadly.

However, it should be noted that the MR-guided LIFU techniques used here carry with them several important limitations. As it stands, the use of a single-element LIFU transducer for modulation, while highly precise in its influence when compared to TMS, tES, is not perfectly so. A single-element array produces an oblong focus, rather than a highly-focal point of influence, in stark comparison to the more sophisticated multi-unit arrays utilized in neurosurgery(Izadifar et al., 2020). Indeed, both the measured (here, < 0.5 cm wide in the X,Y by 1.5 cm long in the Z plane; threshold at -50% maximum pressure, see Figure 2-1) and modeled (see Figure 2-2) dimensions of our ultrasound beam ensure energy deposition into the adjacent nuclei of the putamen and thalamus as well as the large white-matter tracks that surround them. This inherent limitation complicates the placement of these results into canonical network models; thalamic and striatal function may be influenced both indirectly through modulated pallidal output as well as, to some degree, directly from LIFU itself and vice versa. Moreover, it cannot be ruled out that some or all of the apparent effects here result from modulation of the large white matter tracts nearby and passing through our focus (e.g. the internal capsule), a notion difficult to test with the methods

utilized as BOLD signal is widely considered a less effective correlate of neural activity in white matter (Powers et al., 1985). Proposed mechanisms of LIFU, while controversial as discussed above, are not incongruent with direct modulation of axonal projections (Plaksin et al., 2016; Tyler, 2011).

Another principle limitation in human LIFU research remains the variability in propagation and attenuation introduced by transmission through skull. Corroborating other findings (Legon et al., 2014, 2018; Mueller et al., 2017), numerical modeling performed here through a high-resolution CT image (visible human@ (Spitzer & Whitlock, 1998)) suggests a general preservation of the ultrasound waveform observed in free water (Legon et al., 2018; Mueller et al., 2017). However, the degree of preservation in beam shape is likely to vary between individual sessions due to variable positioning, individual skull morphology and individual skull density (Mueller et al., 2017), the latter of which cannot be readily assessed using MRI at this time. Despite an effect found in the GP as a whole, these limitations prevent assertions concerning which aspect of the GP—Globus Pallidus Pars Externa (GPe) or Pars Interna (GPi)—we preferentially targeted, which is why we chose not to parcellate the structure further. However, as modulation of the GPe and GPi may have vastly different impacts on the circuits in which both participate, future research should investigate related methods that may selectively impact these two nuclei (e.g. multi-unit ultrasound arrays). While animal studies, even in large brained (and thick-skulled) animals (Dallapiazza et al., 2017), suggest the general accuracy of linear targeting and human LIFU studies to date (Lee et al., 2017; Legon et al., 2014, 2018; Sanguinetti et al., 2020) have often elected to forgo per-subject modeling of attenuation and refraction through skull, a fuller, more

subject-specific, investigation of possible skull-refractory effects in naturalistic experimental settings in human subjects remains desirable going forward.

Chapter 3. Establish the feasibility, preliminary efficacy, and neural correlates of thalamic LIFU in acute and chronic patient populations.

Abstract

The promotion of recovery in patients who have entered a disorder of consciousness (DOC; e.g., coma, the vegetative state) following severe brain injury remains an enduring medical challenge despite an ever-growing scientific understanding of these conditions. Indeed, recent work has consistently implicated altered cortical modulation by deep brain structures (e.g., thalamus, basal ganglia) following brain damage in the arising of, and recovery from, DOC. The (re)emergence of low intensity focused ultrasound (LIFU) neuromodulation may provide a means to selectively modulate the activity of deep brain structures noninvasively in the study and treatment of DOC. This technique is unique in its combination of relatively high spatial precision and noninvasive implementation. Given the consistent implication of the thalamus in DOC and prior results inducing behavioral recovery through invasive thalamic stimulation, here we stimulate the central thalamus in 11 acute DOC patients and measure behavioral responsiveness before/after sonication as well as functional MRI during sonication. With respect to behavioral responsiveness, we find significant recovery in the week following thalamic LIFU compared to baseline. With respect to functional imaging, we find decreased BOLD signal in frontal cortex and basal ganglia during LIFU. In addition, we also find a relationship between altered connectivity of the sonicated thalamus and the degree of recovery observed post-LIFU.

Introduction

Despite continued advances in life-sustaining intensive care for severe brain injury patients, little can be done to promote behavioral recovery in patients who fall into a Coma, Vegetative state (VS), or Minimally-Conscious State (MCS) (i.e., disorder of consciousness; DOC)(Schnakers & Monti, 2017). This is despite many recent advancements in the science of DOC(Luppi et al., 2021), including a growing emphasis on the role of deep-brain atrophy (e.g., in the thalamus, basal ganglia) in the impaired arousal and cognitive functioning common in DOC(Schiff, 2010a). Several emerging treatment options, some pharmacological(Schnakers & Monti, 2017) (e.g., Amantadine, Zolpidem) and some neuromodulatory (e.g., transcranial direct current stimulation(Thibaut et al., 2017); tDCS, thalamic deep brain stimulation(Schiff, 2008); DBS) ostensibly improve DOC symptoms by way of indirect (e.g., Zolpidem) or direct (e.g., thalamic DBS) promotion of excitatory thalamic output to cortex and, as a result, more neurotypical activity in cortico-basal ganglia-thalamo-cortical (i.e., mesocircuit) (Schiff, 2010a) and cortico-cortical(Luppi et al., 2019, 2021) networks. To date, neurorestorative interventions are either systemic (e.g., pharmacological) or targeted (i.e., neuromodulatory technologies). With respect to the latter, an important trade-off is between the ability of surgical techniques (e.g., DBS) to target the deep nodes of the mesocircuit, with at times remarkable results(Schiff, 2008), at the cost of being applicable to a small subset of patients (Magrassi et al., 2016) and increased risk (Fenoy & Simpson, 2014), and the safety, ease, and broad applicability of non-invasive techniques (e.g., tDCS), which are however limited to only reaching the cortical nodes of the mesocircuit.

A renewed interest in low intensity focused ultrasound (LIFU) as a method for obtaining spatially precise neuromodulation of deep-brain structures without surgery may address this gap. Several

experiments have now demonstrated the neuroactivity and safety of LIFU in both animal models (Dallapiazza et al., 2017; Yoo, Kim, et al., 2011) as well as healthy human volunteers (Cain, Visagan, et al., 2021; Legon et al., 2018; Xia et al., 2021). In addition, small case reports suggest the potential for this technique in both acute and chronic DOC (Cain, Spivak, et al., 2021; Monti et al., 2016). In what follows, we investigate the impact of magnetic resonance (MR)-guided LIFU applied to the thalamus on brain activity and neurobehavioral measures in a convenience sample of acute DOC patients (n=11). This work is part of the acute arm of a *first-in-man* proof-of-concept clinical trial (NCT02522429). While our results must be considered preliminary, we report below three main findings: (i) significant behavioral improvements following LIFU, (ii) evidence of brain engagement during LIFU stimulation, and (iii) a significant correlation between changes in connectivity of the thalamus targeted with LIFU and subsequent behavioral recovery.

Methods

1. Subjects

Subjects included 11 acute DOC patients (see Table 1 for details). Patients were referred to the study following the persistence of DOC despite administration of routine first-line care at Ronald Reagan Hospital after cessation of any sedation protocol. An initial neurobehavioral evaluation with the JFK Coma Recovery Scale – Revised (CRS-R) (Giacino et al., 2004) was conducted prior to enrollment to confirm eligibility (i.e. a persisting DOC).

Inclusion criteria were as follows:

1. < 6 weeks since injury
2. a Glasgow Coma Score < 9 (at the time of injury)
3. an abnormal CT

4. prolonged loss of consciousness (>24h)
5. behavioral profile consistent with a VS or MCS as assessed with the Coma Recovery Scale Revised.
6. Chronic patients:
7. > 3 months post injury for non-traumatic injuries, >12 months post-injury for traumatic injuries
8. behavioral profile consistent with a VS or MCS as assessed with the Coma Recovery Scale Revised.

Excursion Criteria Were as follows:

1. deep sedation
2. history of neurological illness prior to injury
3. inability to safely enter the MR environment (e.g., ferromagnetic non MR safe implants)

PATIENTS #	AGE	SEX	TSI	ETIOLOGY	INITIAL	FINAL	LIFU #	HEM.
A1	25	M	18d	TBI/MVA	MCS+	MCS+	1	R
A2	23	F	16d	TBI/MVA	MCS-	MCS-	1	R
A3	45	M	5d	TBI	MCS+	EMCS	2	L
A4	72	M	5d	Glioma/Stroke	coma	VS	2	L
A5	75	F	28d	TBI	VS	MCS-	1	L
A6	59	M	17d	TBI	VS	MCS+	1	L
A7	67	M	4m	TBI/MVA	MCS+	MCS+	2	L
A8	22	M	13d	TBI	coma	coma	2	R

A9	31	M	1 m	TBI/MVA	MCS+	MCS+	1	L
A10	53	M	1m	TBI/MVA	MCS+	MCS+	1	L
A11	31	M	24d	TBI/MVA	VS	VS	1	L
C1	56	M	14.5m	Stroke	MCS+	eMCS	2	L
C2	50	F	32m	Anoxia	MCS-	MCS+	2	L
C3	58	M	66m	TBI	MCS+	MCS-	2	L
C4	45	F	20m	Anoxia	VS	VS	2	L
C5	37	M	240m	TBI	MCS-	MCS+	1	L
C6	33	M	24m	TBI	MCS-	MCS+	2	L
C7	30	F	30m	Anoxia	VS	VS	2	L
C8	30	M	39m	TBI	MCS-	MCS-	2	L
C9	26	M	56m	Anoxia/TBI	MCS+	MCS+	2	L
C10	26	F	46m	TBI	MCS+	MCS+	2	R

Table 3-1) Relevant patient-specific information in subjects (Acute denoted by A## and Chronic denoted by C##). TSI = time since injury. TBI = traumatic brain injury. MVA = motor vehicle accident. Initial diagnostic category (e.g., MCS+) is based on the highest performance measured using the CRS-R prior to LIFU exposure. Final diagnostic category is based on the highest performance measured using the CRS-R in the week following the final LIFU exposure (regardless if 1 or 2 sonications were performed). The number of sonications (LIFU #) and the hemisphere of the targeted thalamus (Hem.) is reported.

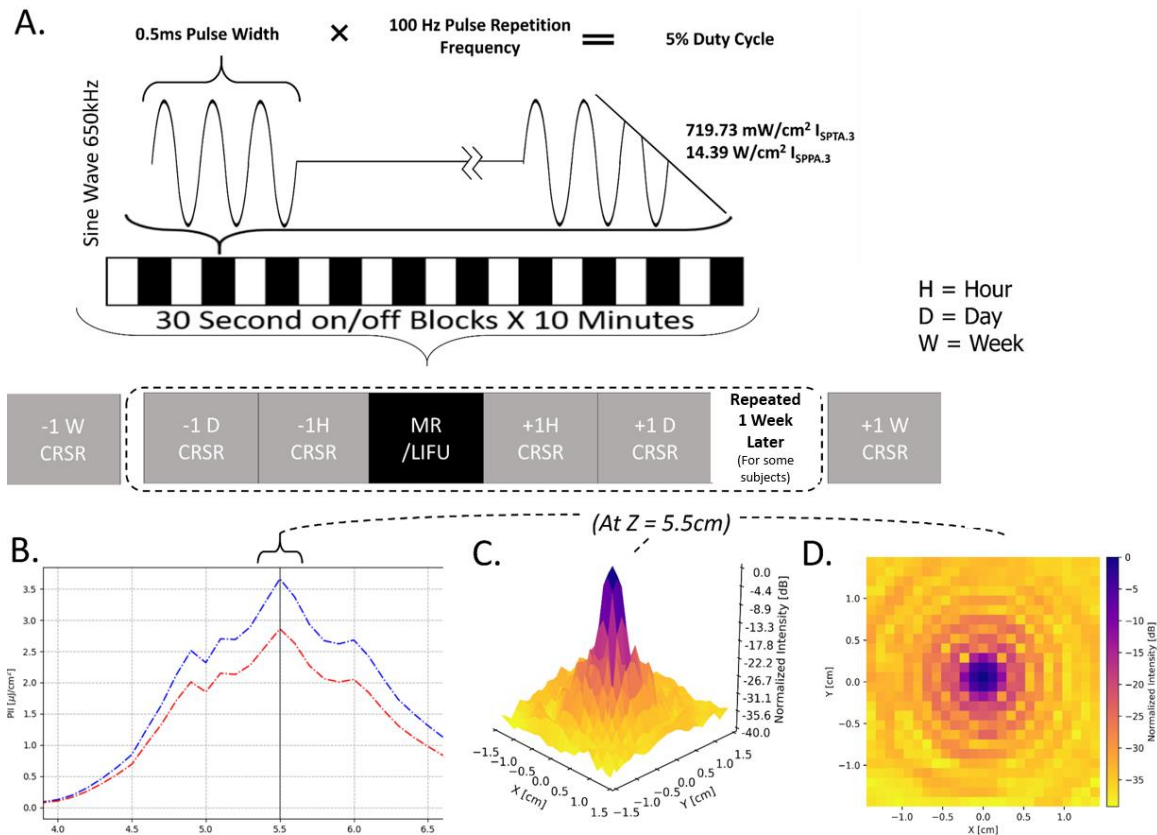


Figure 3-1 Depiction of study protocol involving LIFU parameters and CRS-R (Coma Recovery Scale – Revised) assessments. ISPTA.3 = Spatial Peak Temporal Average Intensity.3. ISPPA.3 = Spatial Peak Pulse Average Intensity.3 (“0.3” denotes deration (attenuation) due to absorption by tissue at 0.3 dB/cm-MHz). **1B**) Intensity in the longitudinal plane (Z plane, extending from transducer) in absolute (pulse intensity integral (PII); “.3”denoting absorption in human tissue at 0.3 dB/cm-MHz) values of Z correspond to distance from the transducer surface. Note the peak intensity 5.5 cm from the transducer surface and that a 50% (– 3 dB) reduction in peak intensity is found in an area approximately 1.5 cm in length. **(1C,1D)** Intensity in the radial plane (X/Y plane, extending from focal point of ultrasound beam 5.5 cm from transducer surface) shown in both 3 **(1C)** and 2 **(1D)** dimensions. A 50% (– 3 dB) reduction in peak

intensity occurs in an area approximately 0.5 cm in width. Note that the decibel scale is nonlinear and -3 dB approximately corresponds to a 50% reduction in intensity; this scale is normalized to maximal intensity, where peak intensity equals 0 dB.

2. Experimental Design

The overall experimental protocol is shown in Figure 3-1A. Briefly, patients underwent two baseline neurobehavioral assessments (at 1 day and 1h prior to LIFU; henceforth, pre-LIFU) followed by a session of MRg-LIFU, and two additional neurobehavioral assessments (at 1h and 1 day following LIFU; henceforth, post-LIFU). While the declared protocol called for a second, identical, cycle neurobehavioral assessments and LIFU, this was only possible for 27% of our acute sample, with the large majority of patients being discharged prior to undergoing the second session of LIFU. However, all but one chronic subject received two LIFU sessions. Finally, a follow-up assessment was conducted 1 week post-LIFU (from the first session, for patients who only underwent one LIFU, or from the second session, for the 3 acute and 9 chronic patients receiving two LIFU sessions).

3. Neurobehavioral Assessments

Neurobehavioral assessments were conducted using the CRS-R (*Giacino et al., 2004*). Baseline responsiveness was assessed 1 day as well as 1 hour prior to LIFU exposure while reresponsiveness following the procedure was assessed 1 hour, 1 day, and 1 week following LIFU exposure. Three subjects, who were in the care of Ronald Reagan hospital for longer periods, underwent the procedure twice, with 1 week separating each LIFU administration.

4. LIFU Sonication Protocol and Procedure

LIFU Sonication Parameters. In each session, LIFU was applied at 100 Hz pulse repetition frequency (PRF), 0.5ms pulse width (PW), 650 kHz carrier wave frequency, 5% duty cycle (DC), and $14.39 \frac{W}{cm^2} I_{SPPA.3} / 719.73 \frac{mW}{cm^2} I_{SPTA.3}$; “.3” denotes tissue absorption at 0.3 dB/cm-MHz. This parameter set (PRF/PW/DC) has been derived from prior work demonstrating its neuroactivity(*Cain, Visagan, et al., 2021; Yoo, Kim, et al., 2011*). Importantly, the energy levels employed in this experiment fall below the FDA limit for diagnostic ultrasound imaging of the human cranium.(*Duck, 2007*) The LIFU waveform was emitted from a single-element transducer (Brainsonix; 71.5mm curvature) positioned, using MR-guidance, such that its theoretical focus (55mm from its surface) lay over the intended target. Once appropriate transducer placement was confirmed visually (see below), ultrasound was delivered inside for a total of ten 30-second on blocks, separated by 30s off periods (see Figure 3-1A).

LIFU Target. In light of the results form DBS applications to DOC(*Magrassi et al., 2016; Schiff, 2008*) and prior theoretical (*Schiff, 2010b*) and empirical (*Lutkenhoff et al., 2015; Lutkenhoff, Johnson, et al., 2020; Yoo, Kim, et al., 2011*)work, the intended LIFU target was the central thalamus. The protocol called for sonication to occur preferentially to the left thalamus, on the basis of prior work documenting a preferential association between atrophy in left thalamus and depth of the disorder of consciousness(*Lutkenhoff et al., 2015; Lutkenhoff, Johnson, et al., 2020*). Nonetheless, flexibility was allowed for patients with left craniectomy, which would result in higher than expected energy deposition into the target tissues, or left cranioplasty, given the unknown penetration and refraction profile of ultrasound through synthetic bone replacement materials. Additional flexibility was excercised in the case of implanted medical devices (e.g., stints, ventricular shunts) position proximally to the intended left hemispheric target and

potentially susceptible to receiving significant energy deposition, thus at risk of creating a potential hazard to the patient. (See Table 3-1 for laterality of LIFU administration in our sample.)

LIFU Procedure. The area around the planned LIFU entry point on the head was shaved prior to positioning in order to minimize the impedance of ultrasound due to air bubbles. Ultrasound gel (aquasonic) was firstly applied to this region and smoothed in order to remove air pockets. The ultrasound transducer was first positioning so that its center lay on the temporal window (the thinnest part of the human skull) in order to minimize ultrasound scatter and refraction through the bone. A thin layer of gel was applied to the surface of the transducer and bubbles were similarly smoothed from this layer. The transducer was then coupled to the head with gel filling any open space between the transducer membrane and the scalp with two straps—one horizontal and one vertical—securing the device to the patient. Conventional soft foam padding and pillows were used to further secure the positioning of the device and decrease the potential for head motion during the procedure. Next, we acquired a rapid (95 s) T1-weighted MPRAGE anatomical image (see 2.6). Using a circular MR fiducial and the visible center of the transducer, reference lines were drawn in the transverse and coronal planes, using the Siemens 3D display GUI available as part of the MRI device’s console software, to locate visually the target of the LIFU beam in three dimensions. Adjustments to the positioning of the transducer on the head were made iteratively, re-acquiring a T1-weighted MPRAGE at each iteration, until the trajectory of the normal from the center of the transducer was assessed to be in-line with the intended target.

5. Behavioral Analysis

Behavioral data analysis was performed using JASP (JASP Team (2019). JASP, Version 0.11.1).

Behavioral responsiveness in patients was assessed using the total score on the CRS-R_{index}(*Annen et al., 2019*), which was calculated from the CRS-R using publically available scripts in R (Rstudio2021; https://github.com/Annen/CRS-R/blob/master/CRS-R_index.R). Prior to analysis, the highest CRS-R_{index} score for each experimental period (i.e., Pre-LIFU 1, Post-LIFU 1, and, for patients who had a second session, Post-LIFU 2) was taken in order to best capture subjects' maximal performance. For patients who had 2 runs (n=3), recovery (POST CRS-R_{index} – PRE CRS-R_{index}) following LIFU 1 and that following LIFU 2 were averaged for inclusion in group-wide statistics. However, behavioral analyses were also performed following the exclusion of run 2 for these subjects. Given that data was found to be non-normal (Shapiro-Wilk), a non-parametric Wilcoxon signed rank test was used to compare Pre-LIFU and Post-LIFU scores for all patients.

6. MRI Sequences and Scanning Procedure

Prior to transducer placement and targetting, a high-resolution T1-weighted MPRAGE (TR = 2.08, TE = 4.14, voxel size = 1x0.5x0.5mm³) was acquired for later processing. Rapid (95 s) T1-weighted structural sequences (TR = 1900 ms, TE = 2.2 ms, voxel size 2 mm³) were used for targetting purposes. Concurrent with LIFU administration, BOLD data was collected with a T2*-weighted Echo Planar Image sequence (TR = 2s, TE = 25ms, voxel size = 3.44x3.44x4.25mm³).

7. MRI Data Analysis: Preprocessing

MRI data preprocessing and analysis was conducted using FSL (FMRIB Software Library v6.0.1)(*Jenkinson et al., 2012*) with in-house Bash shell scripts. In addition, second level data analysis was performed using JASP. JASP Team (2019). JASP (Version 0.11.1).

In order to produce group-level functional results, data from subjects who received LIFU to the right thalamus was flipped such that the right hemisphere became the left hemisphere. This includes structural data for the purpose of co-registration. Next, preprocessing was performed including brain extraction (using optibet (*Lutkenhoff et al., 2014*)), spatial smoothing (using a Gaussian kernel of 5 mm full-width half-max), slice timing correction (Fourier-space time-series phase-shifting), highpass temporal filtering (Gaussian-weighted) at 0.01 Hz, and motion correction (MCFLIRT)(*Jenkinson et al., 2002, 2012*).

Following recent data(*Weiler et al., 2021*), in-scanner head motion was mitigated by including in the statistical model a number of nuisance regressors including individual timepoints with excessive motion (i.e., spike regression (*Weiler et al., 2021*)), 24 head motion parameters, and physiological regressors (for white matter and CSF components). Physiological regressors were produced by segmenting T1 images for each subject using FSL Fast (visually inspected for accuracy). Tissue segmentations for white matter and CSF were moved into functional space (for some subjects, FSL *epi_reg* was employed while some subjects required nonlinear registration using FSL *FNIRT*) and binarized (and again visually inspected for accuracy). Time series for white matter and CSF were then extracted from functional images using *fslmeans*. Framewise displacements for each volume were derived from FSL *MCFLIRT*(*Jenkinson et al., 2002, 2012*) and these were used to exclude unwanted volumes with a framewise displacement exceeding 0.5mm (25% of voxel width). Any functional data not exceeding 4 minutes of total time were excluded (a single functional run, specifically subject 4, run 2) from the rest of data analysis while no subjects were dropped.

In order to register structural images to functional space, we employed a combination of FSL `epi_reg`, which is tailored for coregistration of subcortical regions in particular (including the LIFU target) and conventional 12 dof linear coregistration (using FSL FLIRT). In order to register structural images to standard space, nonlinear registration (FSL FNIRT) was used. For some patients, however, linear registration (FSL FLIRT) resulted in better alignment to the standard MNI template space, as determined by visual inspection conducted prior to analysis.

8. BOLD Data Analysis: Whole Brain Block Design

BOLD data collected during LIFU were first analyzed employing a univariate general linear model (GLM) approach (*Monti, 2011*) including pre-whitening correction for autocorrelation (FILM). A univariate analysis was conducted using a single “task” regressor— which represented the onset time of 30s blocks of LIFU administration. Thus, here, the “baseline” condition used were the inter-sonication periods where no LIFU was applied. For each BOLD sequence, we computed 2 contrasts: LIFU > no LIFU and LIFU < no LIFU and assessed each using a Fixed Effects model given the low sample size. For subjects with two LIFU exposures, results from the two runs were averaged at level two prior to third-level analysis. At the third level, data were cluster corrected for multiple comparisons using a cluster-level threshold of $z > 3.09$ (corrected $p < .05$). A separate level 3 analysis was conducted with cluster correction at $z > 2.57$ (corrected $p < .05$) (*Eklund et al., 2016*).

In order to determine if the degree of LIFU-induced modulation is associated to subsequent neurobehavioral change, an additional regressor was included in the group analysis capturing each subject’s recovery post-LIFU measured using the $CRS-R_{index}$.

9. BOLD Data Analysis: Psychophysiological Interaction

In order to determine whether the connectivity of the targeted thalamus was modulated by LIFU sonication, we performed a psycho-physiological interaction (PPI) analysis, a technique designed to detect changes in connectivity between a seed region and the rest of as a function of the onset and offset of a psychological task (*Friston et al., 1997*). In our design, the task regressor coded the onset and offset periods of the LIFU sonication, thus making it a modulo-physiological interaction. The thalamic seed was obtained by performing subject-specific segmentations obtained from each patient's high-resolution T1-weighted image using FSL FIRST. All segmentations were visually inspected for accuracy prior to conducting the analysis. The time series of thalamic BOLD was extracted from each functional run using *fslmeants*. The MPI was estimated for each subject separately and aggregated at the group level with the same procedure as outline above for the full-brain analysis.

In order to determine if the results of this PPI analysis covaried with behavioral recovery, we included, in the group analysis, a regressor describing each subject's behavioral change post-LIFU as measured using the CRS-R_{index}.

Results Acute

1. Behavioral Analysis

We found a significant increase in maximal responsiveness (i.e., total CRS-R_{index} score) among patients ($p=0.014$; see Figure 3-2) following the LIFUP procedure compare to baseline. The analysis is significant also when repeated on the raw CRS-R total score ($p = 0.014$). The finding was unchanged when analyzing only the data from the first LIFU session for all patients (i.e., when

excluding the data from the second session administered in 4 patients only; $p = 0.009$ and $p = 0.008$ for the CRS-R_{index} and CRS-R total score, respectively). Interestingly, when comparing CRS-R_{index} score immediately prior to and immediately following LIFU administration, no significant change was found ($p=0.820$).

Furthermore, behavioral recovery was found to positively correlate with initial CRS-R_{index} score (Spearman's Rho = 0.651, $p = 0.015$).

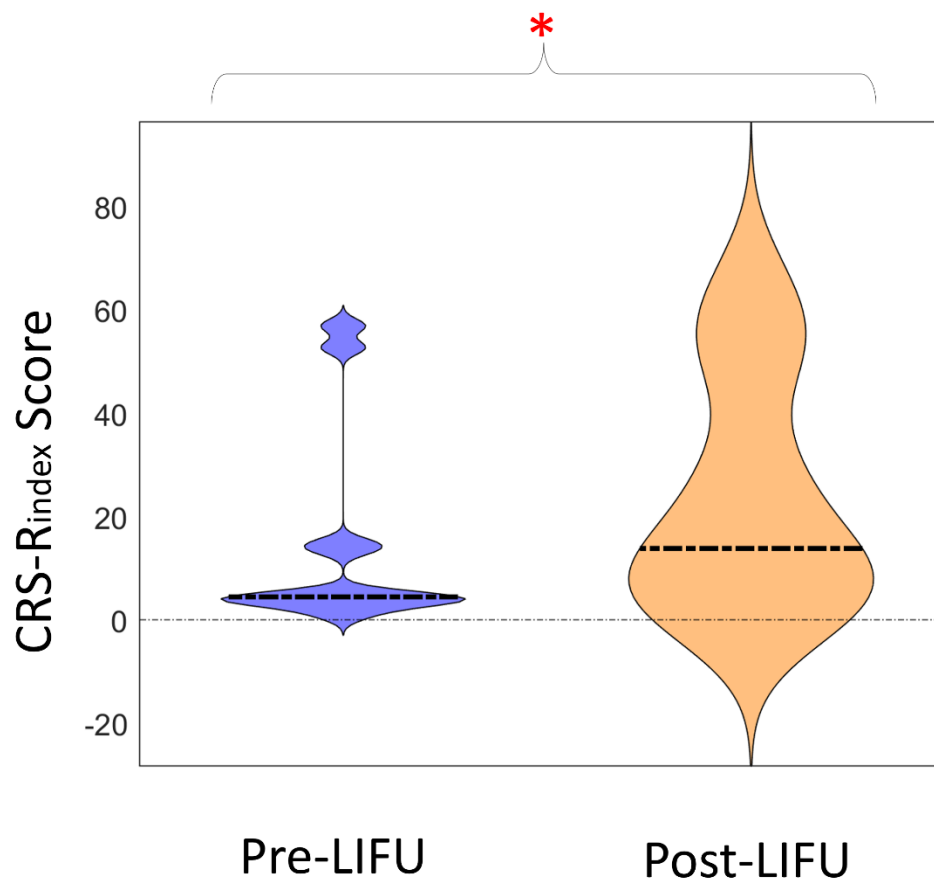


Figure 3-2) Violin plots display the distribution of the highest CRS-R_{index} score prior to and up to 1-week following LIFUP. Dashed lines represent the median data was nonnormal) of each distribution. The red asterisk indicates a significant difference between Pre and Post-LIFU scores.

2. BOLD Data Analysis: Effect of LIFU on Activity

As compared to baseline (i.e., LIFU-off), 30 second of deep brain LIFU sonication resulted in significantly reduced BOLD signal in three anterior clusters (see Figure 3-3a). Specifically, these clusters subsumed portions of the subcallosal prefrontal cortex, anterior cingulate cortex, medial prefrontal cortex and striatum (both caudate and putamen; ipsilateral to the sonication site). None of these activations appeared to correlate with subsequent behavioral recovery (see Figure 3-3b).

3. BOLD Data Analysis: Effect of LIFU on Connectivity

Our psycho-physiological interaction analysis found that, during LIFU sonication, the targeted thalamus increased its connectivity with two clusters—one in the ipsilateral pre and post-central gyrus and one subsuming portions of the contralateral opercular and insular cortex—while decreasing its connectivity with the ipsilateral frontal polar cortex (see Figure 3-3c). When the same analysis was run on the thalamus contralateral to sonication, no significant change in connectivity was observed during LIFU (see Figure 3-3e).

Interestingly, we also found an association between the degree to which thalamic connectivity was modulated during LIFU sonication and subsequent behavioral recovery. Specifically, we found that decreased connectivity between the targeted thalamus and regions in the frontal lobe, spanning bilaterally dorsal and mesial frontal cortices, insula, as well as bilateral subcortical structures was associated with increased behavioral responsiveness following LIFU sonication. Specifically, significant regions included portions of the ipsilateral dorsolateral prefrontal and motor cortex, bilateral striatum, contralateral globus pallidus, contralateral thalamus, the contralateral opercular cortex, the subcallosal frontal cortex, the anterior cingulate cortex, and bilateral orbitofrontal

cortex. Portions of the clusters over the contralateral basal ganglia structures, opercular cortex, amygdala, and anterior cingulate cortex retain significance when using a more conservative CDT of 0.001 and both thresholds are shown in Figure 3-3.

Furthermore, we found that increased connectivity between the targeted thalamus and regions throughout the contralateral motor, parietal, temporal, and occipital cortex was also associated with increased recovery in subjects. Specifically, these regions included portions of the somatomotor cortex, the middle temporal gyrus, the occipital pole, and the precuneus. Portions of the clusters found in the occipital pole and somatomotor cortex retain significance when using a more conservative CDT of 0.001 and both thresholds are shown in Figure 3-3.

When the same analysis was run using the thalamus contralateral to the LIFU sonication as a seed, no significant results were found.

4. Thalamic ROI Effect

An ROI analysis of the targeted thalamus reveals that while the BOLD signal was numerically lower during sonication (as compared to baseline), the change was not statistically significant ($p=0.097$). Nonetheless, the change was significant when compared to the non-targeted thalamus ($p=0.047$).

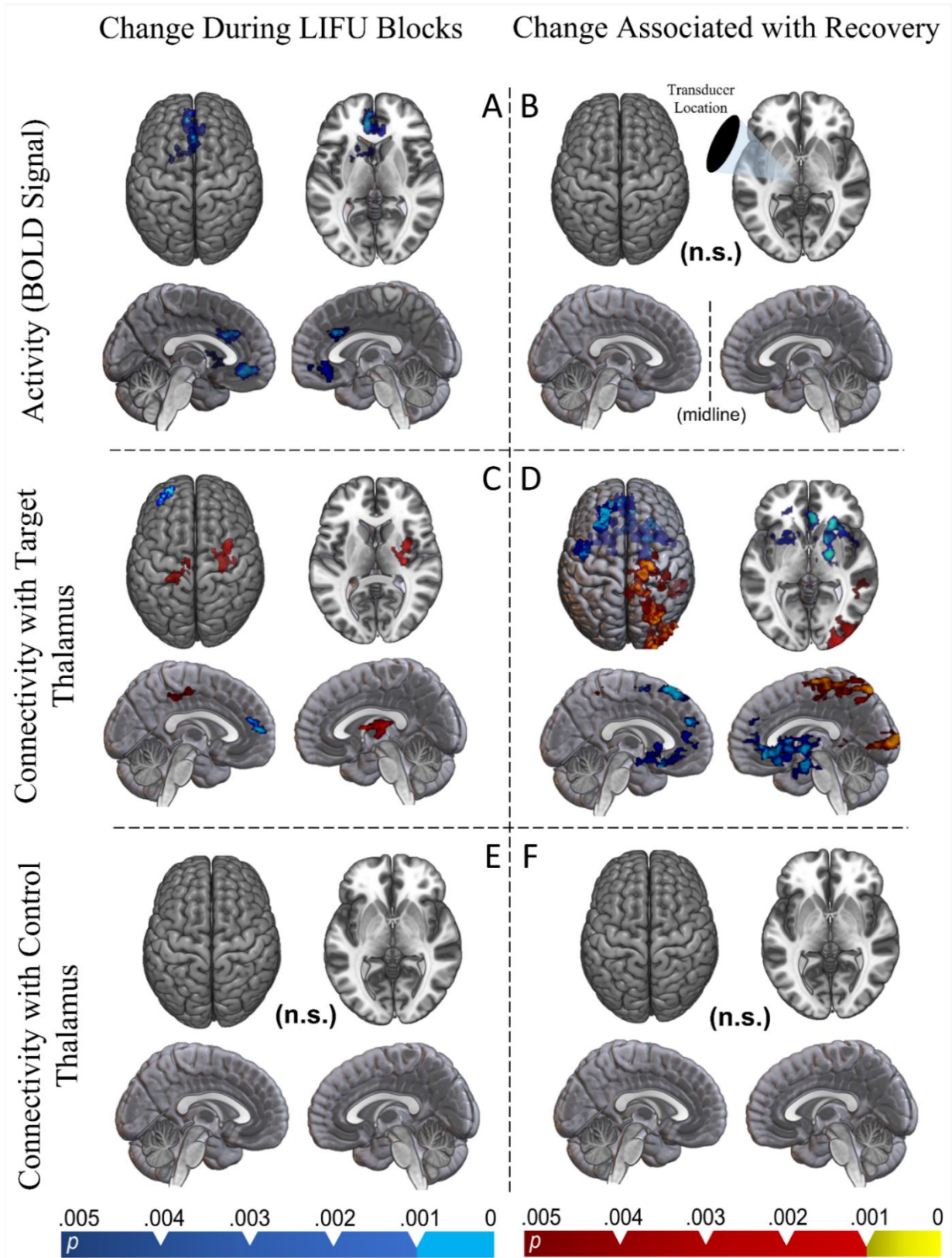


Figure 3-3). Whole brain results. For all analyses, statistical maps were obtained using a fixed

effects model as implemented in FSL6.0.1, and are shown at two levels of cluster correction for multiplicity (CDT set at $p < 0.005$, in blue, and at $p < 0.001$ in violet). Note that sagittal images are shown from the midline and each show one hemisphere. **A)** Regions of significant change in BOLD signal during sonication compared to inter-sonication periods (i.e., baseline). **B)** Regions of significant BOLD change predicted by behavioral recovery. **C)** Connectivity changes observed during LIFU-on blocks compared to LIFU-off blocks (PPI) between the whole brain and the targeted thalamus. **D)** These changes predicted by behavioral recovery. **E)** Connectivity changes observed during LIFU-on blocks compared to LIFU-off blocks (PPI) between the whole brain and the non-targeted (control) thalamus. **F)** These changes predicted by behavioral recovery.

Results Chronic

1. Behavioral Analysis

We observe a significant positive linear trend in maximal responsiveness (total CRS-R_{index} score) among patients (p=0.040; see Figure 3-4) following the LIFU procedure. When taking the CRS-R scores instead, p = 0.019. No correlations were found between recovery (either using the CRS-R or CRS-R_{index} score and age, TSI, or baseline responsiveness). Running the same analysis with CRS_R_{index} (as well as CRS_R) taken immediately prior to and following does not result in a significant linear or “L-Shaped” (a rise in responding following LIFU 1 and then flat performance) trend. Furthermore, no correlations between recovery and baseline responsiveness were found.

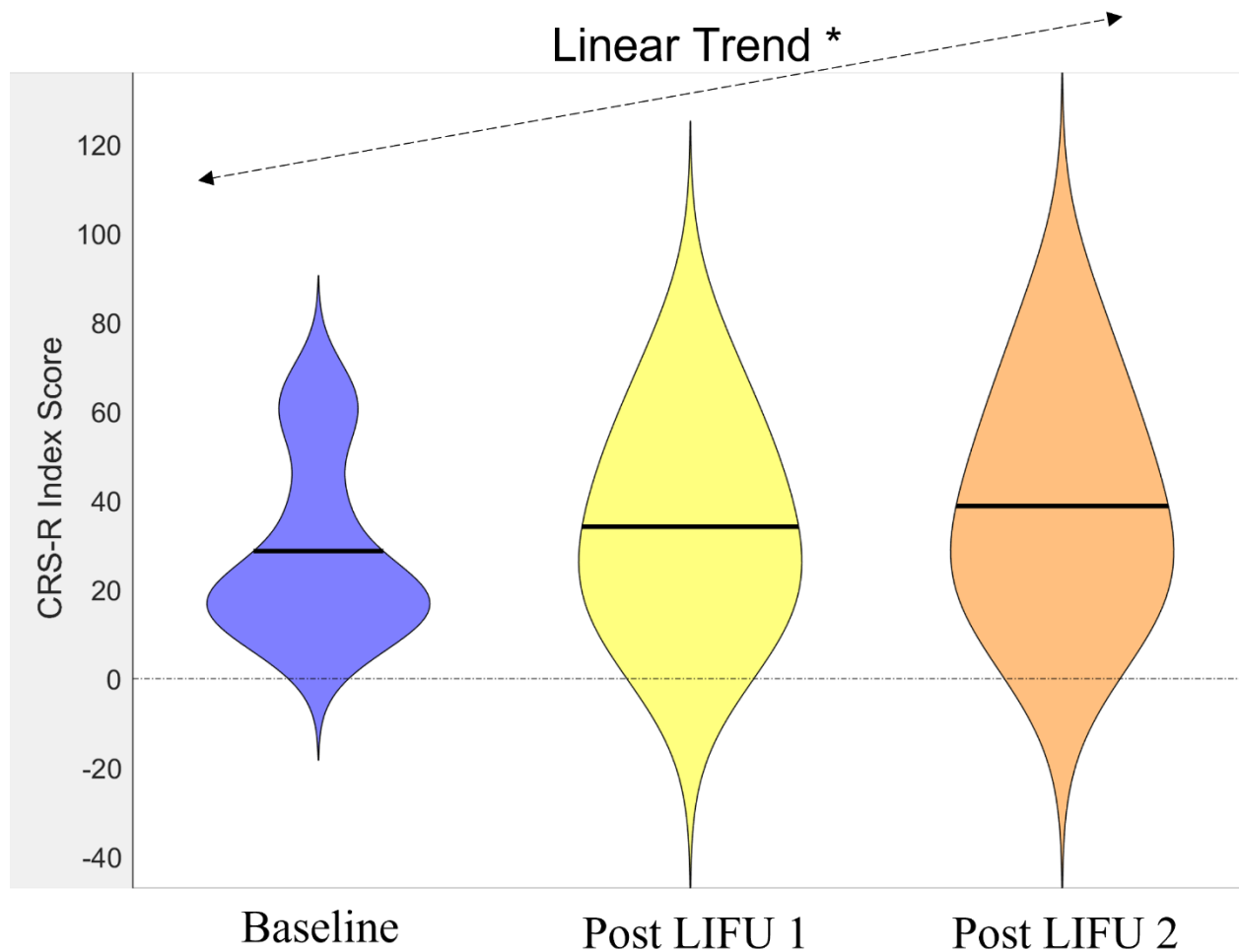


Figure 3-4) Violin plots display the distribution of the highest CRS- R_{index} score prior to and up to 1-week following LIFU 1 and LIFU 2. Solid lines represent the mean of each distribution. A significant positive linear trend was found.

2. *BOLD Data Analysis: Effect of LIFU on Activity*

As compared to baseline (i.e., LIFU-off), 30 second blocks of deep brain LIFU sonication coocurred with significantly reduced BOLD signal in one temporal cluster (see Figure 3-5a), ipsilateral to the site of stimulation. However, behavioral recovery was associated with a reduction in BOLD signal within one cluster located in the ipsilateral subcortex, sepecifically surrounding the ventral striatum in most subjects.

3. *BOLD Data Analysis: Effect of LIFU on Connectivity*

Our psycho-physiological interaction analysis found that, during LIFU sonication, the targeted thalamus increased its connectivity with three clusters (Figure 3-5c)—one extending from the ipsilateral opercular cortex to the ipsilateral supramarginal gyrus, one in the contralateral frontal polar cortex, and one in the ipsilateral insular cortex. Notably, no significant clusters were found when using the non-sonicated thalamus as a seed.

When recovery for each subject (CRS_ R_{index}) was regressed on PPI results, we found that increased connectivity between the targeted thalamus and the contralateral striatum, globus pallidus, and anterior cingulate (cluster 1), as well as the contralateral middle frontal gyrus (cluster 2) predicted recovery. Decreases in connectivity between the targeted thalamus and the posterior cingulate cortex predicted recovery as well (Figure 3-5d).

While using the non-targeted thalamus as seed returned no significant PPI results (Figure 3-5e), connectivity changes between it and the rest of the brain were associated with recovery in a pattern highly similar to that found for the targeted thalamus. Indeed, clusters were found in the same locations as the targetted thalamus, save a unique cluster of heightened activity in the ipsilateral opercular cortex (Figure 3-5f).

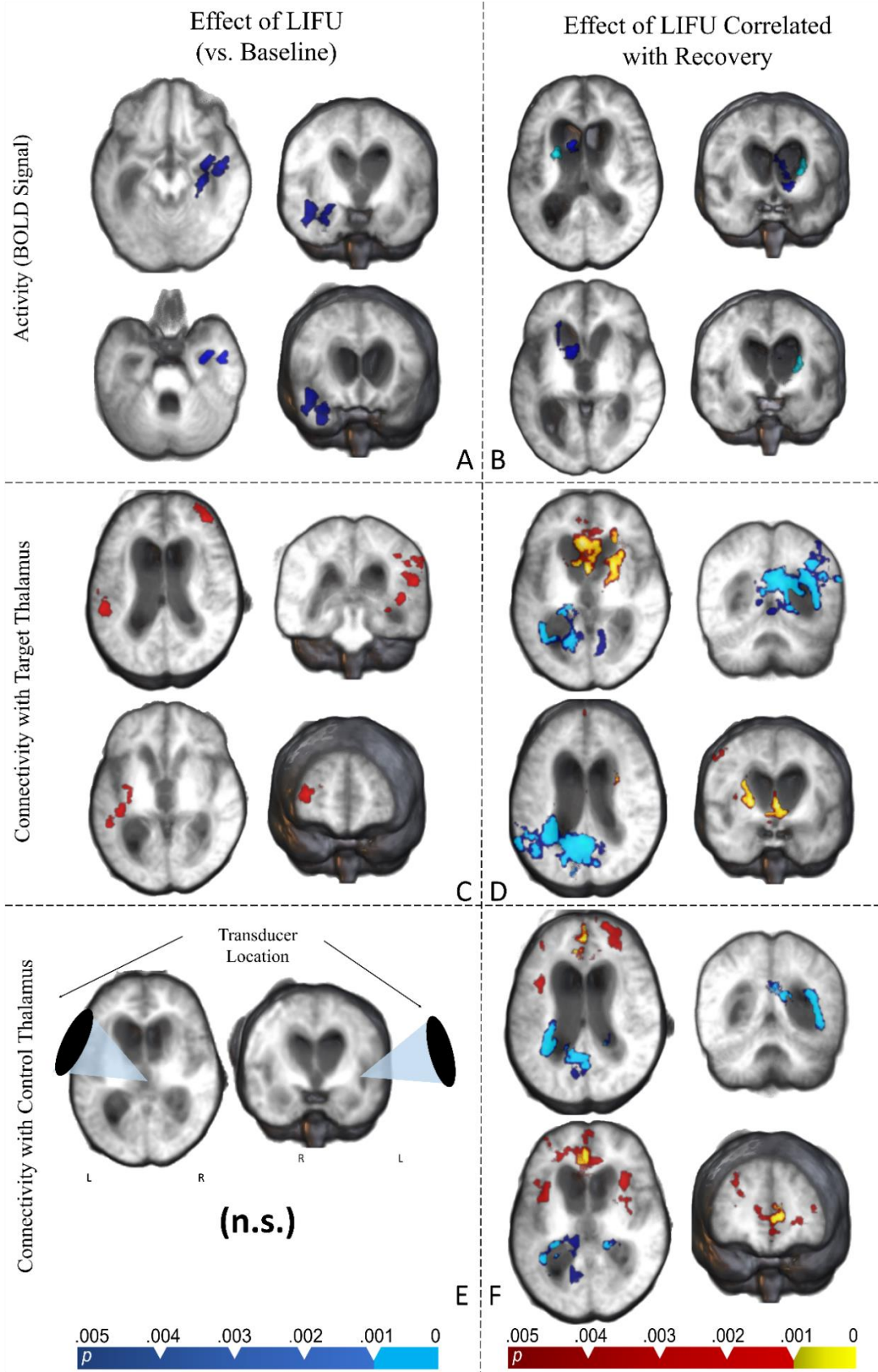


Figure 3-5). Whole brain results. For all analyses, statistical maps were obtained using a fixed effects model as implemented in FSL6.0.1, and are shown at two levels of cluster correction for multiplicity (CDT set at $p < 0.005$, in blue, and at $p < 0.001$ in violet). **A)** Regions of significant change in BOLD signal during sonication compared to inter-sonication periods (i.e., baseline). **B)** Regions of significant BOLD change predicted by behavioral recovery. **C)** Connectivity changes observed during LIFU-on blocks compared to LIFU-off blocks (PPI) between the whole brain and the targeted thalamus. **D)** These changes predicted by behavioral recovery. **E)** Connectivity changes observed during LIFU-on blocks compared to LIFU-off blocks (PPI) between the whole brain and the non-targeted (control) thalamus. **F)** These changes predicted by behavioral recovery.

General Results

Safety of Thalamic LIFU

In regard to safety, no change in vital parameters were observed during the administration of LIFU. While two adverse events occurred to subjects during the study, both were considered unrelated to the LIFU procedure. One AE involved respiratory suppression of a patient prior to any LIFU exposure while the other resulted from a seizure in one patient over 1 week following LIFU in the context of sepsis.

Discussion

Acute Subjects:

Firstly, with respect to feasibility and safety, no adverse events associated with the application of LIFU were observed over the course of this study; thus our results support the apparent safety of thalamic LIFU in acute DOC at the parameters tested, which is in line with the known safety profile

of transcranial ultrasound(Duck, 2007; Gaur et al., 2020). Moreover, our findings suggest that MR-guided LIFU can be accomplished in acute DOC patients while viable functional data is collected despite the challenges that equipment placement and subject motion present to this procedure.

Secondly, with respect to behavior, this cohort increased in their neurobehavioral responsiveness following thalamic LIFU, in line with some prior case reports in acute(Monti et al., 2016) and chronic patients(Cain, Spivak, et al., 2021). Specifically, this reflects an increase in the highest CRS-R_{index} score in the 1-week period following LIFU when compared to the best CRS-R_{index} score at baseline. For four of eleven subjects, this included a shift up in diagnostic category (e.g., VS to MCS). This improvement correlated positively with the initial level of patient functioning, suggesting that the mechanism of this recovery may require some minimal level of neurotypicality. However, this early finding should not deter future investigations in lower-functioning subjects which may confirm or dispel this observation. Indeed, even some VS subjects enrolled in this study demonstrated apparent recovery. Interestingly, no significant difference was found when comparing the CRS-R_{index} immediately preceding and immediately following LIFU application. While this null result cannot bolster or dispel the notion of rapid recovery, our behavioral results, when taken as a whole, suggest that recovery—if indeed induced by thalamic LIFU—may require some time after the 1-hour post-LIFU period to develop. However, a major confound here is that the lengthy procedure is likely to induce fatigue in subjects, which may mask any immediate effect. Finally, our functional MRI results provide initial data on the neural origin of this apparent behavioral effect. The results of our block design model suggest that an acute reduction in activity, instead of acute excitation, is induced by thalamic LIFU when compared to baseline. Portions of

both the anterior cingulate, subcallosal, and medial prefrontal cortex appear inhibited during LIFU-on blocks. Furthermore, the ipsilateral striatum (both caudate and putamen) was inhibited during LIFU-on blocks. While no thalamic cluster appeared in the whole-brain results, the sonicated thalamus had reduced BOLD signal compared to the un-sonicated thalamus during LIFU blocks in an ROI approach. This pattern of results is interesting when considering the intimate connectivity known to exist between cortex (especially fronto-parietal), the basal ganglia, and the targeted central thalamic regions(Jones, 2012; Schiff, 2010b). Whole-brain regions of reduced BOLD with small effects in the targeted nuclei mirror results found in a previous LIFU study targeting the thalamus and adjacent basal ganglia in healthy individuals using the same parameter set(Cain, Visagan, et al., 2021). Moreover, an observation of acute inhibition is in line with recent associations between low duty cycle (here 5%) in LIFU parameter sets and inhibition(Plaksin et al., 2016). As inhibition from LIFU is thought to involve the excitation of inhibitory neurons (cortical interneurons or thalamic reticular cells), a local BOLD effect—driven largely by local glutamate secretion and metabolic changes(Logothetis et al., 2001)—may be difficult to detect(Ai et al., 2016; Plaksin et al., 2016).

Our psychophysiological interaction (PPI) results suggest a more complex change in connectivity between the targeted thalamus and the rest of the brain when LIFU is applied. During LIFU-on blocks, the targeted thalamus decreased in its connectivity with ipsilateral fronto-polar cortex. However, it increased in its connectivity with ipsilateral somatomotor cortex and contralateral opercular/insula cortex. Perhaps more interestingly, changes in thalamic connectivity which predicted recovery were more expansive and generally aligned with changes in BOLD signal during LIFU. Indeed, reduced connectivity between the targeted thalamus and all of the regions which we found to be inhibited during LIFU-on blocks were associated with greater recovery (i.e.,

anterior cingulate, subcallosal frontal cortex, medial prefrontal cortex, ipsilateral striatum). However, the effect expanded to include portions of the ipsilateral prefrontal cortex, contralateral striatum, bilateral opercular cortex, and the contralateral thalamus as well. Furthermore, increased connectivity between the targeted thalamus and large portions of the contralateral parietal, occipital, and motor cortex also predicted recovery. It is interesting that this increase in connectivity was entirely contralateral; one hypothesis is that this may reflect a form of compensation for thalamocortical connectivity changes that were induced ipsilaterally.

Strikingly, no significant changes in connectivity were found between the non-targeted thalamus and the rest of the brain, nor did recovery predict changes in connectivity.

Chronic Subjects:

Firstly, with respect to feasibility and safety, our results support the safety of thalamic LIFU, this time in chronic patients. Again, no adverse events (AE) associated with LIFU were noted. Viable functional MR data may also be collected concurrent with LIFU sonication in this patient population, which presents unique denoising challenges related to their severely altered brain morphology(Weiler et al., 2021).

Secondly, with respect to behavior, we observed a linear increase in the neurobehavioral responsiveness of this cohort following each of two thalamic LIFU sessions. This is in contrast with the possibility of a leveling out of recovery following the first LIFU session (“L-Shaped” recovery); although these results should be considered highly preliminary, this may suggest that multiple LIFU sonication sessions provide additional benefits to patients. For four of eleven subjects, behavioral changes included a shift up in diagnostic category (e.g., VS to MCS). These

observed behavioral changes should be considered more compelling than our approaches in acute subjects because it is well established that DOC patients in the chronic phase of illness are much less likely to recover spontaneously than those in the acute phase—especially in the time frame of weeks for which we observed them in this study (**Whyte et al., 2013**).

Finally, significant fMRI results suggest the neuroactivity of LIFU in chronic subjects and provide preliminary datapoints from which to speculate about the mechanisms of the observed behavioral change. In corroboration with previous results in acute subjects and in healthy individuals (**Cain, Visagan, et al., 2021**), we find reduced BOLD signal during LIFU-on blocks compared to LIFU-off blocks in cortical regions remote to the site of stimulation. Perhaps more compellingly, inhibition of subcortical tissues ipsilateral to the site of stimulation was associated with recovery in chronic subjects (See Figure 3-5b). When projecting this group-wide cluster on single subjects (see Chapter 2 Appendix Figure 3-S1), it can be more easily located to the ventral regions of the ipsilateral striatum; broadly, reduced striatal output has been hypothesized as a mechanism underlying DOC (**Schiff, 2010b**), while, specifically, the ventral striatum is a component of the basal forebrain nuclei, which share intimate reciprocal thalamic connectivity and play a key role in maintaining cortical arousal (**Saper & Fuller, 2017**). These results may conceivably stem from two obvious sources: **1**) Direct inhibition of the region during sonication, given its proximity to thalamus or **2**) circuit-level effects during sonication. The first hypothesis of direct stimulation appears unlikely given the distance of this cluster from the central thalamus (>2cm) and previous estimates of skull-refractory effects (**Mueller et al., 2017**). Instead, hypothesis 2—the downstream inhibition of the striatum following thalamic inhibition—seems plausible considering the intimate relationship between thalamic output and striatal input from the cortex. The established relationship between these regions is such that reduced thalamic output (consistent with the notion

of local inhibition of the thalamus(Cain, Visagan, et al., 2021; Plaksin et al., 2016)) is likely to co-occur with reduced striatal activity; indeed, such a relationship is thought to underlie some aspects of the broad reduction in cortical activity observed in DOC patients(Schiff, 2010b). While the observation that reduced striatal activity—a correlate of DOC—appears to predict recovery in these patients may appear counterintuitive, it should be noted that we have no data from which to understand the longer-term activity of this or any other of the relevant brain regions. The analyses reported only suggest that reduced activity in some regions is altered during LIFU-on compared to LIFU-off blocks; it remains fully possible that this could be driven by increased activity in these regions as a rebound from the immediate effect of LIFU rather than a reduction in activity compared to a pre-LIFU baseline, for which we have no data. Future studies should include more extended pre-LIFU baselines in order to clear up this ambiguity, as discussed more below.

The above results are perhaps better contextualized in the context of our connectivity (PPI) results. During LIFU-on blocks, compared to LIFU-off blocks, the targeted thalamus (and notably, not the untargeted thalamus) increased its connectivity with several cortical clusters. Given that DOC is often hypothesized as a “disconnection syndrome”, where reduced functional communication (especially between subcortical structures and association cortex) underlies dysfunction(Schiff, 2010b), it is interesting to observe enhancement of functional connectivity between thalamus and association cortex during LIFU in these subjects. Yet, the relationship between changes in connectivity and recovery appears more complex. We observe recovery-related increases in connectivity between thalamus and the bilateral frontal cortex as well as recovery-related reductions in connectivity between thalamus and the PCC and ipsilateral parietal cortex during LIFU. This general pattern was observed for both the targeted and untargeted thalamus; however, changes in connectivity with the untargeted thalamus appear notably less expansive. The presence

of activity-related changes in connectivity with the targeted thalamus with large sections of association cortex should likely be emphasized over the specific regions in which those changes are found, especially considering the broad connectivity of the thalamus. However, the observation of recovery-related changes in connectivity between thalamus and the PCC, lateral parietal cortex, and (especially medial) frontal cortex is interesting considering their inclusion in the classical default mode network—dysregulation of which has previously been observed in DOC patients (Di Perri et al., 2016).

Collective Discussion:

LIFU in Acute and Chronic DOC

While some clear differences exist between the studied acute and chronic cohorts (e.g., the precise pattern of fMRI effects), several overarching observations can be emphasized when considering the results stemming from both acute and chronic patients together; namely:

1) Behavioral responsiveness was observed to increase on a group-wide level during the course of this clinical trial for both cohorts. While a control cohort was not feasible in this proof-of-concept trial, behavioral changes observed in chronic subjects are especially interesting considering the low likelihood of spontaneous and/or rapid recovery in these subjects without intervention (Whyte et al., 2013).

2) Changes in connectivity were observed between the targeted thalamus and cortical regions in both cohorts while no changes were observed between the untargeted (control) thalamus and the rest of the brain. These changes largely reflected increases in connectivity, save one cluster of reduced connectivity in our acute cohort. While the precise pattern observed differed between

cohorts, both results show changes in connectivity between thalamus and striatum as well as frontal cortical regions, both of which are known to have intimate connectivity with the intended (central) thalamic target(**Jones, 2012**).

3) Changes in connectivity between the targeted thalamus and the cortex was associated with recovery in both cohorts. Furthermore, for both cohorts, these effects were expansive and highly complex, involving clusters of increased as well as reduced connectivity. For both cohorts, the implicated regions largely surrounded frontal and parietal cortical regions as well as the basal ganglia. Again, these are sensible considering the known structural and functional connectivity of the (central) thalamus(**Jones, 2012; Schiff, 2008**). Moreover, for both cohorts, reductions in connectivity were generally more ipsilateral while increases in connectivity were generally observed more contralateral to the sonicated hemisphere, which may reflect the unilateral nature of our stimulation.

However, some notable differences in the pattern of effects observed for both cohorts were clear. Reduced bold signal was observed during LIFU in the acute cohort within frontal and (ipsilateral) striatal regions while a lone temporal cluster was observed in chronic subjects. The pattern observed in acute subjects can be considered somewhat less surprising considering what we know about (central) thalamic connectivity. Moreover, the clusters of reduced activity in acute subjects more closely aligned with changes in connectivity associated with recovery observed in the same cohort. For instance, reduced BOLD signal and reduced connectivity with the targeted thalamus were both observed in acute subjects within the medial prefrontal cortex and ipsilateral striatum.

Despite identical experimental designs applied to each cohort, such discrepancies could be considered inevitable given the considerable differences in acute and chronic brain morphology.

Although much of the total structural damage has already been done in the acute phase of DOC, the final conformation of neural structures to this damage does not reveal itself until much later. Thus, damaged subcortical (e.g., thalamic) tissues are much smaller and ventricles are much larger in chronic cohorts compared to acute cohorts. Thus, an identical focal point of LIFU may readily subsume different or larger portions of the targeted thalamus (e.g., the gabaergic reticular nucleus) in the chronic cohort, as well as adjacent structures such as the basal ganglia.

The Potential Benefits of Inhibition

Given that DOC is often associated with a gross reduction in neural activity (**Laureys, 2005**) compared to healthy subjects, it may appear counterintuitive that we observe behavioral recovery following apparent inhibition in both cohorts. While reduced activity in large-scale cortico-subcortical networks is a hallmark of the DOC pathology (**Schiff, 2010b**), a more complete description of the neural correlates of DOC may emphasize a more general dysregulation of large-scale networks and the isolation of independent regions (**Luppi et al., 2021**). It's relevant to note here that some DOC patients present with normative levels of whole-brain metabolism (**Laureys, 2005**) while their condition is thought to be result from functional network changes—even in regions distant from the site of injury (diaschisis) (**Carrera & Tononi, 2014**).

From this perspective, interventions which cause acute excitation as well as inhibition may restore more neurotypical states dormant within highly damaged brains (**Pistoia et al., 2014**). Indeed, CNS depressants (e.g., zolpidem, baclofen, lamotrigine, lorazepam) have been associated with recovery in select DOC patients (**Pistoia et al., 2010; B. Zhang et al., 2021**). Although the mechanisms behind these effects remain debated, it is interesting that CNS depressants can, even in healthy brains, increase functional connectivity (**Fingelkurts et al., 2004**). As has been previously

proposed(Pistoia et al., 2014), inducing inhibition within the brains of DOC patients may induce recovery by bolstering the inhibitory gating mechanisms necessary to conduct the large-scale connectivity presumed to underlie goal-directed activity. It could be argued that this perspective is especially relevant to thalamic modulation as the role of this structure in cognition appears to rely greatly on sensorimotor gating (Fiebelkorn & Kastner, 2019; Jones, 2012; Saalman, 2014). Once reestablished, improved functional connectivity may evolve or become self-sustaining(Schiff, 2010b), which may explain reports of the CNS depressants baclofen and lamotrigine being associated with improved symptoms in DOC patients weeks after administration and in a pattern unrelated to these drugs' pharmacodynamic profile(Pistoia et al., 2014). This may similarly explain why we do not observe recovery in our patients in the immediate post-LIFU assessment but only after.

So, in the perspective that perturbation of not only brain activity, but especially brain connectivity is important for recovery from DOC, it is fascinating that we find a complex pattern of altered connectivity with the targeted thalamus during LIFU that was related to behavioral recovery. Based on these results, we may hypothesize that acute perturbation of thalamic connectivity induced by thalamic LIFU may have a beneficial effect on restoring the more normative patterns necessary for behavioral recovery. However, this should remain a tentative hypothesis awaiting more extensive future investigations.

Limitations and Future Directions

Though we find some marginal evidence for of the targeted thalamus as a whole during LIFU, such an approach neglects the thalamus' complexity—its many nuclei, their possible interactions (mediated by the thalamic reticular nucleus), and subtypes of thalamic neurons. Recent

computational models suggests that LIFU applied at a 5% duty cycle preferentially causes action potentials in excitatory thalamocortical cells compared to inhibitory thalamic reticular cells (RE); however, raising the DC to just 7% produces equal action potentials between both thalamic cell subtypes(Plaksin et al., 2016). Thus, passing a beam of LIFU at a DC of 5% and thus near the critical threshold of RE neuron activity through a large portion of the residual thalamus likely has a complicated effect on individual thalamocortical circuit relationships; these likely depend strongly on the precise shape of local connectivity. This complexity may be mirrored in our connectivity results, which show a pattern of both increases and decreases in thalamic connectivity, which could reflect differences in the local thalamic effect of LIFU or cortical target cell types. Similarly, even this perspective ignores the fact that the ultrasound applied here reaches adjacent structures (though likely at a lower intensity), such as aspects of the basal ganglia. Some of these interpretational challenges could be avoided in the future by employing functional localizers and more advanced structural imaging techniques(Iglehart et al., 2020) to locate thalamic subregions in damaged brains alongside more spatially-precise multi-transducer arrays.

Furthermore, many of the ambiguities that remain could be alleviated by larger datasets with more numerous time points and the addition of a control condition. For instance, we could not probe the effect of LIFU on individual sub-scores of the CRS-R_{index} (e.g., arousal, auditory components) due to insufficient power. Future analyses of this kind may reveal the mechanisms behind the general recovery observed here—whether it be mediated by improved arousal or increased complex command following, which imply different neural underpinnings. Similarly, behavioral and neuroimaging data with more time-points could map the path of recovery following LIFU and provide a richer dataset from which to probe network interactions underlying that recovery. Future investigations may opt for jittered event-related designs when collecting neuroimaging data; our

contrast of LIFU-on vs. LIFU-off blocks may be unable to disambiguate acute effects from regularly lagged (i.e., a lag of ~30 seconds) rebound effects from LIFU administration. Thus, assertions about the valence of thalamic LIFU's influence on brain activity in DOC should be confirmed with more complex designs.

A major limitation of the present work, typical of a proof-of-concept trials, is the absence of a sham-control group. While these patients were enrolled in our trial specifically because they were not showing spontaneous recovery, it is not impossible that they spontaneously recovered in the week following LIFU. Yet, while the change behavioral responsiveness after sonication needs to be interpreted with caution, it is particularly noteworthy that the degree to which LIFU modulated the connectivity of thalamus with fronto-parietal and subcortical areas is associated with the behavioral recovery observed following LIFU. Of course, whether this indicates a positive effect of LIFU on brain dynamics – and, subsequently, behavioral responsiveness – or whether we are detecting, through thalamic responsiveness to LIFU, patients with sufficiently preserved thalamo-cortical connectivity – such that they are more likely to recover – remains to be assessed.

Conclusion

We find preliminary evidence for the safety and feasibility of LIFU in DOC. In addition, we found that the degree to which LIFU could alter thalamic connectivity was associated with subsequent behavioral recovery. Functional data collected during LIFU administration suggests that the acute effect of LIFU may be inhibitory at these parameters, in line with prior investigations. However, these data emphasize the role of changes in connectivity (both increases and decreases) with the thalamic target in the behavioral recovery of subjects. Future investigations would benefit greatly by including neuroimaging at more time points to better parse the neural underpinnings of apparent

recovery from thalamic LIFU, especially considering that this recovery appears to develop over time. While many unknowns remain, these preliminary results should help compel and define future efforts to assess the efficacy of thalamic LIFU as a treatment for DOC and its associated mechanisms.

Chapter 4. Establish improved methods for rapidly estimating the effects of skull on transcranial focused ultrasound.

Abstract

Low-intensity focused ultrasound (LIFU) is an increasingly applied method for achieving non-invasive brain stimulation. However, transmission of ultrasound through the human skull can substantially affect focal point characteristics of LIFU, including dramatic attenuation in intensity and refraction of focal point location. These effects depend on a high-dimensional parameter space, making these effects difficult to estimate from previous work. Instead, focal point properties of LIFU experiments are often estimated using numerical simulation of LIFU sonication through skull. However, this procedure presents many entry barriers to even computationally savvy investigators and often requires expensive computational hardware, impeding LIFU research. We present a novel MATLAB toolbox (<https://doi.org/10.5068/D1QD60>) for rapidly estimating beam properties of LIFU transmitted through bone. Users provide specific values for frequency of LIFU, bone thickness, angle at which LIFU is applied, depth of the LIFU focal point, and diameter of the transducer used and receive an estimation of the degree of refraction/attenuation expected for the given parameters.

Introduction

In recent years, low-intensity focused ultrasound (LIFU) has gained popularity as a novel neuromodulation method due to its noninvasive implementation, relative ease-of-use, and theoretically highly precise targeting of both cortical and sub-cortical brain regions (Baek et al., 2017). A major challenge in the implementation of LIFU is the degree to which skull absorbs, reflects, and diffracts ultrasound (Blackmore et al., 2019). Skull dramatically affects the intensity

of LIFU reaching the brain, often attenuating it by more than 50% in humans.(Cain, Visagan, et al., 2021; Lee et al., 2016) Skull also affects the location of LIFU foci by refracting incoming sound waves (a total translation of 1cm is not uncommon(Mueller et al., 2017)). Thus, the realization of LIFU as a safe and highly precise form of neuromodulation depends on the proper estimation of these qualities. However, the relationship between relevant LIFU parameters and the energy pattern realized inside the skull have been relatively underexplored compared to other noninvasive techniques (e.g., TMS).

While pioneering studies provide a general understanding of the relationship between some of these parameters and skull propagation,(Deffieux & Konofagou, 2010; Mueller et al., 2017) their results may not be readily used to estimate effects of skull in the context of any singular experimental preparation, which likely differs from previous investigations in at least one parameter. Although many studies employ simulations to estimate energy deposition inside the brain given specific parameters and experimental settings(Treeby & Cox, 2010), this procedure is often impractical due to the computational power and sophistication required.

We introduce the Surrogate Model of Attenuation and Refraction in Transcranial Focused Ultrasound (SMART FUS) toolkit, which provides users the ability to estimate the effects of skull without intensive simulations of acoustic propagation. We achieve this using precomputed simulations that sample a wide range of the LIFU parameter space (a surrogate model). We distribute this dataset with a user-friendly MATLAB program (<https://doi.org/10.5068/D1QD60>) that enables users to input study-specific experimental parameters and rapidly receive: **1)** estimated attenuation in focal intensity inside the brain; **2)** estimation of the degree of translation of the focal

point; and 3) visualizations of the precomputed simulations nearest to the provided parameters. SMART FUS aims to greatly streamline the process of planning LIFU parameter sets and trajectories that are reasonable given the often dramatic impact of the human skull.

Methods

We defined a five-dimensional parameter space, comprising carrier frequency, bone thickness, trajectory, transducer size, and focal depth (detailed in Figure 4-2A), in which we simulated acoustic waves through bone. Some portions of this parameter space placed the theoretical focus either inside bone or outside the head entirely; inputting these values into SMART_FUS will return an error. Similarly, inputting values outside the parameter space studied will also return an error. In all, 12,096 simulations were run using an NVIDIA RTX 3080 GPU with each simulation taking roughly 10 seconds to complete, making for approximately fourteen days of simulation time.

We applied the MATLAB-based pseudospectral solver toolbox k-Wave (Treeby & Cox, 2010) to perform the simulations. A simulation space of $256 \times 256 \times 256$ voxels with isotropic dimensions of 0.5mm each was created. Using dimensions that were powers of two maximized the speed of the Fast Fourier Transform used in k-Wave's Fourier collocation method. A perfectly matched layer (PML) was created to absorb energy at the edge of the simulation; default values of 10 voxels and a PML_{α} of 2 were used. A Courant-Friedrichs-Lewy (CFL) of 0.3 (the default value for k-Wave) was chosen. A trade-off between runtime and simulation fidelity exists for CFL values. A value of 0.3 is appropriate for simple simulations, such as these, and maintains feasible simulation times. When ignoring the PLM layer, our simulations represent a space of 11.8 cm in each direction, capable of subsuming the necessary components of each simulation: a transducer up to 80mm in diameter with a focal depth up to 80mm, and a bone thickness up to 12mm. These

dimensions, given the frequencies sampled, result in a points-per-wavelength (PPW) ranging from 11.86 (at the lowest frequency) to 2.96 (at the highest frequency). Homogenous 3D simulations have been observed to converge (in terms of recorded intensity and focal location) at a PPW of 3.5, even with more complex skull models (Robertson et al., 2017) with values lower than this introducing some error. As our medium contains non-aliased skull-models (discussed more below) and a lower CFL of 0.3 (resulting in higher fidelity), compared to the cited study's CFL of 0.5, a slightly lower PPW of 2.96 (compared to 3.5) at our high-range remains valid.

For each simulation, a single-element transducer was modeled and assigned as the source of the acoustic waveform. The modeled transducer has dimensions that corresponded to a certain radius of curvature and diameter. The radius of curvature was determined using the desired focal depth of the transducer with the simple formula:

$$\textit{Radius of Curvature} = \sqrt{(\textit{Transducer Focal Depth})^2 + (\textit{Transducer Radius})^2}$$

Transducers were generated in voxel space using k-Wave's `makeBowl` function and placed such that they met the upper-left corner of the PML. Bone was assigned to a flat wall of voxels in front of and meeting the transducer face. While transducers assigned to a perpendicular trajectory met bone along its entire face, those assigned a non-perpendicular trajectory were tilted away from the PML so their foci fully avoid the perimeter of the space. Regardless of trajectory, the voxel structure of bone remained flat to avoid an aliased surface (see Figure 4-1). Since aliasing has been characterized as the most significant source of error in simulations of this type (Robertson et al., 2017), this likely enhances the fidelity of our simulations considerably.

Each voxel in the space not corresponding to bone was assigned a density of 1000 kg/m^3 and speed of sound of 1482 m/s , corresponding to that of water. A simulation time of $8.0375e^{-5} \text{ s}$ was chosen as this allowed the simulated acoustic wave to reach the opposing end of the simulation space. The intensity emitted from the transducer was set to 1.0558 MPa . Because all outputs from this function reflect the relative attenuation/refraction between water and bone simulations, this value is arbitrary but was selected from measurements taken from a previous empirical study (Cain, Visagan, et al., 2021) (see **Discussion**). Because the absorption coefficient for water changes in relation to the frequency of sound being simulated, we calculated it using k-Wave's waterAbsorption function by inputting the frequency used and a temperature of 37°C (body temperature). Bone attenuation was set to $85 \text{ Np MHz}^{-1} \text{ m}^{-1}$, while speed of sound in bone was set to 2850 m/s , and Bone density was set to 1732 kg/m^3 as has been defined previously for Bulk Bone (Mueller et al., 2017; White et al., 2006) and appropriate for homogeneous simulations.

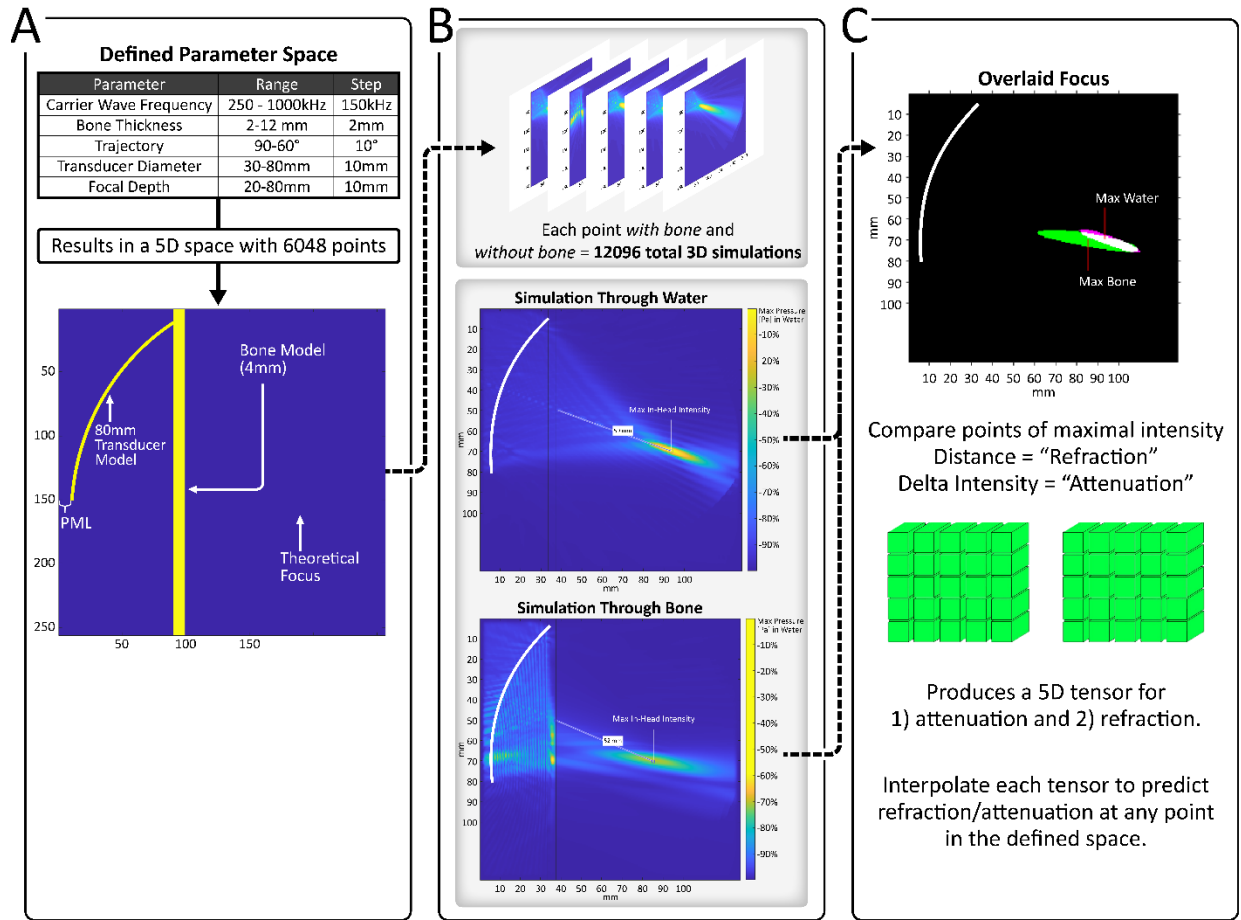


Figure 4-1 This figure depicts the workflow for the creation of the dataset provided in SMART_FUS. As described in more detail in the methods section, a 5-dimensional parameter space was first defined and discretized. From this, 6048 unique simulation environments were constructed (shown in **A**). Simulations with bone and through only water were run for each of these environments (resulting in 12096 total simulations). The value and position of the peak intensity were located for “bone” and “water” simulations at each of the 6048 points in the space defined. The distance between these points defined the observed “refraction” and the difference in intensity between these points defined the observed “attenuation” at each point in the space. Thus, one 5D “refraction” tensor (an array of 3D matrices) and one 5D “attenuation” tensor were created.

These tensors are linearly interpolated according to the values input into SMART_FUS and are used to predict attenuation/refraction at any point within the described parameter space.

Results/Usage

SMART_FUS includes two functions: SMART_FUS and SMART_FUS_vis2d.

SMART_FUS takes as input values for each dimension studied and returns an estimate of attenuation and refraction based on linear interpolation of two datasets that sample the attenuation and refraction in the parameter space (see below). Additionally, the nearest simulation point is visualized, providing the user an estimate of focal shape for the given parameters (see Figure 4-1A).

SMART_FUS_vis2d takes as input values for any three of the five dimensions studied and returns two 2D images depicting the refraction and attenuation expected at points across the two unspecified dimensions, which represent 2D slices through the full 5D parameter space. These 2D arrays are extracted and linearly interpolated to upscale the output matrix and provide a smooth space for visualization (see Figure 4-1B).

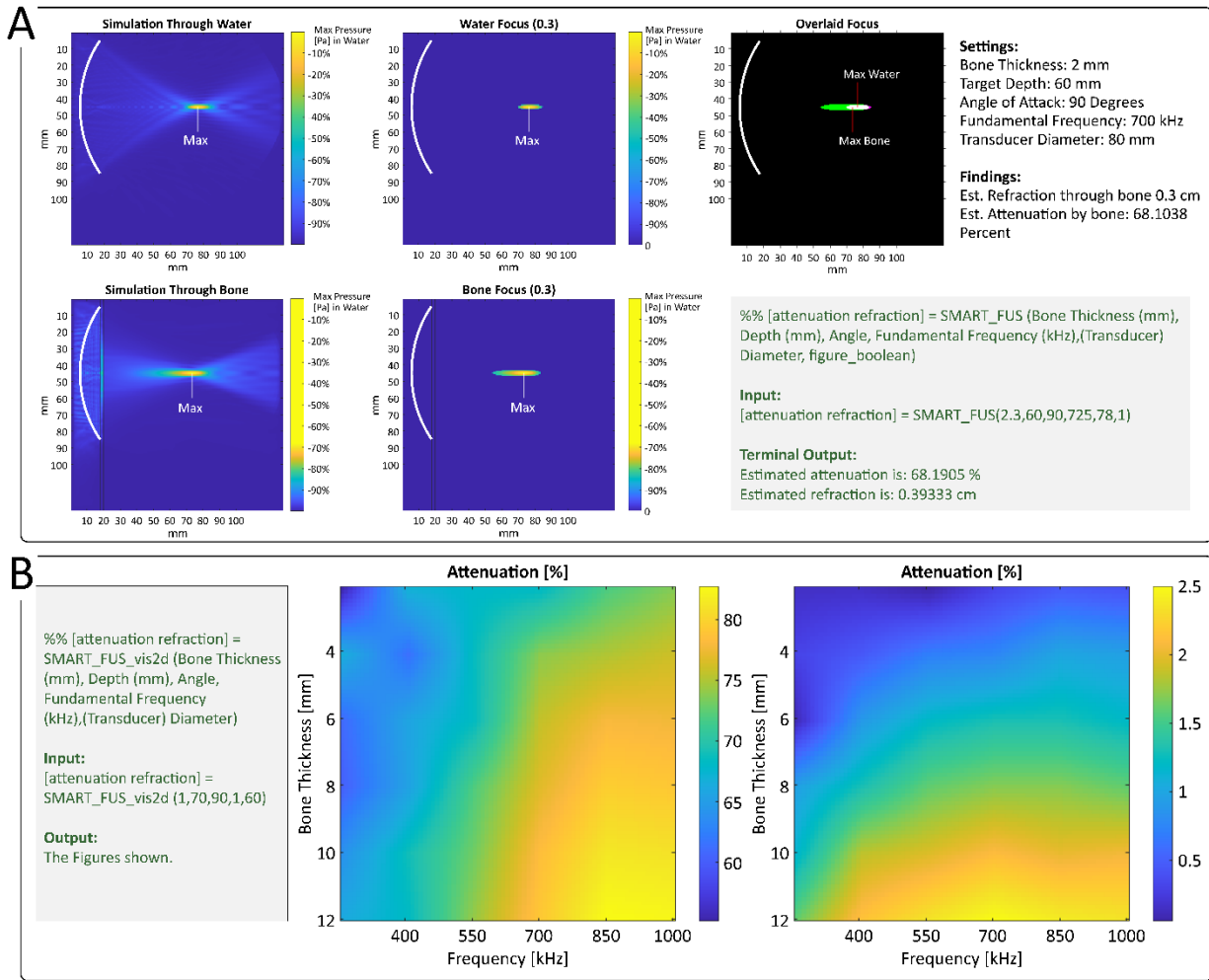


Figure 4-2 The primary visual outputs from SMART_FUS are depicted here. **A)** SMART_FUS estimates attenuation and refraction of specific inputs through linear interpolation and also provides a depiction of the simulation with the parameters closest to those input. Here, a simulation conducted with a bone thickness of 2mm, target depth of 60mm, angle of entry of 90 degrees, a fundamental frequency of 700kHz, and a transducer diameter of 80mm is shown both when performed through a medium containing bone and when performed through a medium containing only water. The -3dB focal region (equivalent to the region exposed to 50% or more of the maximum intensity) is depicted to the right of the full simulations. The point of maximum intensity is highlighted. Finally, against a black background, these -3dB focal regions are overlaid and their

points of maximum intensity highlighted again to clearly demonstrate the impact of bone on focus properties. It is important to note that this output would be provided if a close but not identical parameter set was provided (e.g., with a bone thickness of 2.5mm and all other parameters remaining constant). However, the estimated attenuation and refraction with this unique parameter set would be provided through interpolation and output in the MATLAB terminal. **B)** A sample output from the script SMARTF_FUS_vis2d.m. Here, the user selected to visualize the impact of bone thickness and carrier-wave frequency at specific values for the remaining 3 free parameters. This 2-dimensional space is shown for both attenuation and refraction.

Discussion

SMART FUS enables simple and rapid estimation of skull attenuation and refractory effects when using LIFU in human subjects. This function is intended to aid in planning experiments and parameter selection. Furthermore, SMART FUS may be used to select parameters prior to performing higher-fidelity simulations. It provides an estimate of skull attenuation and refractory effects but should not be considered a replacement for high-resolution subject-specific simulations, which may provide higher validity for individual experimental settings and should be considered.

We selected methods that maximize validity while reducing individual simulation time to feasible levels to produce such a large dataset. Thus, some limitations exist. Several sacrifices regarding bone shape were made to reduce simulation time and avoid aliased skull models. The skull here was a simple flat, homogenous bone layer and did not approximate the heterogenous density and complex shape of real skull. While homogenous simulations are often used to reduce simulation complexity, skull-shape and reflection of energy off the back of the skull appear to dictate focal properties to some extent (Mueller et al., 2017). Furthermore, true skull models would not display

homogenous density and material properties across the skull volume and can include areas of markedly lower density and pockets of air and fluid. The short simulation time and homogeneous bone layer chosen here do not allow us to account for these effects. However, the curved structures of more realistic skull models necessitate aliased simulation media, which are likely to reduce the validity of simulations considerably (Robertson et al., 2017). These were intentionally avoided here.

Similarly, complexity was reduced by assuming constant values for skull density and the intensity of emitted ultrasound. Skull density is known to differ substantially between individuals, which may dramatically impact the effect of skull on ultrasound propagation. We avoided a skull-density dimension to reduce simulation run-time and because skull-density of participants is usually unknown by experimenters unless computed tomography (CT) images are taken. In clinical settings where CT images are available, subject-specific simulations become much easier and are recommended. Future procedures may take advantage of increased computational power and add dimensions such as bone density or increase the resolution of the parameter space explored.

Chapter 5. This Work in Context

The three approaches covered in this dissertation—**1)** focused ultrasound in healthy individuals, **2)** focused ultrasound in a clinical setting involving DOC patients and **3)** numerical modelling of LIFU—reflect the need for interdisciplinary approaches when moving nascent techniques towards fuller implementation. In recent years, we have seen LIFU neuromodulation quickly bootstrapped by a focus on both "its use in science" and the "science of its use"; my Ph.D. work can be seen as a microcosm of this dual-focus.

At the time of the first development of the methods detailed here (~2014; see clinical trial NCT02522429), the reemergence of focused ultrasound neuromodulation had just arrived and the understanding of its effects and how they change in response to LIFU parameters was in its infancy (Bystritsky et al., 2011). More specifically, the use of LIFU in humans was between 1 and 2 years old (Legon et al., 2014), and the field was just beginning to uncover the unique effects, use cases (e.g., clinical applications(Bystritsky & Korb, 2015)), and challenges (e.g., the thick human skull(Mueller et al., 2017); safety(Pasquinelli et al., 2019)) associated with LIFU applied to healthy human brains. The recent development of this field is apparent in the volume of google scholar results shown in Figures 5-1,5-3 between 1999 and 2022. It is clear that LIFU as a technique is dwarfed in popularity compared to more established forms of neuromodulation like TMS(Figure 5-1), but that its implementation has been gaining momentum in recent years (Figure 5-2,5-3).

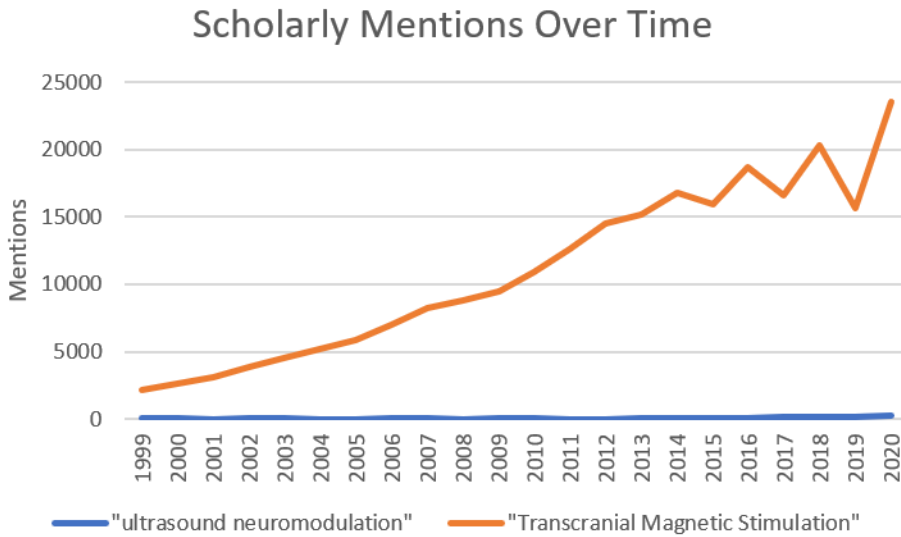


Figure 5-1: Scholarly mentions (results on google scholar) since 1999 of “ultrasound neuromodulation” and “transcranial magnetic stimulation”. Quotes ensure the exact phrases were present in these results. Note that the amount of results for ultrasound neuromodulation is dwarfed by those for the most established transcranial magnetic stimulation. This demonstrates the still esoteric nature of LIFU, even within the field of neuromodulation.

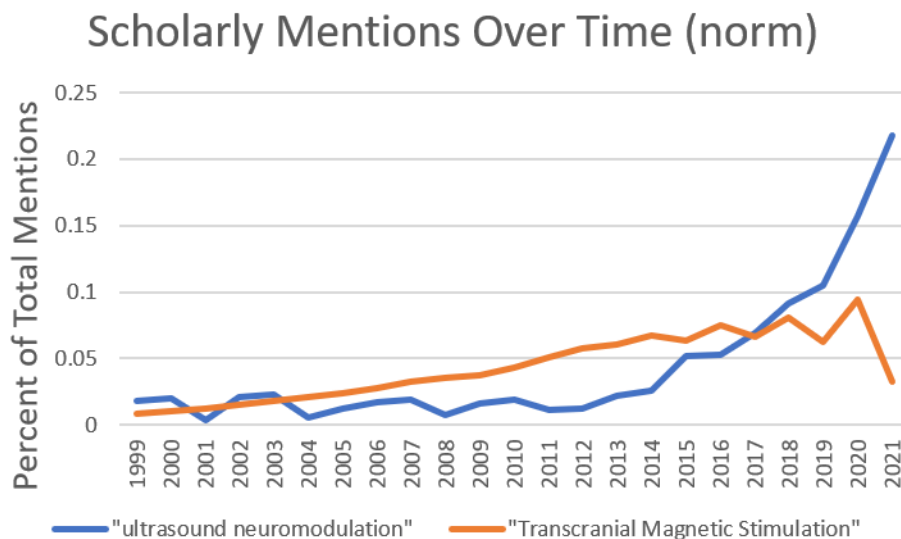


Figure 5-2: Scholarly mentions (results on google scholar) since 1999 of “ultrasound neuromodulation” (blue) and “transcranial magnetic stimulation” (orange), normalized by the total results from each search query since 1999. Thus, the percent of total mentions since 1999 for each year is shown. The rapid increase in the rate of scholarly mentions of ultrasound neuromodulation is clear, with nearly 25% occurring in 2021.

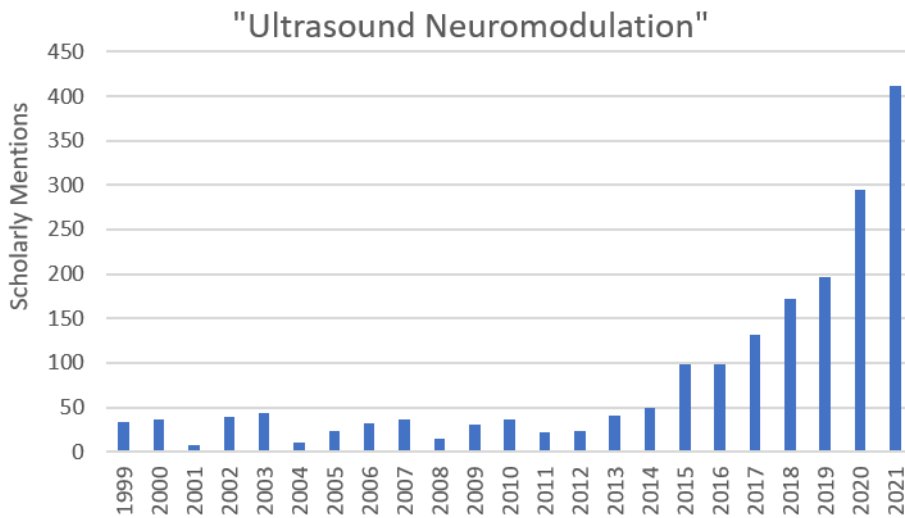


Figure 5-3: Scholarly mentions (results on google scholar) since 1999 of “ultrasound neuromodulation”. Here, the total number of mentions are clear, with a large increase occurring following 2014, which marks its first use in humans and the time at which the methods in this dissertation were first being developed.

Thus, despite the first publishing of these results in only the past two years, how this work has interlaced with and been informed by concurrent developments in the field is already apparent to some degree. Here, I will try to briefly contextualize this dissertation within the greater field of LIFU research.

1) Given LIFU's novelty, the simple feasibility of the techniques detailed in this dissertation make up a great deal of its value. For instance, Chapter 2 details the first group-wide fMRI effect from subcortical focused ultrasound in humans. Indeed, only two studies demonstrating fMRI effects from concurrent focused ultrasound predated these findings (Lee et al., 2015, 2016) and ours is the first study to investigate effects which persist following focused ultrasound using MRI (specifically, using arterial spin labelling). Our process of transducer positioning in the MRI scanner (e.g., using circular MR-fiducials) was in-part developed in this study. The idea that concurrent fMRI may be used to effectively understand LIFU applied to the subcortex as well as methods for positioning ultrasound in the MRI scanner have influenced other recent works (Badran et al., 2020; Stern et al., 2021; Zielinski et al., 2021). Moreover, the parameters first used in chapter 2 and 3 have also been employed in a number of more recent investigations (Badran et al., 2020; Stern et al., 2021; Zielinski et al., 2021).

Similarly, Chapter 3 details data which represents the first ever use of focused ultrasound neuromodulation in a clinical setting (the DOC patient population) and only its second ever use in humans (Legon et al., 2014). Given the ability of focused ultrasound to target deep-brain structures non-invasively and with an accuracy that far surpasses other non-invasive neuromodulatory techniques, this may be the first of many attempts to investigate the clinical implications of LIFU (Bystritsky & Korb, 2015). Indeed, some other applications have already begun (Badran et al., 2020; Stern et al., 2021; Zielinski et al., 2021). Our investigations in DOC patients have provided some early data-points considering the safety and feasibility of clinical LIFU in vulnerable patient populations. Specifically, our methods for the use of focused ultrasound in both inpatient, outpatient, acute, and chronic patients—with an emphasis on fMRI data collection,

preprocessing, and analysis methods—will certainly inform any future investigations for the use of LIFU in the treatment of these conditions.

2) While many ambiguities in how the parameters of focused ultrasound relate to its effects remain, great advances have occurred in recent years. As early as 2013 (King et al., 2013), attempts to understand how these parameters (e.g., carrier wave frequency, intensity, pulse repetition frequency, duty cycle, etc.) impact neuroactivity in animals were made. However, these studies were conducted with few previous datapoints from which to base their designs and were also denied an understanding of the still-unclear mechanistic underpinning of ultrasound's neuroactivity. Given the high dimensional nature of LIFU parameters, this led to a relatively thin sampling of the total parameter space of LIFU and one quite different than what would be selected today given recent discoveries. Likely as an analogy to more established forms of neuromodulation (tDCS, TMS, DBS), the field spent a great deal of attention understanding the effects of pulse repetition frequency on neuroactivity and some apparent influences of PRF on neuroactivity have been found (Cain, Visagan, et al., 2021; King et al., 2013). For instance, Chapter 2 details the investigation of the relative neuroactivity of a parameter set using a 100Hz PRF and one using a 10Hz PRF with all other parameters held constant, as measured using fMRI. Indeed, we did find effects when PRF was changed—at least in terms of the acute impact of LIFU. This is certainly important and finds its way into a small group of publications showing the potential impact of PRF, which has perhaps culminated in the recent development of complex PRF designs—e.g., theta-burst LIFU built around the PRF frequency (Y. Zhang et al., 2021).

However, computational modelling which supports the notion of a capacitance-related mechanism for LIFU's neuroactivity has found increasing support in the field (Blackmore et al., 2019; Plaksin et al., 2014, 2016). These models suggest that duty cycle (for how long ultrasound

is “on” in a given time period, e.g., 50%) is a particularly impactful parameter as it may alter which cell-types (e.g., inhibitory interneurons vs. excitatory pyramidal cells) in a targeted tissue are preferentially activated, and, thus, the valence of LIFU’s effect. The ever-growing body of experimental evidence generally continues to support these models, adding to their credibility (Kim et al., 2021; Yoon et al., 2019). In general, lower duty cycles (e.g., 5%) appear to induce suppressive effects, with higher duty cycles (e.g., 70%) inducing excitation (Plaksin et al., 2016). This appears true for both cortical and thalamic targets (Yoon et al., 2019). Though we did not design our parameters with this in mind, our results have supported this notion. In both healthy subjects and DOC patients, we find that our 5% duty cycle parameter set appears to induce acute inhibition both locally and throughout the brain, though the local effects were less clear in patients. These results add to and bolster this growing consensus.

3) In addition, the time-course of LIFU’s influence has also been an area of focus over recent years and our results have emerged alongside many recent findings of long term (sometimes called “offline”) effects from LIFU in primate subjects, including humans (Folloni et al., 2018, 2019; Fouragnan et al., 2019; Sanguinetti et al., 2020; Verhagen et al., 2019; Y. Zhang et al., 2021). The findings detailed in chapter 2 and 3 bolster the notion of possible long-term effects from focused ultrasound. Specifically, we find broad-ranging inhibition in the minutes following subcortical focused ultrasound with both of the parameter sets used in chapter 2, as determined using arterial spin labelling. Moreover, our behavioral findings in DOC patients—which derive their first datapoint from an assessment given 1-hour following LIFU—suggest that long term impacts may be found. Indeed, we note that the behavior changes we find are driven by changes that occur after this immediate 1-hour post-LIFU period, perhaps suggesting an impact which may

develop or persist for days. However, see chapter 3 for a discussion of the limitations of these findings.

4) Finally, this technique which was very recently only used by a small group of individuals—most of which knew each other personally—has expanded and is expanding to a broader group of scientists interested in the possibilities provided by precise noninvasive neuromodulation. This was first gradual, but has become rapid in the last two years—evident in a large increase in the rate of publications mentioning the technique (see Figure 5-2,5-3). While this is certain to be a good thing for the field, newcomers are much less likely to possess some of the esoteric skills necessary for LIFU's use—namely the ability to conduct valid computer simulations of beam properties. Most extant publications using LIFU, especially early ones, include numerical modelling of skull-refractory effects alongside their findings(Cain, Visagan, et al., 2021; Lee et al., 2015, 2016; Legon et al., 2014). While we have gained a lot of knowledge about the general degree of refraction, attenuation, etc., that occurs when passing ultrasound through the human skull (Mueller et al., 2017), it remains important to ensure one's own parameter sets are valid to use in thick-skulled humans or through particular portions of the human skull. This is inevitably a particularly large entry barrier to conducting LIFU research professionally due to the expertise and computational resources needed to conduct one's own simulations. Chapter 4 details how I have attempted to reduce this entry barrier by providing a way to rapidly estimate the attenuation/refraction to be expected throughout nearly the entire relevant parameter space for human LIFU. While SMART_FUS does not eliminate the need for more detailed modelling in some circumstances, it can certainly aid in the planning of future LIFU experiments—where candidate parameter sets, target depths, and likely skull thicknesses at planned entry points can be checked for skull-refractory effects quickly and easily. While the dataset and tools detailed in

chapter 4 are still under review, I am certain that it will be eagerly used by an expanding field of researchers aiming to use LIFU in ways that it has not been used before, but who may fear the unique challenges that skull may present in those situations.

In conclusion, the work detailed in this dissertation is best understood in not only a scientific, but a methodological context; focused ultrasound neuromodulation is indeed finding its way into the tool-kit of cognitive neuroscientists interested in understanding the brain, but this is often seen as secondary to what our findings tell us about the technique itself. The work presented here is intended as a prelude to the concurrent and near-future use of LIFU to unlock the many secrets of deep-brain structures once unable to be explored causally in healthy human subjects. In particular, it is hoped that this work especially acts as a suitable foundation from which to better understand the thalamocortical interactions often deemed so important for mediating arousal(Baker et al., 2016; Redinbaugh et al., 2020), cognitive functions(Saalman & Kastner, 2015), and consciousness(Boly et al., 2013; Schiff, 2008). May this become reality in time.

Appendices

Chapter 2 Appendix

Region	Voxels	Z-Max	<u>Z-Max (MNI)</u>		
			x	y	z
<hr/> LIFU Mode 1 – Baseline <hr/>					
*Midline Precentral Ctx.	4127	5.01	4	-18	76
*Posterior Cingulate Ctx.	855	4.1	6	-40	0
*Heschel's Gyrus	484	3.71	60	-6	8
*Frontal Polar Ctx.	457	4.15	-2	62	32
Frontal Medial Ctx.	234	3.6	-4	46	-16
<hr/> LIFU Mode 1 – LIFU Mode 2 <hr/>					
Midline Postcentral Gyrus	510	4.31	38	-34	64
Midline Precentral Gyrus	245	4.04	-4	-30	74
Posterior Cingulate Ctx.	218	3.87	8	-40	0

Table S1: BOLD Changes in Whole-Brain During 100Hz Sonication Compared to Baseline, 10Hz Sonication. Significant clusters as defined by a cluster significance level of $p < 0.05$ with a cluster defining threshold (CDT) of $p < 0.005$. Regions that also survived a more conservative CDT of $p < 0.001$ are marked with an asterisk *.

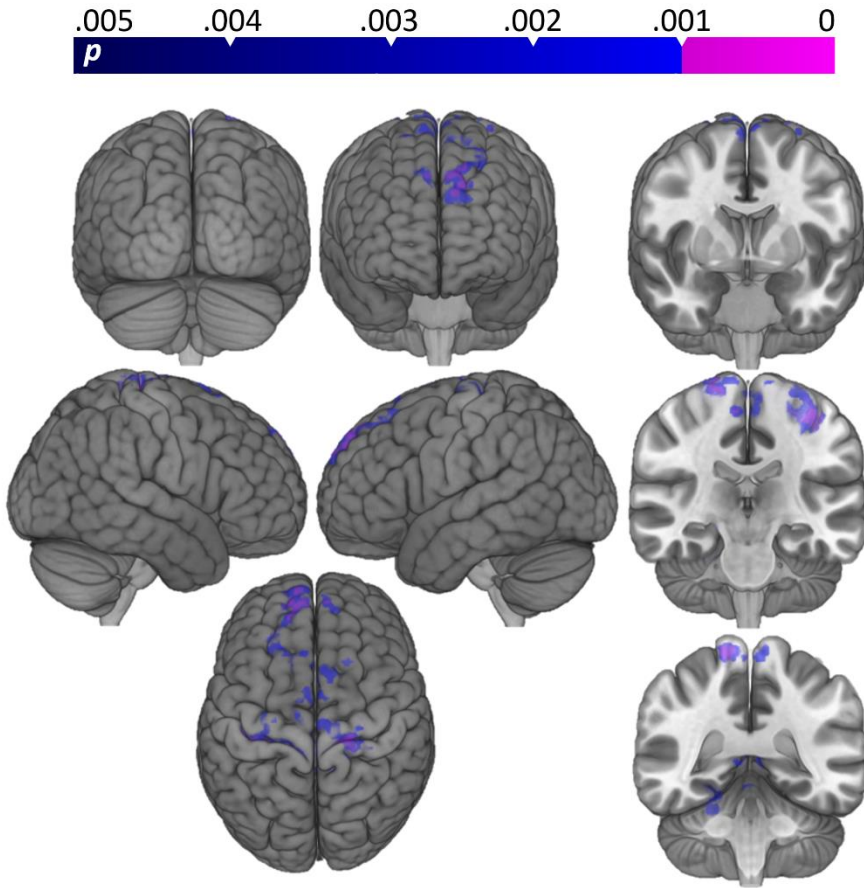


Figure 2-S1: Aggregating LIFU Mode 1 and LIFU Mode 2 data. Shown here are the results of modeling our block design on data captured during both LIFU modes (Mixed Effects FLAME 1+2; cluster significance: $p < 0.05$; cluster defining threshold: $p < 0.005$ (blue), $p < 0.001$ (violet)). Despite the boost in statistical power theoretically provided by doubling the data included, no new clusters are added to the results obtained when analyzing LIFU Mode 1 alone.

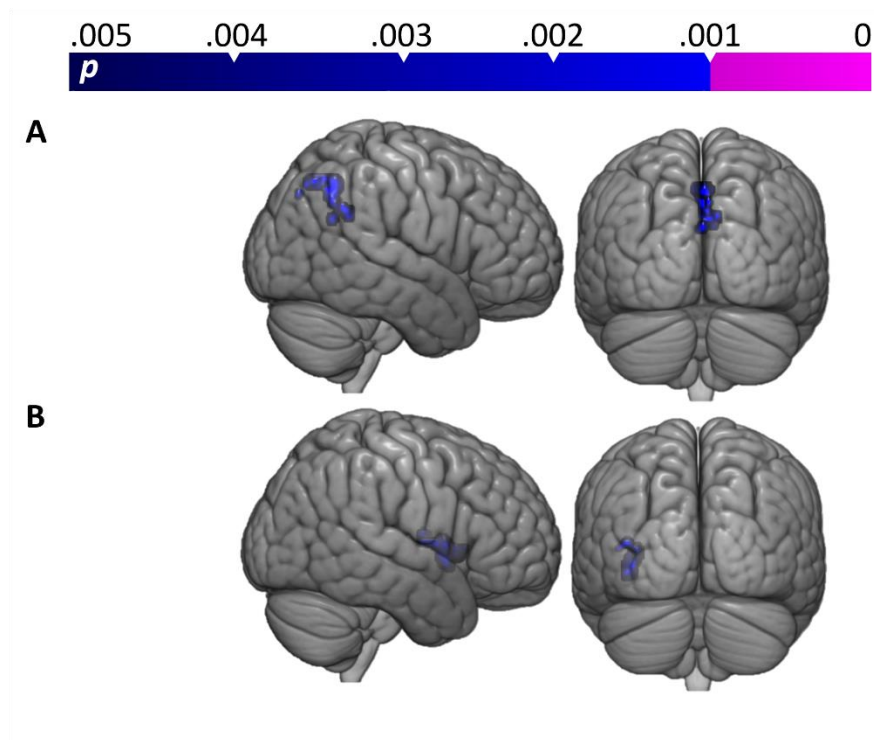


Figure 2-S2: Comparisons between Run1 and Run2 for LIFU in Mode 1 (PRF = 100Hz). Shown here is a statistical map (Mixed Effects FLAME 1+2; cluster significance: $p < 0.05$; cluster defining threshold: $p < 0.005$ (blue), $p < 0.001$ (violet)) of results obtained when subtracting successive LIFU runs (two data sets were collected per session) during Mode 1 (PRF = 100Hz) LIFU. **A)** Run1 -Run2 **B)** Run2-Run1. Significant voxels denote regions of relatively decreased BOLD (i.e., more suppression of BOLD signal from baseline). Minor differences exist, suggesting no major sensitization or habituation to LIFU’s influence.

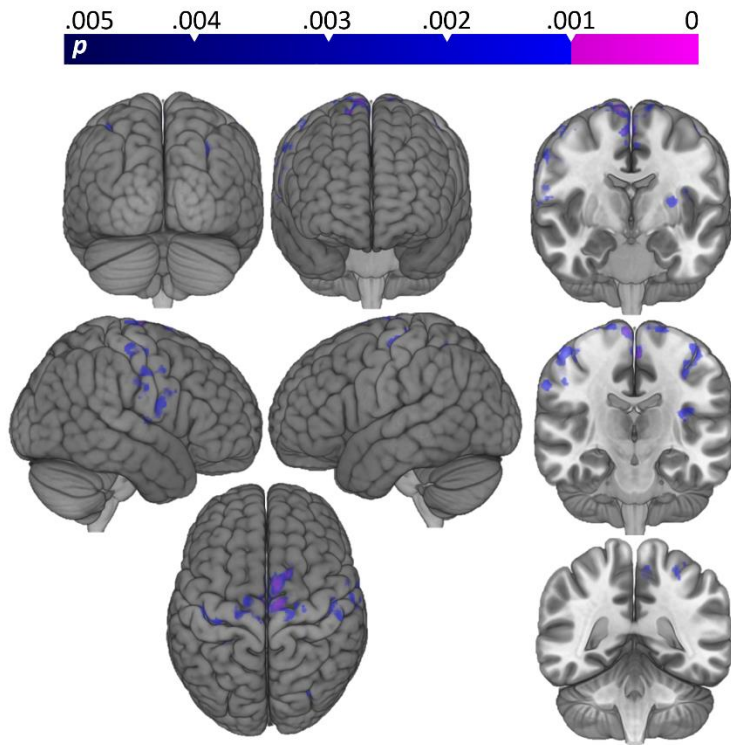
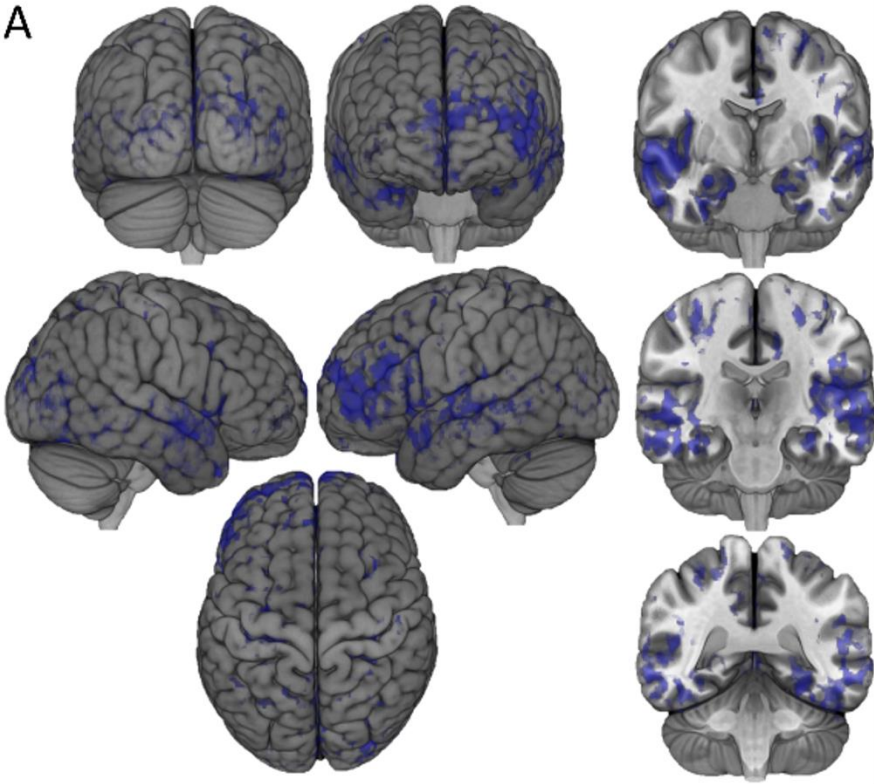


Figure 2-S3: Comparisons between Run1 and Run2 for LIFU in Mode 2 (PRF = 10Hz).

Shown here is a statistical map (Mixed Effects FLAME 1+2; cluster significance: $p < 0.05$; cluster defining threshold: $p < 0.005$ (blue), $p < 0.001$ (violet)) of results obtained when subtracting successive LIFU runs (two data sets were collected per session) during Mode 2 (PRF = 10Hz) LIFU. Significant voxels denote regions of relatively decreased BOLD (i.e., more suppression of BOLD signal from baseline). We find a greater inhibition of BOLD signal in Run 2 compared to Run 1, in regions generally in line with inhibition found when comparing LIFU Mode 1 to baseline, suggesting that perhaps a sensitization occurs during LIFU in Mode 2 over time.

A



B

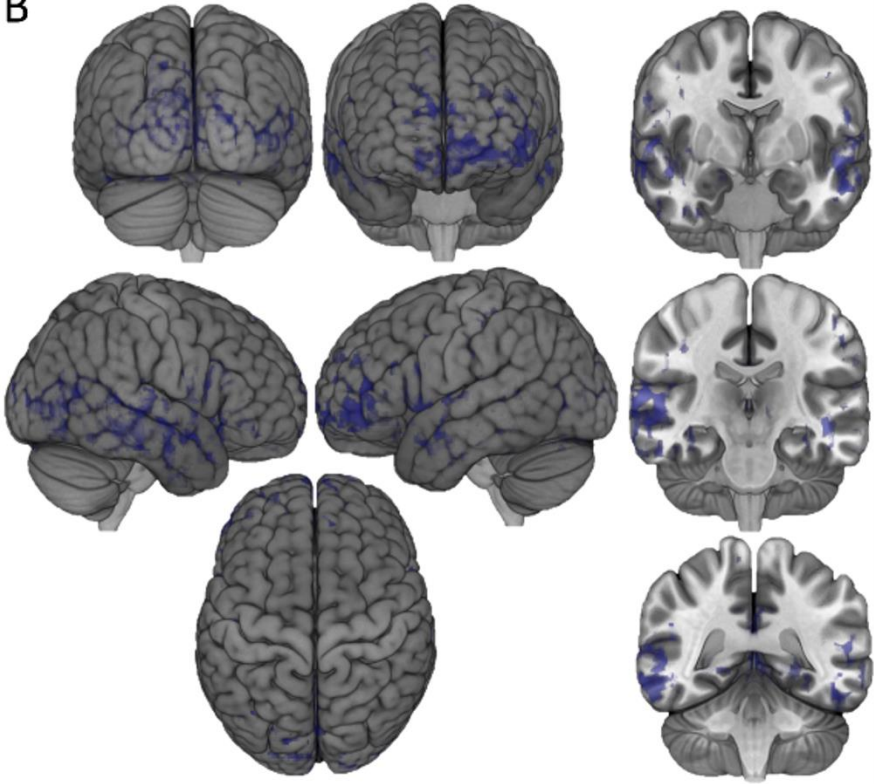


Figure 2-S4: Whole-Brain Perfusion Linear Model. Statistical maps of Blood Perfusion resulting from ASL analysis for all subjects (n=16), including 3 total ASL captures per subject per parameter set—taken immediately before and after each pallidal LIFU in **A**) Mode 1 (100Hz PRF; 5ms PW) and **B**) Mode 2 (10Hz PRF; 0.5ms PW). Color voxels indicate those that fit a linear shaped model such that activity decreased following sonication 1 and decreased further following sonication 2. The colored bar indicates the p-value window with $p < 0.05$. No increase in blood perfusion at these parameters is indicated because none was found. No subtraction between parameters is shown because none was found.

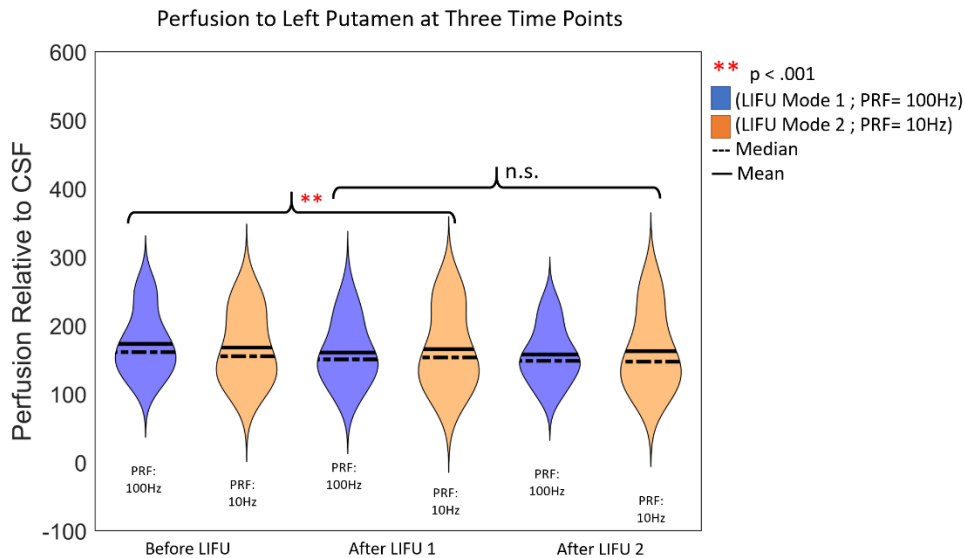


Figure 2-S5: ASL ROI Putamen. The perfusion signal from the Left Putamen at three time points: Before LIFU 1, After LIFU 1, and After LIFU 2. A main effect of Time was found, while a significant decrease in perfusion was found following LIFU 1. However, perfusion was not found to decrease further following LIFU 2.

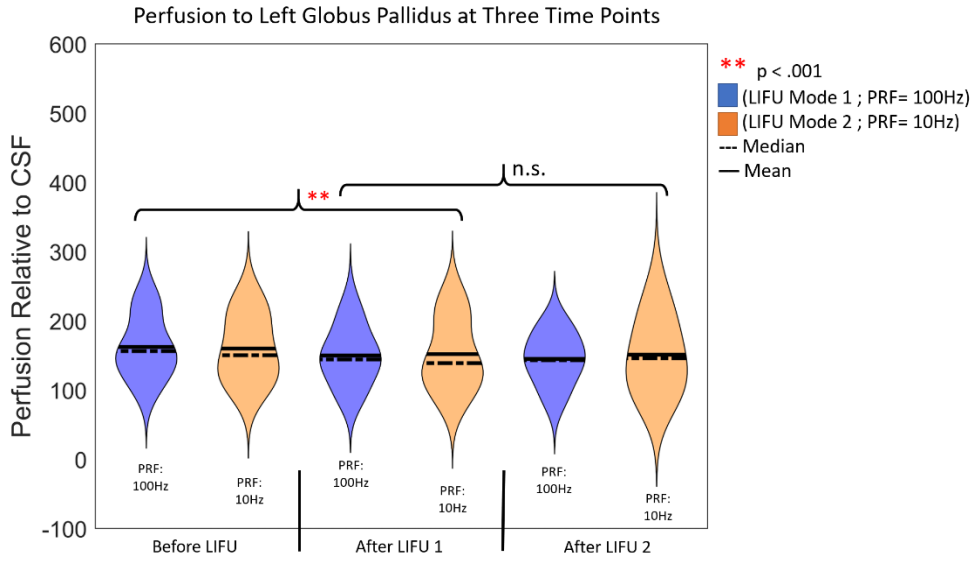


Figure 2-S6: ASL ROI Left Globus Pallidus. The perfusion signal from the Left Globus Pallidus at three time points: Before LIFU 1, After LIFU 1, and After LIFU 2. A main effect of Time was found, while a significant decrease in perfusion was found following LIFU 1. However, perfusion was not found to decrease further following LIFU 2.

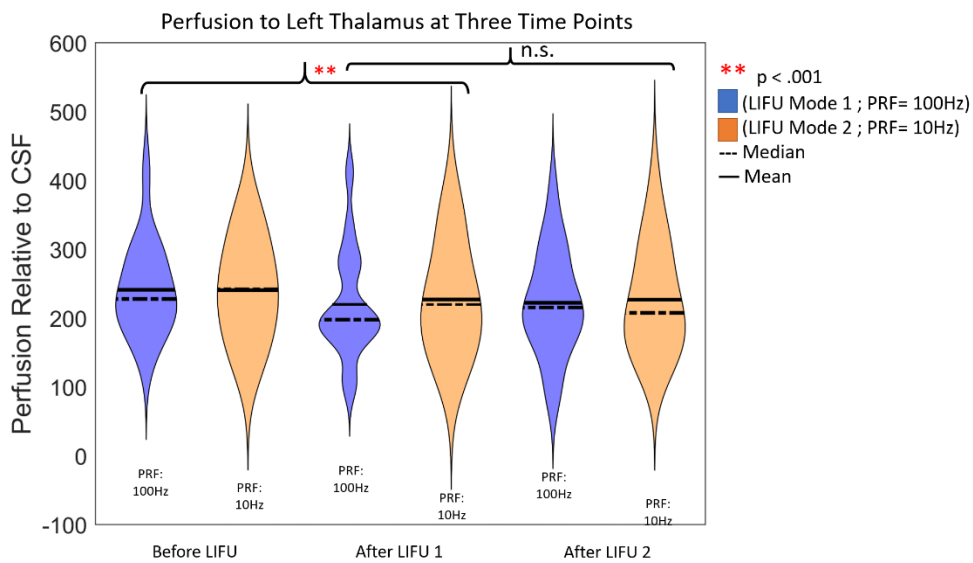


Figure 2-S7: ASL ROI Left Thalamus. The perfusion signal from the Left Thalamus at three time points: Before LIFU 1, After LIFU 1, and After LIFU 2. A main effect of Time was found while a significant decrease in perfusion was found following LIFU 1. However, perfusion was not found to decrease further following LIFU 2.

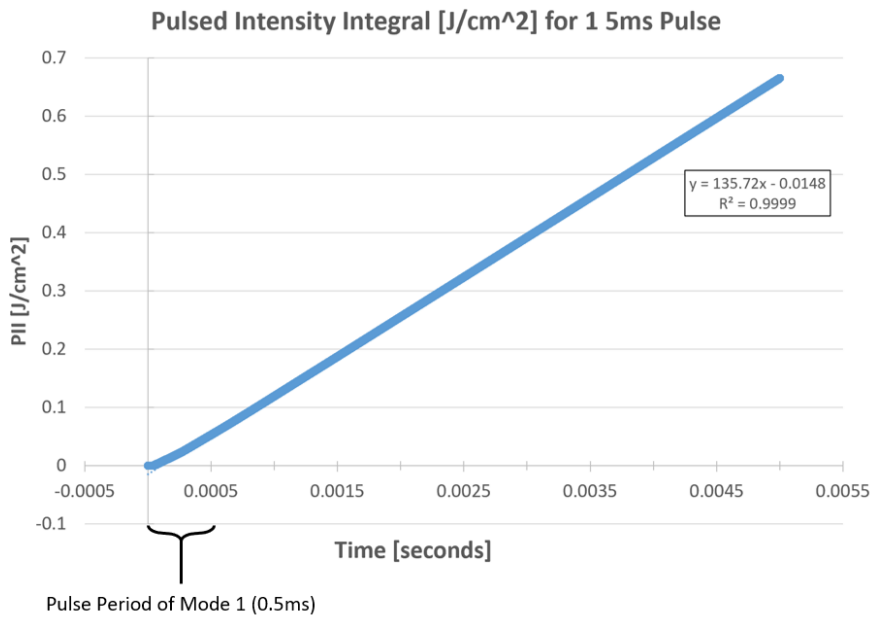


Figure 2-S8: Cumulative Pressure Over Time. Results from monitoring the pressure at the voxel of maximum intensity (see Figure 2) when simulating a 5ms pulse over the full course of that pulse. The simulation scheme is the through-skull scheme described in Methods. As demonstrated by an R^2 of effectively 1, the pressure experienced by the brain appears highly linear over the time period of this pulse. This suggests a highly similar pressure distribution over-time for both pulse lengths used here. Note the length of the shorter pulse (0.5ms) represented here.

**Group-Wide Activation from
Figure 6b in Subject Space**

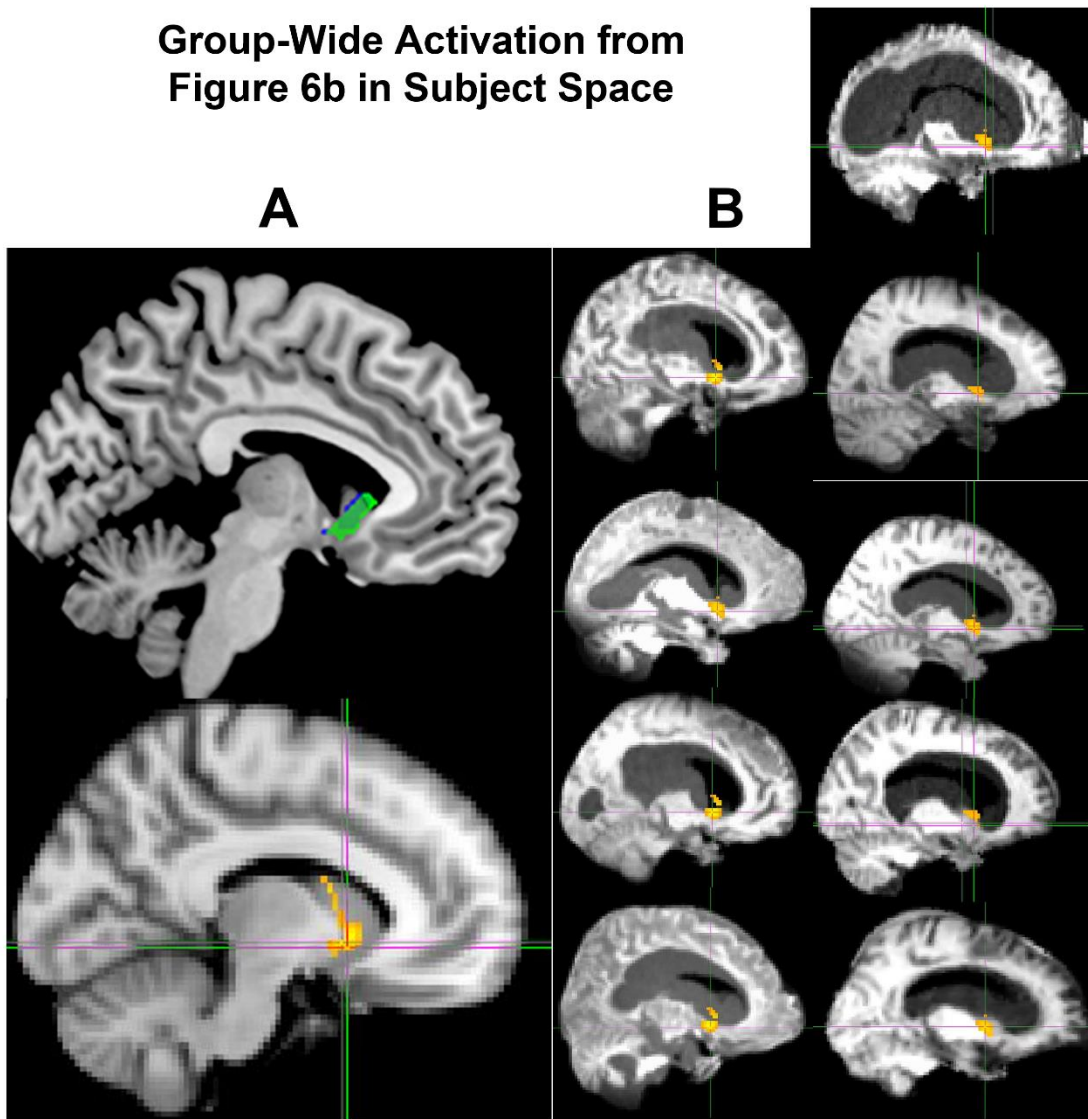


Figure 3-S1: Group Wide Activations in Subject Space. Here, the activation seen in Figure 6b, which represents changes in BOLD signal during LIFU blocks correlated with behavioral recovery, are shown in MNI(A bottom) and subject space(B). For reference the ventral striatum is shown in green (A, top) (Satterfield et al., 2019).

References

- Agnesi, F., Johnson, M. D., & Vitek, J. L. (2013). Chapter 4 - Deep brain stimulation: How does it work? In A. M. Lozano & M. Hallett (Eds.), *Handbook of Clinical Neurology* (Vol. 116, pp. 39–54). Elsevier. <https://doi.org/10.1016/B978-0-444-53497-2.00004-8>
- Aguirre, G. K., Detre, J. A., Zarahn, E., & Alsop, D. C. (2002). Experimental Design and the Relative Sensitivity of BOLD and Perfusion fMRI. *NeuroImage*, *15*(3), 488–500. <https://doi.org/10.1006/nimg.2001.0990>
- Ai, L., Mueller, J. K., Grant, A., Eryaman, Y., & Legon, W. (2016). Transcranial focused ultrasound for BOLD fMRI signal modulation in humans. *2016 38th Annual International Conference of the IEEE Engineering in Medicine and Biology Society (EMBC)*, 1758–1761. <https://doi.org/10.1109/EMBC.2016.7591057>
- Alkire, M. T., Asher, C. D., Franciscus, A. M., & Hahn, E. L. (2009). Thalamic microinfusion of antibody to a voltage-gated potassium channel restores consciousness during anesthesia. *Anesthesiology*, *110*(4), 766–773. <https://doi.org/10.1097/aln.0b013e31819c461c>
- Alkire, M. T., Hudetz, A. G., & Tononi, G. (2008). Consciousness and anesthesia. *Science (New York, N.Y.)*, *322*(5903), 876–880. <https://doi.org/10.1126/science.1149213>
- Alkire, M. T., McReynolds, J. R., Hahn, E. L., & Trivedi, A. N. (2007). Thalamic Microinjection of Nicotine Reverses Sevoflurane-induced Loss of Righting Reflex in the Rat. *Anesthesiology: The Journal of the American Society of Anesthesiologists*, *107*(2), 264–272. <https://doi.org/10.1097/01.anes.0000270741.33766.24>
- Annen, J., Filippini, M. M., Bonin, E., Cassol, H., Aubinet, C., Carrière, M., Gosseries, O., Thibaut, A., Barra, A., Wolff, A., Sanz, L. R. D., Martial, C., Laureys, S., & Chatelle, C. (2019). Diagnostic

- accuracy of the CRS-R index in patients with disorders of consciousness. *Brain Injury*, 33(11), 1409–1412. <https://doi.org/10.1080/02699052.2019.1644376>
- Badran, B. W., Caulfield, K., Stomberg-Firestein, S., Summers, P., Dowdle, L. T., Savoca, M., Li, X., Austelle, C. W., Short, B., Borckardt, J. J., Spivak, N., Bystritsky, A., & George, M. S. (2020). *Sonication of the Anterior Thalamus with MRI-Guided Low Intensity Focused Ultrasound Pulsation (LIFUP) Changes Pain Thresholds in Healthy Adults: A Double-Blind, Concurrent LIFUP/MRI Study* [Preprint]. *Pain Medicine*. <https://doi.org/10.1101/2020.04.08.20042853>
- Baek, H., Pahk, K. J., & Kim, H. (2017). A review of low-intensity focused ultrasound for neuromodulation. *Biomedical Engineering Letters*, 2(7), 135–142. <https://doi.org/10.1007/s13534-016-0007-y>
- Baker, J. L., Ryou, J.-W., Wei, X. F., Butson, C. R., Schiff, N. D., & Purpura, K. P. (2016). Robust modulation of arousal regulation, performance, and frontostriatal activity through central thalamic deep brain stimulation in healthy nonhuman primates. *Journal of Neurophysiology*, 116(5), 2383–2404. <https://doi.org/10.1152/jn.01129.2015>
- Bestmann, S., & Feredoes, E. (2013). Combined neurostimulation and neuroimaging in cognitive neuroscience: Past, present, and future. *Annals of the New York Academy of Sciences*, 1296, 11–30. <https://doi.org/10.1111/nyas.12110>
- Bestmann, S., & Walsh, V. (2017). Transcranial electrical stimulation. *Current Biology : CB*, 27(23), R1258–R1262. <https://doi.org/10.1016/j.cub.2017.11.001>
- Blackmore, J., Shrivastava, S., Sallet, J., Butler, C. R., & Cleveland, R. O. (2019). Ultrasound Neuromodulation: A Review of Results, Mechanisms and Safety. *Ultrasound in Medicine & Biology*, 45(7), 1509–1536. <https://doi.org/10.1016/j.ultrasmedbio.2018.12.015>
- Bolkan, S. S., Stujenske, J. M., Parnaudeau, S., Spellman, T. J., Rauffenbart, C., Abbas, A. I., Harris, A. Z., Gordon, J. A., & Kellendonk, C. (2017). Thalamic projections sustain prefrontal activity during

- working memory maintenance. *Nature Neuroscience*, 20(7), 987–996.
<https://doi.org/10.1038/nn.4568>
- Boly, M., Seth, A. K., Wilke, M., Ingmundson, P., Baars, B., Laureys, S., Edelman, D., & Tsuchiya, N. (2013). Consciousness in humans and non-human animals: Recent advances and future directions. *Frontiers in Psychology*, 4. <https://doi.org/10.3389/fpsyg.2013.00625>
- Brinker, S. T., Preiswerk, F., McDannold, N. J., Parker, K. L., & Mariano, T. Y. (2019). Virtual Brain Projection for Evaluating Trans-skull Beam Behavior of Transcranial Ultrasound Devices. *Ultrasound in Medicine & Biology*, 45(7), 1850–1856.
<https://doi.org/10.1016/j.ultrasmedbio.2019.03.009>
- Brunoni, A. R., Moffa, A. H., Fregni, F., Palm, U., Padberg, F., Blumberger, D. M., Daskalakis, Z. J., Bennabi, D., Haffen, E., Alonzo, A., & Loo, C. K. (2016). Transcranial direct current stimulation for acute major depressive episodes: Meta-analysis of individual patient data. *The British Journal of Psychiatry*, 208(6), 522–531. <https://doi.org/10.1192/bjp.bp.115.164715>
- Buzsáki, G. (2006). *Rhythms of the Brain*. Oxford University Press.
<https://doi.org/10.1093/acprof:oso/9780195301069.001.0001>
- Bystritsky, A., & Korb, A. S. (2015). A Review of Low-Intensity Transcranial Focused Ultrasound for Clinical Applications. *Current Behavioral Neuroscience Reports*, 2(2), 60–66.
<https://doi.org/10.1007/s40473-015-0039-0>
- Bystritsky, A., Korb, A. S., Douglas, P. K., Cohen, M. S., Melega, W. P., Mulgaonkar, A. P., DeSalles, A., Min, B.-K., & Yoo, S.-S. (2011). A review of low-intensity focused ultrasound pulsation. *Brain Stimulation*, 4(3), 125–136. <https://doi.org/10.1016/j.brs.2011.03.007>
- Cain, J. A., Spivak, N. M., Coetzee, J. P., Crone, J. S., Johnson, M. A., Lutkenhoff, E. S., Real, C., Buitrago-Blanco, M., Vespa, P. M., Schnakers, C., & Monti, M. M. (2021). Ultrasonic thalamic stimulation

- in chronic disorders of consciousness. *Brain Stimulation: Basic, Translational, and Clinical Research in Neuromodulation*, 14(2), 301–303. <https://doi.org/10.1016/j.brs.2021.01.008>
- Cain, J. A., Visagan, S., Johnson, M. A., Crone, J., Blades, R., Spivak, N. M., Shattuck, D. W., & Monti, M. M. (2021). Real time and delayed effects of subcortical low intensity focused ultrasound. *Scientific Reports*, 11(1), 6100. <https://doi.org/10.1038/s41598-021-85504-y>
- Carrera, E., & Tononi, G. (2014). Diaschisis: Past, present, future. *Brain: A Journal of Neurology*, 137(Pt 9), 2408–2422. <https://doi.org/10.1093/brain/awu101>
- Casarotto, S., Comanducci, A., Rosanova, M., Sarasso, S., Fecchio, M., Napolitani, M., Pigorini, A., G. Casali, A., Trimarchi, P. D., Boly, M., Gosseries, O., Bodart, O., Curto, F., Landi, C., Mariotti, M., Devalle, G., Laureys, S., Tononi, G., & Massimini, M. (2016). Stratification of unresponsive patients by an independently validated index of brain complexity. *Annals of Neurology*, 80(5), 718–729. <https://doi.org/10.1002/ana.24779>
- Castaigne, P., Lhermitte, F., Buge, A., Escourolle, R., Hauw, J. J., & Lyon-Caen, O. (1981). Paramedian thalamic and midbrain infarcts: Clinical and neuropathological study. *Annals of Neurology*, 10(2), 127–148. <https://doi.org/10.1002/ana.410100204>
- Chang, C., & Glover, G. H. (2009). Relationship between respiration, end-tidal CO₂, and BOLD signals in resting-state fMRI. *NeuroImage*, 47(4), 1381–1393. <https://doi.org/10.1016/j.neuroimage.2009.04.048>
- Chappell, M. A., Groves, A. R., Whitcher, B., & Woolrich, M. W. (2009). Variational Bayesian Inference for a Nonlinear Forward Model. *IEEE TRANSACTIONS ON SIGNAL PROCESSING*, 57(1). <https://ora.ox.ac.uk/objects/uuid:1e31142d-b892-4910-807f-7cf44f290a9b>
- Chen, M. C., Ferrari, L., Sacchet, M. D., Foland-Ross, L. C., Qiu, M.-H., Gotlib, I. H., Fuller, P. M., Arrigoni, E., & Lu, J. (2015). Identification of a direct GABAergic pallidocortical pathway in rodents. *The European Journal of Neuroscience*, 41(6), 748–759. <https://doi.org/10.1111/ejn.12822>

- Cho, S. B., Baars, B. J., & Newman, J. (1997). A Neural Global Workspace Model for Conscious Attention. *Neural Networks: The Official Journal of the International Neural Network Society*, *10*(7), 1195–1206. [https://doi.org/10.1016/s0893-6080\(97\)00060-9](https://doi.org/10.1016/s0893-6080(97)00060-9)
- Constantinople, C. M., & Bruno, R. M. (2011). Effects and mechanisms of wakefulness on local cortical networks. *Neuron*, *69*(6), 1061–1068. <https://doi.org/10.1016/j.neuron.2011.02.040>
- Crick, F. (1984). Function of the thalamic reticular complex: The searchlight hypothesis. *Proceedings of the National Academy of Sciences of the United States of America*, *81*(14), 4586–4590.
- Crick, F., & Koch, C. (1995). Are we aware of neural activity in primary visual cortex? *Nature*, *375*(6527), 121–123. <https://doi.org/10.1038/375121a0>
- Crone, J. S., Lutkenhoff, E. S., Bio, B. J., Laureys, S., & Monti, M. M. (2017). Testing Proposed Neuronal Models of Effective Connectivity Within the Cortico-basal Ganglia-thalamo-cortical Loop During Loss of Consciousness. *Cerebral Cortex*, *27*(4), 2727–2738. <https://doi.org/10.1093/cercor/bhw112>
- Crone, J. S., Soddu, A., Höller, Y., Vanhaudenhuyse, A., Schurz, M., Bergmann, J., Schmid, E., Trinka, E., Laureys, S., & Kronbichler, M. (2014). Altered network properties of the fronto-parietal network and the thalamus in impaired consciousness. *NeuroImage: Clinical*, *4*, 240–248. <https://doi.org/10.1016/j.nicl.2013.12.005>
- Dallapiazza, R. F., Timbie, K. F., Holmberg, S., Gatesman, J., Lopes, M. B., Price, R. J., Miller, G. W., & Elias, W. J. (2017). Noninvasive neuromodulation and thalamic mapping with low-intensity focused ultrasound. *Journal of Neurosurgery*, *128*(3), 875–884. <https://doi.org/10.3171/2016.11.JNS16976>
- Deffieux, T., & Konofagou, E. E. (2010). Numerical Study of a Simple Transcranial Focused Ultrasound System Applied to Blood-Brain Barrier Opening. *IEEE Transactions on Ultrasonics, Ferroelectrics, and Frequency Control*, *57*(12), 2637–2653. <https://doi.org/10.1109/TUFFC.2010.1738>

- Deng, Z.-D., Lisanby, S. H., & Peterchev, A. V. (2013). Electric field depth-focality tradeoff in transcranial magnetic stimulation: Simulation comparison of 50 coil designs. *Brain Stimulation*, *6*(1), 1–13.
<https://doi.org/10.1016/j.brs.2012.02.005>
- Di Perri, C., Bahri, M. A., Amico, E., Thibaut, A., Heine, L., Antonopoulos, G., Charland-Verville, V., Wannez, S., Gomez, F., Hustinx, R., Tshibanda, L., Demertzi, A., Soddu, A., & Laureys, S. (2016). Neural correlates of consciousness in patients who have emerged from a minimally conscious state: A cross-sectional multimodal imaging study. *The Lancet. Neurology*, *15*(8), 830–842.
[https://doi.org/10.1016/S1474-4422\(16\)00111-3](https://doi.org/10.1016/S1474-4422(16)00111-3)
- Donoghue, J. A., Bastos, A. M., Yanar, J., Kornblith, S., Mahnke, M., Brown, E. N., & Miller, E. K. (2019). *Neural signatures of loss of consciousness and its recovery by thalamic stimulation* [Preprint]. Neuroscience. <https://doi.org/10.1101/806687>
- Duck, F. A. (2007). Medical and non-medical protection standards for ultrasound and infrasound. *Progress in Biophysics and Molecular Biology*, *93*(1), 176–191.
<https://doi.org/10.1016/j.pbiomolbio.2006.07.008>
- Edelman, G. M., & Tononi, G. (2000). *A universe of consciousness: How matter becomes imagination* (pp. xiii, 274). Basic Books.
- Edwards, T. C., Zrinzo, L., Limousin, P., & Foltynie, T. (2012). Deep brain stimulation in the treatment of chorea. *Movement Disorders*, *27*(3), 357–363. <https://doi.org/10.1002/mds.23967>
- Eklund, A., Nichols, T. E., & Knutsson, H. (2016). Cluster failure: Why fMRI inferences for spatial extent have inflated false-positive rates. *Proceedings of the National Academy of Sciences of the United States of America*, *113*(28), 7900–7905. <https://doi.org/10.1073/pnas.1602413113>
- Fenoy, A. J., & Simpson, R. K. (2014). Risks of common complications in deep brain stimulation surgery: Management and avoidance. *Journal of Neurosurgery*, *120*(1), 132–139.
<https://doi.org/10.3171/2013.10.JNS131225>

- Fiebelkorn, I. C., & Kastner, S. (2019). A Rhythmic Theory of Attention. *Trends in Cognitive Sciences*, 23(2), 87–101. <https://doi.org/10.1016/j.tics.2018.11.009>
- Fingelkurts, A. A., Fingelkurts, A. A., Kivisaari, R., Pekkonen, E., Ilmoniemi, R. J., & Kähkönen, S. (2004). Enhancement of GABA-related signalling is associated with increase of functional connectivity in human cortex. *Human Brain Mapping*, 22(1), 27–39. <https://doi.org/10.1002/hbm.20014>
- Folloni, D., Verhagen, L., Mars, R. B., Fouragnan, E., Constans, C., Aubry, J.-F., Rushworth, M. F. S., & Sallet, J. (2018). *Manipulation of subcortical and deep cortical activity in the primate brain using transcranial focused ultrasound stimulation* [Preprint]. Neuroscience. <https://doi.org/10.1101/342303>
- Folloni, D., Verhagen, L., Mars, R. B., Fouragnan, E., Constans, C., Aubry, J.-F., Rushworth, M. F. S., & Sallet, J. (2019). Manipulation of Subcortical and Deep Cortical Activity in the Primate Brain Using Transcranial Focused Ultrasound Stimulation. *Neuron*, 101(6), 1109-1116.e5. <https://doi.org/10.1016/j.neuron.2019.01.019>
- Fouragnan, E. F., Chau, B. K. H., Folloni, D., Kolling, N., Verhagen, L., Klein-Flügge, M., Tankelevitch, L., Papageorgiou, G. K., Aubry, J.-F., Sallet, J., & Rushworth, M. F. S. (2019). The macaque anterior cingulate cortex translates counterfactual choice value into actual behavioral change. *Nature Neuroscience*, 22(5), 797–808. <https://doi.org/10.1038/s41593-019-0375-6>
- Friston, K. J., Buechel, C., Fink, G. R., Morris, J., Rolls, E., & Dolan, R. J. (1997). Psychophysiological and Modulatory Interactions in Neuroimaging. *NeuroImage*, 6(3), 218–229. <https://doi.org/10.1006/nimg.1997.0291>
- Fuller, P. M., Sherman, D., Pedersen, N. P., Saper, C. B., & Lu, J. (2011). Reassessment of the structural basis of the ascending arousal system. *The Journal of Comparative Neurology*, 519(5), 933–956. <https://doi.org/10.1002/cne.22559>

- Gaur, P., Casey, K. M., Kubanek, J., Li, N., Mohammadjavadi, M., Saenz, Y., Glover, G. H., Bouley, D. M., & Pauly, K. B. (2020). Histologic safety of transcranial focused ultrasound neuromodulation and magnetic resonance acoustic radiation force imaging in rhesus macaques and sheep. *Brain Stimulation, 13*(3), 804–814. <https://doi.org/10.1016/j.brs.2020.02.017>
- Giacino, J. T., Kalmar, K., & Whyte, J. (2004). The JFK Coma Recovery Scale-Revised: Measurement characteristics and diagnostic utility. *Archives of Physical Medicine and Rehabilitation, 85*(12), 2020–2029.
- Greenberg, B. D., Gabriels, L. A., Malone Jr, D. A., Rezai, A. R., Friehs, G. M., Okun, M. S., Shapira, N. A., Foote, K. D., Cosyns, P. R., Kubu, C. S., Malloy, P. F., Salloway, S. P., Giftakis, J. E., Rise, M. T., Machado, A. G., Baker, K. B., Stypulkowski, P. H., Goodman, W. K., Rasmussen, S. A., & Nuttin, B. J. (2010). Deep brain stimulation of the ventral internal capsule/ventral striatum for obsessive-compulsive disorder: Worldwide experience. *Molecular Psychiatry, 15*(1), 64–79. <https://doi.org/10.1038/mp.2008.55>
- Greve, D. N., & Fischl, B. (2009). Accurate and Robust Brain Image Alignment using Boundary-based Registration. *NeuroImage, 48*(1), 63–72. <https://doi.org/10.1016/j.neuroimage.2009.06.060>
- Grillner, S., Hellgren, J., Ménard, A., Saitoh, K., & Wikström, M. A. (2005). Mechanisms for selection of basic motor programs—Roles for the striatum and pallidum. *Trends in Neurosciences, 28*(7), 364–370. <https://doi.org/10.1016/j.tins.2005.05.004>
- Groves, A. R., Chappell, M. A., & Woolrich, M. W. (2009). Combined spatial and non-spatial prior for inference on MRI time-series. *NeuroImage, 45*(3), 795–809. <https://doi.org/10.1016/j.neuroimage.2008.12.027>
- Guldenmund, J. P., Demertzi, A., Boveroux, P., Boly, M., Vanhaudenhuyse, A., Bruno, M.-A., Gosseries, O., Noirhomme, Q., Brichant, J.-F., Bonhomme, V., Laureys, S., & Soddu, A. (2013). Thalamus,

- Brainstem and Salience Network Connectivity Changes During Propofol-Induced Sedation and Unconsciousness. *Brain Connectivity*, 3. <https://orbi.uliege.be/handle/2268/158733>
- Hajjar Ihab, Zhao Peng, Alsop David, & Novak Vera. (2010). Hypertension and Cerebral Vasoreactivity. *Hypertension*, 56(5), 859–864. <https://doi.org/10.1161/HYPERTENSIONAHA.110.160002>
- Hannawi, Y., Lindquist, M. A., Caffo, B. S., Sair, H. I., & Stevens, R. D. (2015). Resting brain activity in disorders of consciousness: A systematic review and meta-analysis. *Neurology*, 84(12), 1272–1280. <https://doi.org/10.1212/WNL.0000000000001404>
- Hofle, N., Paus, T., Reutens, D., Fiset, P., Gotman, J., Evans, A. C., & Jones, B. E. (1997). Regional Cerebral Blood Flow Changes as a Function of Delta and Spindle Activity during Slow Wave Sleep in Humans. *Journal of Neuroscience*, 17(12), 4800–4808. <https://doi.org/10.1523/JNEUROSCI.17-12-04800.1997>
- Honjoh, S., Sasai, S., Schiereck, S. S., Nagai, H., Tononi, G., & Cirelli, C. (2018). Regulation of cortical activity and arousal by the matrix cells of the ventromedial thalamic nucleus. *Nature Communications*, 9. <https://doi.org/10.1038/s41467-018-04497-x>
- Iglehart, C., Monti, M., Cain, J., Tourdias, T., & Saranathan, M. (2020). A systematic comparison of structural-, structural connectivity-, and functional connectivity-based thalamus parcellation techniques. *Brain Structure & Function*, 225(5), 1631–1642. <https://doi.org/10.1007/s00429-020-02085-8>
- Izadifar, Z., Izadifar, Z., Chapman, D., & Babyn, P. (2020). An Introduction to High Intensity Focused Ultrasound: Systematic Review on Principles, Devices, and Clinical Applications. *Journal of Clinical Medicine*, 9(2). <https://doi.org/10.3390/jcm9020460>
- Jech, R. (2008). Functional Imaging of Deep Brain Stimulation: FMRI, SPECT, and PET. In D. Tarsy, J. L. Vitek, P. A. Starr, & M. S. Okun (Eds.), *Deep Brain Stimulation in Neurological and Psychiatric Disorders* (pp. 179–201). Humana Press. https://doi.org/10.1007/978-1-59745-360-8_9

- Jenkinson, M., Bannister, P., Brady, M., & Smith, S. (2002). Improved optimization for the robust and accurate linear registration and motion correction of brain images. *NeuroImage*, *17*(2), 825–841. [https://doi.org/10.1016/s1053-8119\(02\)91132-8](https://doi.org/10.1016/s1053-8119(02)91132-8)
- Jenkinson, M., Beckmann, C. F., Behrens, T. E. J., Woolrich, M. W., & Smith, S. M. (2012). FSL. *NeuroImage*, *62*(2), 782–790. <https://doi.org/10.1016/j.neuroimage.2011.09.015>
- Jerath, R., & Beveridge, C. (2019). Multimodal Integration and Phenomenal Spatiotemporal Binding: A Perspective From the Default Space Theory. *Frontiers in Integrative Neuroscience*, *13*. <https://doi.org/10.3389/fnint.2019.00002>
- Jones, E. G. (2009). Synchrony in the Interconnected Circuitry of the Thalamus and Cerebral Cortex. *Annals of the New York Academy of Sciences*, *1157*(1), 10–23. <https://doi.org/10.1111/j.1749-6632.2009.04534.x>
- Jones, E. G. (2012). *The Thalamus*. Springer Science & Business Media.
- Kajimura, N., Uchiyama, M., Takayama, Y., Uchida, S., Uema, T., Kato, M., Sekimoto, M., Watanabe, T., Nakajima, T., Horikoshi, S., Ogawa, K., Nishikawa, M., Hiroki, M., Kudo, Y., Matsuda, H., Okawa, M., & Takahashi, K. (1999). Activity of Midbrain Reticular Formation and Neocortex during the Progression of Human Non-Rapid Eye Movement Sleep. *Journal of Neuroscience*, *19*(22), 10065–10073. <https://doi.org/10.1523/JNEUROSCI.19-22-10065.1999>
- Kass, R. E., & Raftery, A. E. (1995). Bayes Factors. *Journal of the American Statistical Association*, *90*(430), 773–795. JSTOR. <https://doi.org/10.2307/2291091>
- Kim, H.-C., Lee, W., Kunes, J., Yoon, K., Lee, J. E., Foley, L., Kowsari, K., & Yoo, S.-S. (2021). Transcranial focused ultrasound modulates cortical and thalamic motor activity in awake sheep. *Scientific Reports*, *11*(1), 19274. <https://doi.org/10.1038/s41598-021-98920-x>

- King, R. L., Brown, J. R., Newsome, W. T., & Pauly, K. B. (2013). Effective Parameters for Ultrasound-Induced In Vivo Neurostimulation. *Ultrasound in Medicine & Biology*, 39(2), 312–331.
<https://doi.org/10.1016/j.ultrasmedbio.2012.09.009>
- Kinomura, S., Larsson, J., Gulyás, B., & Roland, P. E. (1996). Activation by attention of the human reticular formation and thalamic intralaminar nuclei. *Science (New York, N.Y.)*, 271(5248), 512–515.
- Kolmac, C., & Mitrofanis, J. (1999). Organization of the basal forebrain projection to the thalamus in rats. *Neuroscience Letters*, 272(3), 151–154. [https://doi.org/10.1016/s0304-3940\(99\)00614-x](https://doi.org/10.1016/s0304-3940(99)00614-x)
- Kubaneck, J. (2018). Neuromodulation with transcranial focused ultrasound. *Neurosurgical Focus*, 44(2), E14. <https://doi.org/10.3171/2017.11.FOCUS17621>
- Lanciego, J. L., Luquin, N., & Obeso, J. A. (2012). Functional Neuroanatomy of the Basal Ganglia. *Cold Spring Harbor Perspectives in Medicine*, 2(12). <https://doi.org/10.1101/cshperspect.a009621>
- Laureys, S. (2005). The neural correlate of (un)awareness: Lessons from the vegetative state. *Trends in Cognitive Sciences*, 9(12), 556–559. <https://doi.org/10.1016/j.tics.2005.10.010>
- Laureys, S., Faymonville, M., Luxen, A., Lamy, M., Franck, G., & Maquet, P. (2000). Restoration of thalamocortical connectivity after recovery from persistent vegetative state. *The Lancet*, 355(9217), 1790–1791. [https://doi.org/10.1016/S0140-6736\(00\)02271-6](https://doi.org/10.1016/S0140-6736(00)02271-6)
- Laureys, S., Goldman, S., Phillips, C., Van Bogaert, P., Aerts, J., Luxen, A., Franck, G., & Maquet, P. (1999). Impaired Effective Cortical Connectivity in Vegetative State: Preliminary Investigation Using PET. *NeuroImage*, 9(4), 377–382. <https://doi.org/10.1006/nimg.1998.0414>
- Lee, W., Kim, H., Jung, Y., Song, I.-U., Chung, Y. A., & Yoo, S.-S. (2015). Image-Guided Transcranial Focused Ultrasound Stimulates Human Primary Somatosensory Cortex. *Scientific Reports*, 5. <https://doi.org/10.1038/srep08743>

- Lee, W., Kim, H.-C., Jung, Y., Chung, Y. A., Song, I.-U., Lee, J.-H., & Yoo, S.-S. (2016). Transcranial focused ultrasound stimulation of human primary visual cortex. *Scientific Reports*, *6*, 34026.
<https://doi.org/10.1038/srep34026>
- Lee, W., Kim, S., Kim, B., Lee, C., Chung, Y. A., Kim, L., & Yoo, S.-S. (2017). Non-invasive transmission of sensorimotor information in humans using an EEG/focused ultrasound brain-to-brain interface. *PLOS ONE*, *12*(6), e0178476. <https://doi.org/10.1371/journal.pone.0178476>
- Legon, W., Ai, L., Bansal, P., & Mueller, J. K. (2018). Neuromodulation with single-element transcranial focused ultrasound in human thalamus. *Human Brain Mapping*, *39*(5), 1995–2006.
<https://doi.org/10.1002/hbm.23981>
- Legon, W., Sato, T. F., Opitz, A., Mueller, J., Barbour, A., Williams, A., & Tyler, W. J. (2014). Transcranial focused ultrasound modulates the activity of primary somatosensory cortex in humans. *Nature Neuroscience*, *17*(2), 322–329. <https://doi.org/10.1038/nn.3620>
- Liu, J., Lee, H. J., Weitz, A. J., Fang, Z., Lin, P., Choy, M., Fisher, R., Pinskiy, V., Tolpygo, A., Mitra, P., Schiff, N., & Lee, J. H. (2015). Frequency-selective control of cortical and subcortical networks by central thalamus. *eLife*, *4*, e09215. <https://doi.org/10.7554/eLife.09215>
- Logothetis, N. K., Pauls, J., Augath, M., Trinath, T., & Oeltermann, A. (2001). Neurophysiological investigation of the basis of the fMRI signal. *Nature*, *412*(6843), 150–157.
<https://doi.org/10.1038/35084005>
- Luppi, A. I., Cain, J., Spindler, L. R. B., Górska, U. J., Toker, D., Hudson, A. E., Brown, E. N., Diringier, M. N., Stevens, R. D., Massimini, M., Monti, M. M., Stamatakis, E. A., Boly, M., & the Curing Coma Campaign and Its Contributing Collaborators. (2021). Mechanisms Underlying Disorders of Consciousness: Bridging Gaps to Move Toward an Integrated Translational Science. *Neurocritical Care*, *35*(1), 37–54. <https://doi.org/10.1007/s12028-021-01281-6>

- Luppi, A. I., Craig, M. M., Pappas, I., Finoia, P., Williams, G. B., Allanson, J., Pickard, J. D., Owen, A. M., Naci, L., Menon, D. K., & Stamatakis, E. A. (2019). Consciousness-specific dynamic interactions of brain integration and functional diversity. *Nature Communications*, *10*(1), 4616. <https://doi.org/10.1038/s41467-019-12658-9>
- Lutkenhoff, E. S., Chiang, J., Tshibanda, L., Kamau, E., Kirsch, M., Pickard, J. D., Laureys, S., Owen, A. M., & Monti, M. M. (2015). Thalamic and extrathalamic mechanisms of consciousness after severe brain injury. *Annals of Neurology*, *78*(1), 68–76. <https://doi.org/10.1002/ana.24423>
- Lutkenhoff, E. S., Johnson, M. A., Casarotto, S., Massimini, M., & Monti, M. M. (2020). Subcortical atrophy correlates with the perturbational complexity index in patients with disorders of consciousness. *Brain Stimulation: Basic, Translational, and Clinical Research in Neuromodulation*, *13*(5), 1426–1435. <https://doi.org/10.1016/j.brs.2020.07.012>
- Lutkenhoff, E. S., McArthur, D. L., Hua, X., Thompson, P. M., Vespa, P. M., & Monti, M. M. (2013). Thalamic atrophy in antero-medial and dorsal nuclei correlates with six-month outcome after severe brain injury. *NeuroImage. Clinical*, *3*, 396–404. <https://doi.org/10.1016/j.nicl.2013.09.010>
- Lutkenhoff, E. S., Rosenberg, M., Chiang, J., Zhang, K., Pickard, J. D., Owen, A. M., & Monti, M. M. (2014). Optimized Brain Extraction for Pathological Brains (optiBET). *PLOS ONE*, *9*(12), e115551. <https://doi.org/10.1371/journal.pone.0115551>
- Lutkenhoff, E. S., Wright, M. J., Shrestha, V., Real, C., McArthur, D. L., Buitrago-Blanco, M., Vespa, P. M., & Monti, M. M. (2020). The subcortical basis of outcome and cognitive impairment in TBI: A longitudinal cohort study. *Neurology*, *95*(17), e2398–e2408. <https://doi.org/10.1212/WNL.0000000000010825>
- Magrassi, L., Maggioni, G., Pistarini, C., Di Perri, C., Bastianello, S., Zippo, A. G., Iotti, G. A., Biella, G. E. M., & Imberti, R. (2016). Results of a prospective study (CATS) on the effects of thalamic

- stimulation in minimally conscious and vegetative state patients. *Journal of Neurosurgery*, 125(4), 972–981. <https://doi.org/10.3171/2015.7.JNS15700>
- Mair, R. G., Onos, K. D., & Hembrook, J. R. (2011). Cognitive Activation by Central Thalamic Stimulation: The Yerkes-Dodson Law Revisited. *Dose-Response*, 9(3), dose-response.10-017.Mair. <https://doi.org/10.2203/dose-response.10-017.Mair>
- Min, B.-K., Bystritsky, A., Jung, K.-I., Fischer, K., Zhang, Y., Maeng, L.-S., In Park, S., Chung, Y.-A., Jolesz, F. A., & Yoo, S.-S. (2011). Focused ultrasound-mediated suppression of chemically-induced acute epileptic EEG activity. *BMC Neuroscience*, 12, 23. <https://doi.org/10.1186/1471-2202-12-23>
- Min, B.-K., Yang, P. S., Bohlke, M., Park, S., R.Vago, D., Maher, T. J., & Yoo, S.-S. (2011). Focused ultrasound modulates the level of cortical neurotransmitters: Potential as a new functional brain mapping technique. *International Journal of Imaging Systems and Technology*, 21(2), 232–240. <https://doi.org/10.1002/ima.20284>
- Min, H.-K., Hwang, S.-C., Marsh, M. P., Kim, I., Knight, E., Striemer, B., Felmlee, J. P., Welker, K. M., Blaha, C. D., Chang, S.-Y., Bennet, K. E., & Lee, K. H. (2012). Deep brain stimulation induces BOLD activation in motor and non-motor networks: An fMRI comparison study of STN and EN/GPi DBS in large animals. *NeuroImage*, 63(3), 1408–1420. <https://doi.org/10.1016/j.neuroimage.2012.08.006>
- Mitchell, A. S., & Chakraborty, S. (2013). What does the mediodorsal thalamus do? *Frontiers in Systems Neuroscience*, 7. <https://doi.org/10.3389/fnsys.2013.00037>
- Monti, M. M. (2011). Statistical Analysis of fMRI Time-Series: A Critical Review of the GLM Approach. *Frontiers in Human Neuroscience*, 5. <https://doi.org/10.3389/fnhum.2011.00028>
- Monti, M. M., Laureys, S., & Owen, A. M. (2010). The vegetative state. *BMJ (Clinical Research Ed.)*, 341, c3765. <https://doi.org/10.1136/bmj.c3765>

- Monti, M. M., & Sannita, W. G. (Eds.). (2016). *Brain Function and Responsiveness in Disorders of Consciousness*. Springer International Publishing.
<https://www.springer.com/us/book/9783319214245>
- Monti, M. M., Schnakers, C., Korb, A. S., Bystritsky, A., & Vespa, P. M. (2016). Non-Invasive Ultrasonic Thalamic Stimulation in Disorders of Consciousness after Severe Brain Injury: A First-in-Man Report. *Brain Stimulation*, *9*(6), 940–941. <https://doi.org/10.1016/j.brs.2016.07.008>
- Mueller, J. K., Ai, L., Bansal, P., & Legon, W. (2017). Numerical evaluation of the skull for human neuromodulation with transcranial focused ultrasound. *Journal of Neural Engineering*, *14*(6), 066012. <https://doi.org/10.1088/1741-2552/aa843e>
- Murphy, M., Bruno, M.-A., Riedner, B. A., Boveroux, P., Noirhomme, Q., Landsness, E. C., Brichant, J.-F., Phillips, C., Massimini, M., Laureys, S., Tononi, G., & Boly, M. (2011). Propofol Anesthesia and Sleep: A High-Density EEG Study. *Sleep*, *34*(3), 283–291.
- Nagai, Y., Critchley, H. D., Featherstone, E., Fenwick, P. B. C., Trimble, M. R., & Dolan, R. J. (2004). Brain activity relating to the contingent negative variation: An fMRI investigation. *NeuroImage*, *21*(4), 1232–1241. <https://doi.org/10.1016/j.neuroimage.2003.10.036>
- Naito, E., Kinomura, S., Geyer, S., Kawashima, R., Roland, P. E., & Zilles, K. (2000). Fast reaction to different sensory modalities activates common fields in the motor areas, but the anterior cingulate cortex is involved in the speed of reaction. *Journal of Neurophysiology*, *83*(3), 1701–1709. <https://doi.org/10.1152/jn.2000.83.3.1701>
- Parvizi, J., & Damasio, A. (2001). Consciousness and the brainstem. *Cognition*, *79*(1–2), 135–160.
[https://doi.org/10.1016/s0010-0277\(00\)00127-x](https://doi.org/10.1016/s0010-0277(00)00127-x)
- Pasquinelli, C., Hanson, L. G., Siebner, H. R., Lee, H. J., & Thielscher, A. (2019). Safety of transcranial focused ultrasound stimulation: A systematic review of the state of knowledge from both

- human and animal studies. *Brain Stimulation*, 12(6), 1367–1380.
<https://doi.org/10.1016/j.brs.2019.07.024>
- Paus, T. (2000). Functional anatomy of arousal and attention systems in the human brain. *Progress in Brain Research*, 126, 65–77. [https://doi.org/10.1016/S0079-6123\(00\)26007-X](https://doi.org/10.1016/S0079-6123(00)26007-X)
- Pergola, G., Danet, L., Pitel, A.-L., Carlesimo, G. A., Segobin, S., Pariente, J., Suchan, B., Mitchell, A. S., & Barbeau, E. J. (2018). The Regulatory Role of the Human Mediodorsal Thalamus. *Trends in Cognitive Sciences*, 22(11), 1011–1025. <https://doi.org/10.1016/j.tics.2018.08.006>
- Pichardo, S., Milleret, R., Curiel, L., Pichot, O., & Chapelon, J.-Y. (2006). In vitro experimental study on the treatment of superficial venous insufficiency with high-intensity focused ultrasound. *Ultrasound in Medicine & Biology*, 32(6), 883–891.
<https://doi.org/10.1016/j.ultrasmedbio.2006.02.1419>
- Pistoia, F., Mura, E., Govoni, S., Fini, M., & Sarà, M. (2010). Awakenings and awareness recovery in disorders of consciousness: Is there a role for drugs? *CNS Drugs*, 24(8), 625–638.
<https://doi.org/10.2165/11535940-000000000-00000>
- Pistoia, F., Sara, M., Sacco, S., Franceschini, M., & Carolei, A. (2014). Silencing the Brain May be Better than Stimulating it. The GABA Effect. *Current Pharmaceutical Design*, 20(26), 4154–4166.
- Plaksin, M., Kimmel, E., & Shoham, S. (2016). Cell-Type-Selective Effects of Intramembrane Cavitation as a Unifying Theoretical Framework for Ultrasonic Neuromodulation. *ENeuro*, 3(3).
<https://doi.org/10.1523/ENEURO.0136-15.2016>
- Plaksin, M., Shoham, S., & Kimmel, E. (2014). Intramembrane Cavitation as a Predictive Bio-Piezoelectric Mechanism for Ultrasonic Brain Stimulation. *Physical Review X*, 4(1), 011004.
<https://doi.org/10.1103/PhysRevX.4.011004>
- Powers, W. J., Grubb, R. L., Darriet, D., & Raichle, M. E. (1985). Cerebral blood flow and cerebral metabolic rate of oxygen requirements for cerebral function and viability in humans. *Journal of*

- Cerebral Blood Flow and Metabolism: Official Journal of the International Society of Cerebral Blood Flow and Metabolism*, 5(4), 600–608. <https://doi.org/10.1038/jcbfm.1985.89>
- Qiu, M.-H., Vetrivelan, R., Fuller, P. M., & Lu, J. (2010). Basal ganglia control of sleep-wake behavior and cortical activation. *The European Journal of Neuroscience*, 31(3), 499–507. <https://doi.org/10.1111/j.1460-9568.2009.07062.x>
- Qiu, M.-H., Yao, Q.-L., Vetrivelan, R., Chen, M. C., & Lu, J. (2016). Nigrostriatal Dopamine Acting on Globus Pallidus Regulates Sleep. *Cerebral Cortex*, 26(4), 1430–1439. <https://doi.org/10.1093/cercor/bhu241>
- Redinbaugh, M. J., Phillips, J. M., Kambi, N. A., Mohanta, S., Andryk, S., Dooley, G. L., Afrasiabi, M., Raz, A., & Saalman, Y. B. (2019). Central thalamus modulates consciousness by controlling layer-specific cortical interactions. *BioRxiv*, 776591. <https://doi.org/10.1101/776591>
- Redinbaugh, M. J., Phillips, J. M., Kambi, N. A., Mohanta, S., Andryk, S., Dooley, G. L., Afrasiabi, M., Raz, A., & Saalman, Y. B. (2020). Thalamus Modulates Consciousness via Layer-Specific Control of Cortex. *Neuron*, 106(1), 66-75.e12. <https://doi.org/10.1016/j.neuron.2020.01.005>
- Robertson, J. L. B., Cox, B. T., Jaros, J., & Treeby, B. E. (2017). Accurate simulation of transcranial ultrasound propagation for ultrasonic neuromodulation and stimulation. *The Journal of the Acoustical Society of America*, 141(3), 1726–1738. <https://doi.org/10.1121/1.4976339>
- Saalman, Y. B. (2014). Intralaminar and medial thalamic influence on cortical synchrony, information transmission and cognition. *Frontiers in Systems Neuroscience*, 8. <https://doi.org/10.3389/fnsys.2014.00083>
- Saalman, Y. B., & Kastner, S. (2009). Gain control in the visual thalamus during perception and cognition. *Current Opinion in Neurobiology*, 19(4), 408–414. <https://doi.org/10.1016/j.conb.2009.05.007>

- Saalmann, Y. B., & Kastner, S. (2015). The cognitive thalamus. *Frontiers in Systems Neuroscience*, 9. <https://doi.org/10.3389/fnsys.2015.00039>
- Saalmann, Y. B., Pinsk, M. A., Wang, L., Li, X., & Kastner, S. (2012). Pulvinar regulates information transmission between cortical areas based on attention demands. *Science (New York, N.Y.)*, 337(6095), 753–756. <https://doi.org/10.1126/science.1223082>
- Sanguinetti, J. L., Hameroff, S., Smith, E. E., Sato, T., Daft, C. M. W., Tyler, W. J., & Allen, J. J. B. (2020). Transcranial Focused Ultrasound to the Right Prefrontal Cortex Improves Mood and Alters Functional Connectivity in Humans. *Frontiers in Human Neuroscience*, 14. <https://doi.org/10.3389/fnhum.2020.00052>
- Saper, C. B., & Fuller, P. M. (2017). Wake-Sleep Circuitry: An Overview. *Current Opinion in Neurobiology*, 44, 186–192. <https://doi.org/10.1016/j.conb.2017.03.021>
- Sato, T., Shapiro, M. G., & Tsao, D. Y. (2018). Ultrasonic Neuromodulation Causes Widespread Cortical Activation via an Indirect Auditory Mechanism. *Neuron*, 98(5), 1031-1041.e5. <https://doi.org/10.1016/j.neuron.2018.05.009>
- Saunders, A., Oldenburg, I. A., Berezovskii, V. K., Johnson, C. A., Kingery, N. D., Elliott, H. L., Xie, T., Gerfen, C. R., & Sabatini, B. L. (2015). A direct GABAergic output from the basal ganglia to frontal cortex. *Nature*, 521(7550), 85–89. <https://doi.org/10.1038/nature14179>
- Schiff, N. D. (2008). Central thalamic contributions to arousal regulation and neurological disorders of consciousness. *Annals of the New York Academy of Sciences*, 1129, 105–118. <https://doi.org/10.1196/annals.1417.029>
- Schiff, N. D. (2010a). Recovery of consciousness after brain injury: A mesocircuit hypothesis. *Trends in Neurosciences*, 33(1), 1–9. <https://doi.org/10.1016/j.tins.2009.11.002>
- Schiff, N. D. (2010b). Recovery of consciousness after brain injury: A mesocircuit hypothesis. *Trends in Neurosciences*, 33(1), 1–9. <https://doi.org/10.1016/j.tins.2009.11.002>

- Schiff, N. D., Giacino, J. T., Kalmar, K., Victor, J. D., Baker, K., Gerber, M., Fritz, B., Eisenberg, B., O'Connor, J., Kobylarz, E. J., Farris, S., Machado, A., McCagg, C., Plum, F., Fins, J. J., & Rezai, A. R. (2007). Behavioural improvements with thalamic stimulation after severe traumatic brain injury. *Nature*, *448*(7153), 600–603. <https://doi.org/10.1038/nature06041>
- Schiff, N. D., Shah, S. A., Hudson, A. E., Nauvel, T., Kalik, S. F., & Purpura, K. P. (2012). Gating of attentional effort through the central thalamus. *Journal of Neurophysiology*, *109*(4), 1152–1163. <https://doi.org/10.1152/jn.00317.2011>
- Schmitt, L. I., Wimmer, R. D., Nakajima, M., Happ, M., Mofakham, S., & Halassa, M. M. (2017). Thalamic amplification of cortical connectivity sustains attentional control. *Nature*, *545*(7653), 219–223. <https://doi.org/10.1038/nature22073>
- Schnakers, C., & Monti, M. M. (2017). Disorders of consciousness after severe brain injury: Therapeutic options. *Current Opinion in Neurology*, *30*(6), 573–579. <https://doi.org/10.1097/WCO.0000000000000495>
- Schrock, L. E., Mink, J. W., Woods, D. W., Porta, M., Servello, D., Visser-Vandewalle, V., Silburn, P. A., Foltynie, T., Walker, H. C., Shahed-Jimenez, J., Savica, R., Klassen, B. T., Machado, A. G., Foote, K. D., Zhang, J.-G., Hu, W., Ackermans, L., Temel, Y., Mari, Z., ... Okun, M. S. (2015). Tourette syndrome deep brain stimulation: A review and updated recommendations. *Movement Disorders*, *30*(4), 448–471. <https://doi.org/10.1002/mds.26094>
- Smith, J. C., Paulson, E. S., Cook, D. B., Verber, M. D., & Tian, Q. (2010). Detecting changes in human cerebral blood flow after acute exercise using arterial spin labeling: Implications for fMRI. *Journal of Neuroscience Methods*, *191*(2), 258–262. <https://doi.org/10.1016/j.jneumeth.2010.06.028>
- Smith, S. M., Jenkinson, M., Woolrich, M. W., Beckmann, C. F., Behrens, T. E. J., Johansen-Berg, H., Bannister, P. R., De Luca, M., Drobnjak, I., Flitney, D. E., Niazy, R. K., Saunders, J., Vickers, J.,

- Zhang, Y., De Stefano, N., Brady, J. M., & Matthews, P. M. (2004). Advances in functional and structural MR image analysis and implementation as FSL. *NeuroImage*, *23 Suppl 1*, S208-219. <https://doi.org/10.1016/j.neuroimage.2004.07.051>
- Smith, S. M., & Nichols, T. E. (2009). Threshold-free cluster enhancement: Addressing problems of smoothing, threshold dependence and localisation in cluster inference. *NeuroImage*, *44*(1), 83–98. <https://doi.org/10.1016/j.neuroimage.2008.03.061>
- Spitzer, V. M., & Whitlock, D. G. (1998). The visible human dataset: The anatomical platform for human simulation. *The Anatomical Record*, *253*(2), 49–57. [https://doi.org/10.1002/\(SICI\)1097-0185\(199804\)253:2<49::AID-AR8>3.0.CO;2-9](https://doi.org/10.1002/(SICI)1097-0185(199804)253:2<49::AID-AR8>3.0.CO;2-9)
- Steriade, M., & Timofeev, I. (2003). Neuronal plasticity in thalamocortical networks during sleep and waking oscillations. *Neuron*, *37*(4), 563–576. [https://doi.org/10.1016/s0896-6273\(03\)00065-5](https://doi.org/10.1016/s0896-6273(03)00065-5)
- Stern, J. M., Spivak, N. M., Becerra, S. A., Kuhn, T. P., Korb, A. S., Kronemyer, D., Khanlou, N., Reyes, S. D., Monti, M. M., Schnakers, C., Walshaw, P., Keselman, I., Cohen, M. S., Yong, W., Fried, I., Jordan, S. E., Schafer, M. E., Engel, J., & Bystritsky, A. (2021). Safety of focused ultrasound neuromodulation in humans with temporal lobe epilepsy. *Brain Stimulation*, *14*(4), 1022–1031. <https://doi.org/10.1016/j.brs.2021.06.003>
- Thibaut, A., Wannez, S., Donneau, A.-F., Chatelle, C., Gosseries, O., Bruno, M.-A., & Laureys, S. (2017). Controlled clinical trial of repeated prefrontal tDCS in patients with chronic minimally conscious state. *Brain Injury*, *31*(4), 466–474. <https://doi.org/10.1080/02699052.2016.1274776>
- Treeby, B. E., & Cox, B. T. (2010). k-Wave: MATLAB toolbox for the simulation and reconstruction of photoacoustic wave fields. *Journal of Biomedical Optics*, *15*(2), 021314. <https://doi.org/10.1117/1.3360308>
- Tyler, W. J. (2011). Noninvasive Neuromodulation with Ultrasound? A Continuum Mechanics Hypothesis. *The Neuroscientist*, *17*(1), 25–36. <https://doi.org/10.1177/1073858409348066>

- Vanderwolf, C. H., & Stewart, D. J. (1988). Thalamic control of neocortical activation: A critical re-evaluation. *Brain Research Bulletin*, 20(4), 529–538. [https://doi.org/10.1016/0361-9230\(88\)90143-8](https://doi.org/10.1016/0361-9230(88)90143-8)
- Verhagen, L., Gallea, C., Folloni, D., Constans, C., Jensen, D. E., Ahnine, H., Roumazeilles, L., Santin, M., Ahmed, B., Lehericy, S., Klein-Flügge, M. C., Krug, K., Mars, R. B., Rushworth, M. F., Pouget, P., Aubry, J.-F., & Sallet, J. (2019). Offline impact of transcranial focused ultrasound on cortical activation in primates. *eLife*, 8, e40541. <https://doi.org/10.7554/eLife.40541>
- Ward, L. M. (2011). The thalamic dynamic core theory of conscious experience. *Consciousness and Cognition*, 20(2), 464–486. <https://doi.org/10.1016/j.concog.2011.01.007>
- Weiler, M., Casseb, R. F., Campos, B. M. de, Crone, J. S., Lutkenhoff, E. S., Monti, M. M., & Vespa, P. M. (2021). *Evaluating denoising strategies in resting-state fMRI in traumatic brain injury (EpiBioS4Rx)* (p. 2021.12.10.472139). <https://doi.org/10.1101/2021.12.10.472139>
- White, P. J., Clement, G. T., & Hynynen, K. (2006). Longitudinal and shear mode ultrasound propagation in human skull bone. *Ultrasound in Medicine & Biology*, 32(7), 1085–1096. <https://doi.org/10.1016/j.ultrasmedbio.2006.03.015>
- Whyte, J., Nakase-Richardson, R., Hammond, F. M., McNamee, S., Giacino, J. T., Kalmar, K., Greenwald, B. D., Yablon, S. A., & Horn, L. J. (2013). Functional Outcomes in Traumatic Disorders of Consciousness: 5-Year Outcomes From the National Institute on Disability and Rehabilitation Research Traumatic Brain Injury Model Systems. *Archives of Physical Medicine and Rehabilitation*, 94(10), 1855–1860. <https://doi.org/10.1016/j.apmr.2012.10.041>
- Winkler, A. M., Ridgway, G. R., Webster, M. A., Smith, S. M., & Nichols, T. E. (2014). Permutation inference for the general linear model. *NeuroImage*, 92, 381–397. <https://doi.org/10.1016/j.neuroimage.2014.01.060>

- Wise, E. S., & Treeby, B. E. (2013). Full-wave nonlinear ultrasound simulation in an axisymmetric coordinate system using the discrete sine and cosine transforms. *2013 IEEE International Ultrasonics Symposium (IUS)*, 1374–1377. <https://doi.org/10.1109/ULTSYM.2013.0349>
- Woo, C.-W., Krishnan, A., & Wager, T. D. (2014). Cluster-extent based thresholding in fMRI analyses: Pitfalls and recommendations. *NeuroImage*, *91*, 412–419. <https://doi.org/10.1016/j.neuroimage.2013.12.058>
- Xia, X., Fomenko, A., Nankoo, J.-F., Zeng, K., Wang, Y., Zhang, J., Lozano, A. M., & Chen, R. (2021). Time course of the effects of low-intensity transcranial ultrasound on the excitability of ipsilateral and contralateral human primary motor cortex. *NeuroImage*, *243*, 118557. <https://doi.org/10.1016/j.neuroimage.2021.118557>
- Yang, P. S., Kim, H., Lee, W., Bohlke, M., Park, S., Maher, T. J., & Yoo, S.-S. (2012). Transcranial Focused Ultrasound to the Thalamus Is Associated with Reduced Extracellular GABA Levels in Rats. *Neuropsychobiology*, *65*(3), 153–160. <https://doi.org/10.1159/000336001>
- Yerkes, R. M., & Dodson, J. D. (1908). The relation of strength of stimulus to rapidity of habit-formation. *Journal of Comparative Neurology and Psychology*, *18*(5), 459–482. <https://doi.org/10.1002/cne.920180503>
- Yoo, S.-S., Bystritsky, A., Lee, J.-H., Zhang, Y., Fischer, K., Min, B.-K., McDannold, N. J., Pascual-Leone, A., & Jolesz, F. A. (2011). Focused ultrasound modulates region-specific brain activity. *NeuroImage*, *56*(3), 1267–1275. <https://doi.org/10.1016/j.neuroimage.2011.02.058>
- Yoo, S.-S., Kim, H., Min, B.-K., & Eric Franck, S. P. (2011). Transcranial Focused Ultrasound to the Thalamus Alters Anesthesia Time in Rats. *Neuroreport*, *22*(15), 783–787. <https://doi.org/10.1097/WNR.0b013e32834b2957>

- Yoon, K., Lee, W., Lee, J. E., Xu, L., Croce, P., Foley, L., & Yoo, S.-S. (2019). Effects of sonication parameters on transcranial focused ultrasound brain stimulation in an ovine model. *PLOS ONE*, *14*(10), e0224311. <https://doi.org/10.1371/journal.pone.0224311>
- Yuan, X.-S., Wang, L., Dong, H., Qu, W.-M., Yang, S.-R., Cherasse, Y., Lazarus, M., Schiffmann, S. N., d'Exaerde, A. de K., Li, R.-X., & Huang, Z.-L. (2017). Striatal adenosine A2A receptor neurons control active-period sleep via parvalbumin neurons in external globus pallidus. *ELife*, *6*, e29055. <https://doi.org/10.7554/eLife.29055>
- Zhang, B., O'Brien, K., Won, W., & Li, S. (2021). A Retrospective Analysis on Clinical Practice-Based Approaches Using Zolpidem and Lorazepam in Disorders of Consciousness. *Brain Sciences*, *11*(6), 726. <https://doi.org/10.3390/brainsci11060726>
- Zhang, Y., Ren, L., Liu, K., Tong, S., Yuan, T.-F., & Sun, J. (2021). Transcranial ultrasound stimulation of the human motor cortex. *iScience*, *24*(12), 103429. <https://doi.org/10.1016/j.isci.2021.103429>
- Zheng, Z. S., & Monti, M. M. (2019). Thalamic and extra-thalamic connections of the Globus Pallidus in the human brain: The ultradirect pathway. *BioRxiv*, 688283. <https://doi.org/10.1101/688283>
- Zheng, Z. S., Reggente, N., Lutkenhoff, E., Owen, A. M., & Monti, M. M. (2017). Disentangling disorders of consciousness: Insights from diffusion tensor imaging and machine learning. *Human Brain Mapping*, *38*(1), 431–443. <https://doi.org/10.1002/hbm.23370>
- Zhou, J., Liu, X., Song, W., Yang, Y., Zhao, Z., Ling, F., Hudetz, A. G., & Li, S.-J. (2011). Specific and Nonspecific Thalamocortical Functional Connectivity in Normal and Vegetative States. *Consciousness and Cognition*, *20*(2), 257–268. <https://doi.org/10.1016/j.concog.2010.08.003>
- Zielinski, M., Mahdavi, K., Jordan, S., Haroon, J., Habelhah, B., Beccera, S., Spivak, N., Kuhn, T., & Bystrisky, A. (2021). A case study of low-intensity focused ultrasound for treatment-resistant generalized anxiety disorder and major depressive disorder. *Brain Stimulation: Basic*,

Translational, and Clinical Research in Neuromodulation, 14(6), 1667.

<https://doi.org/10.1016/j.brs.2021.10.252>